Defining and Characterizing Cell Signal Transduction in the Sestrin2 Pathway

by

Allison Ho Kowalsky

A dissertation submitted in partial fulfillment
of the requirements for the degree of
Doctor of Philosophy
(Molecular and Integrative Physiology)
in The University of Michigan
2020

Doctoral Committee:

Associate Professor Jun Hee Lee, Co-Chair
Professor Santiago Schnell, Co-Chair
Associate Professor Diane C. Fingar
Associate Professor Ken Inoki
Professor Ling Qi

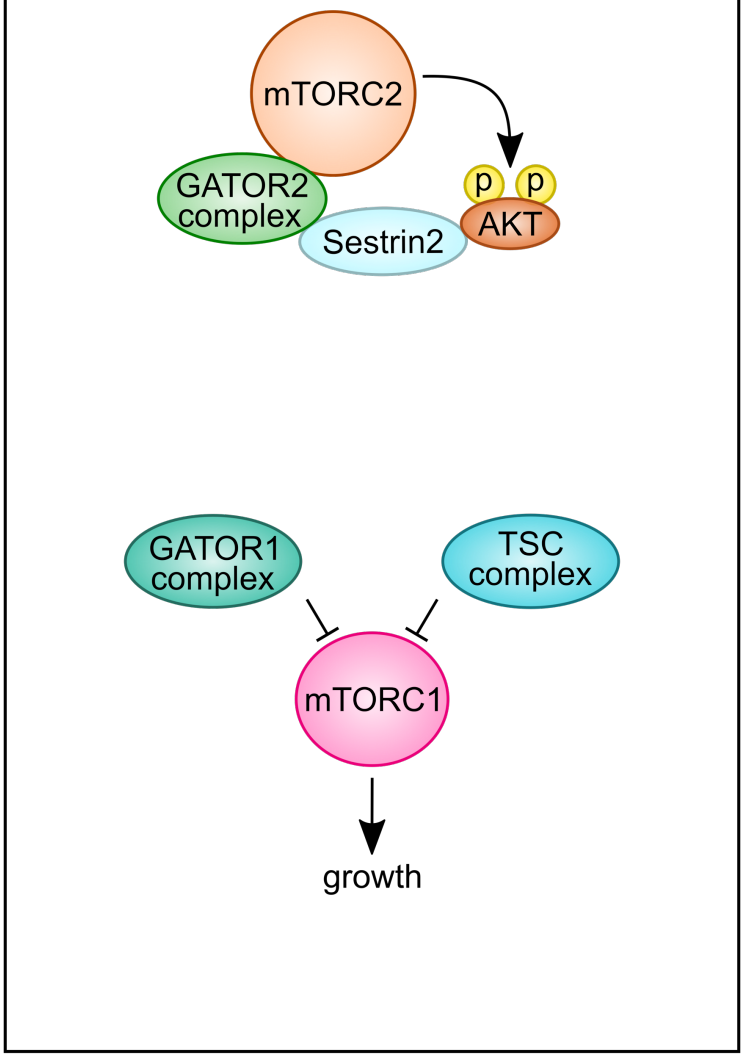
mTORC2
GATOR2
complex
p
p
AKT
Sestrin2
GATOR1
complex
TSC
complex
mTORC1
growth

Allison H. Kowalsky

allho@umich.edu

ORCID iD: 0000-0002-0922-0910

DEDICATION

I would like to dedicate this dissertation to my father, Herbert Ho (何平生).

ACKNOWLEDGEMENTS

This work could not have been completed without the support of everyone on this journey with me for the past six years. First and foremost, I have to thank my co-mentor, Santiago Schnell. If it were not for him, I would never have even considered pursuing a PhD. He has been a constant guide, inspiration, and life coach throughout my entire graduate education. He has pushed me to succeed in both science and life, even winning a doubles tennis tournament together during my Master's! Secondly, I would like to thank my co-mentor Jun Hee Lee, who has embarked on this adventure with me since the beginning of my PhD. He has spent countless hours editing my grants and papers, coaching me on my presentations, and somehow has an infinite generator in his head for exciting experimental ideas. His dedication to science has been a constant source of inspiration and guidance in training me to be an experimental scientist.

Next, I would like to thank all members of my dissertation committee Diane Fingar, Ken Inoki, and Ling Qi for their commitment to my success, quick doodle response times, and attendance at all meetings. The scientific input and career advice you have given me over the years has been invaluable, and I have been so lucky to have a "dream team" of signaling and metabolism experts to guide me throughout my PhD.

The Molecular & Integrative Physiology (MIP) Department has been incredibly supportive and provided me with a wonderful training environment. The graduate chairs during my training, Sue Moenter and Dan Michele, were always there when I needed them. Sue, an aspirational role model for me, and Dan, making sure my thesis defense could actually happen virtually through the coronavirus craze! In addition, I would like to thank the administrators in the department,

Michele Boggs, Rachel Anderson, and Jason Yunk who have helped me throughout the course of my training. I also had the opportunity to work with many other faculty both within and outside the department. Yatrik Shah, Scott Pletcher, and Malcolm Low from MIP all contributed to my training. Yatrik always attended my seminars and asked great questions, Scott taught a grant writing course and directed the Aging Training Grant, and Malcolm directed the Systems & Integrative Physiology Training Grant. I also had the opportunity to work with Uhn-Soo Cho from the Department of Biological Chemistry, where I learned about protein biochemistry and had many opportunities to present my work to his lab.

I also want to thank past and present members of both the Lee and Schnell Labs. Sim Namkoong, Chun-Seok Cho, Sung Rye Park, Hwan-Woo Park, Seung Hyun Ro, Myungjin Kim, Boyoung Kim, Frank Gu, Ian Semple, Jeong Sig Kim, Insook Jang, Eric Mettetal, Amanda Jones, Janae Hurd, and Alexandra Kiers from the Lee lab. Caroline Adams, Michele Wynn, Mark Whidden, Justin Eilertson, Wylie Stroberg, Suzie Shoffner, Dan DeWoskin, Max Denies, Mike Vincent, Malgorzata Tyczynska, and Joseph Cavataio from the Schnell lab. Your support, guidance, and friendship have made this journey unforgettable and achievable.

I would also like to thank many of my classmates. Jacob Johnson, thanks for being such a great friend and lab neighbor! You have made the day-to-day exceedingly more exciting and fun, and thank you for pushing me to new heights, literally! Andrew Schwartz, thank you for your friendship and helping me all along the PhD. I shamelessly skipped along the trail you blazed for all of the graduate school milestones! Thank you also to Owen Funk, Bree Doering, Paloma Garcia, Alyssa Kruger, Alivia Wu, Jeff Phumsatitpong, Anabel Flores, and Edith Jones. You have been great supporters and friends these past years, some even flying to Taiwan to attend my wedding!

Finally, I would like to thank my family for supporting me. Herbert and Shumei Ho, Steven Kowalsky and Ilene Burk, and my dear husband, Daniel Kowalsky. I could not have made it without your love and support!

TABLE OF CONTENTS

LIST OF FIGURES

LIST OF TABLES

ABSTRACT

Sestrins are highly conserved, stress-inducible proteins that protect against cellular damage and the progression of age-associated and diabetic pathologies. These include fat accumulation, insulin resistance, muscle degeneration, cardiac dysfunction, mitochondrial pathologies, and tumorigenesis. Sestrin has two established anti-aging functions: reducing oxidative stress and regulating the mechanistic target of rapamycin (mTOR) signaling network. This thesis focuses on the regulation of mTOR signaling.

First, I defined a new pathway in the Sestrin2 signaling network. Sestrin2 strongly activates AKT, a major metabolic regulator downstream of the insulin signaling cascade. I found that the mechanism for Sestrin2-induced AKT activation occurred through two large protein complexes: GAP Activity TOwards Rags 2 (GATOR2), a pentameric protein complex that binds to Sestrin2, and mTOR Complex 2 (mTORC2), a kinase upstream of AKT. GATOR2 bridged Sestrin2 and mTORC2 and was functionally required for Sestrin2-induced AKT activation. In addition, Sestrin2 bound to AKT's pleckstrin homology (PH) domain and induced AKT translocation to the plasma membrane. Although Sestrin2 and GATOR2 were known to inhibit mTORC1, this work defined a new mechanism for Sestrin2 and GATOR2 in activating mTORC2.

Next, I characterized other components in the Sestrin2 signaling network by generating transgenic mice with liver-specific knockouts. mTORC1 has two signaling arms required for full activation: nutrient sensing and growth factors. Nutrients input to the GATOR1 complex, which consists of Nprl2, Nprl3, and DEPDC5, while growth factors input to the TSC complex. First, I generated a *DEPDC5* knockout mouse to constitutively activate the nutrient sensing arm of

mTORC1. I found that liver-specific *DEPDC5* deletion (*Depdc5*$^{\Delta hep}$) showed enlarged zone 3 hepatocytes, increased sensitivity to acetaminophen toxicity, and decreased lipid accumulation in the liver. Next, I generated *Depdc5*$^{\Delta hep}$/*Tsc1*$^{\Delta hep}$ double knockout (DKO) mice to concurrently activate both the growth factor and nutrient sensing arms of mTORC1 in the liver. The DKO mice showed severe phenotypes by two months with significantly lower body weights and more liver injury. Interestingly, the severe pathological phenotypes were all reversed after only 10 days of intraperitoneal injections of either rapamycin, an mTORC1 inhibitor, or Tempol, an oxidative stress reducer. Surprisingly, tauroursodeoxycholic acid (TUDCA), an ER stress reliever, was lethal to the DKO mice, suggesting a potential feedback mechanism for ER stress in the context of hyperactive mTORC1. In addition, transcriptomic analysis of WT, *Depdc5*$^{\Delta hep}$, *Tsc1*$^{\Delta hep}$, and DKO livers showed that DKO livers had distinct transcriptomic profiles with selective upregulation of oxidative stress genes. Taken together with the Tempol experiment, this suggests that hyperactive hepatic mTORC1 induces liver injury through oxidative stress signaling. Finally, systemic characterization without any interventions showed that 2-month-old DKO mice had insulin resistance, and 5-month-old DKO mice exhibited spontaneous hepatocellular carcinoma (HCC). Overall, this work developed and characterized a new mouse model of hyperactive mTOR that could potentially be utilized for future studies as a 2-month nonalcoholic steatohepatitis (NASH) model or 5-month HCC model.

In summary, the work from this thesis has furthered our understanding of Sestrin2 signaling. First, we defined a novel mechanism where Sestrin2 and GATOR2 activate the mTORC2 pathway. Secondly, we developed and characterized a genetic mouse model with a hyperactive mTORC1 liver that spontaneously develops NASH by two months and HCC by five months. This work

provides a mechanistic understanding of how Sestrin is able to protect against diabetic pathological progression and provide a new tool for future studies of liver disease.

CHAPTER I[1]

Introduction

Sestrin, a versatile anti-aging molecule

One theory for the cause of aging is the accumulation of cellular damage, facilitated by environmental stressors that induce genotoxic or oxidative stress (1). Although appropriate levels of reactive oxygen species (ROS) are necessary for physiological homeostasis (2), excessive ROS accumulation can cause damage to DNA and proteins, thereby facilitating the aging process (1,2). Nutritional overabundance and obesity are also well-established promoters of aging, while appropriate dietary restriction extends longevity and healthspan in virtually all model organisms (1). One of the major signaling components that can mediate the nutritional effect on aging is mechanistic target of rapamycin complex 1 (mTORC1). Genetic or pharmacological inhibition of mTORC1 extends longevity and healthspan in most organisms including mammals (3-5), suggesting a central role of mTORC1 in the acceleration of aging.

Sestrins are a family of highly conserved proteins that are induced upon various conditions of stress, including DNA damage and oxidative stress. Invertebrates have a single orthologue, while vertebrates have three paralogues, Sestrin1-3 (Table 1.1) (6). In cultured cells, Sestrin1 and Sestrin2 reduced ROS (7) and suppressed mTORC1 activity (8), suggesting that this family of proteins may perform anti-aging functions through the inhibition of these two well-characterized aging facilitators. Indeed, genetic depletion of Sestrin in many animal models, including

[1] This chapter represents a published manuscript: Ho A, Cho CS, Namkoong S, Cho US, Lee JH. Biochemical Basis of Sestrin Physiological Activities. *Trends in Biochemical Sciences* (2016)

Table 1.1. Identified functions of mammalian Sestrin isoforms

Functions	Inhibits ROS in cells	In vitro [a]Ahp activity	Binds to Keap1	Inhibits mTORC1 in cells	Binds to GATOR2	Binds to mTORC2	Activates Akt in cells	Activates AMPK in cells	In vitro leucine binding
Sesn1	O	-	O	O	O	-	O	O	O
Sesn2	O	O	O	O	O	O	O	O	O
Sesn3	O	-	-	O	O	O	O	O	▲
Ref	(7,9)	(10)	(11)	(8,12)	(13-15)	(16)	(16,17)	(8,12)	(18)

[a]alkylhydroperoxidase
O = Functional
▲ = Weak
- = Undetermined

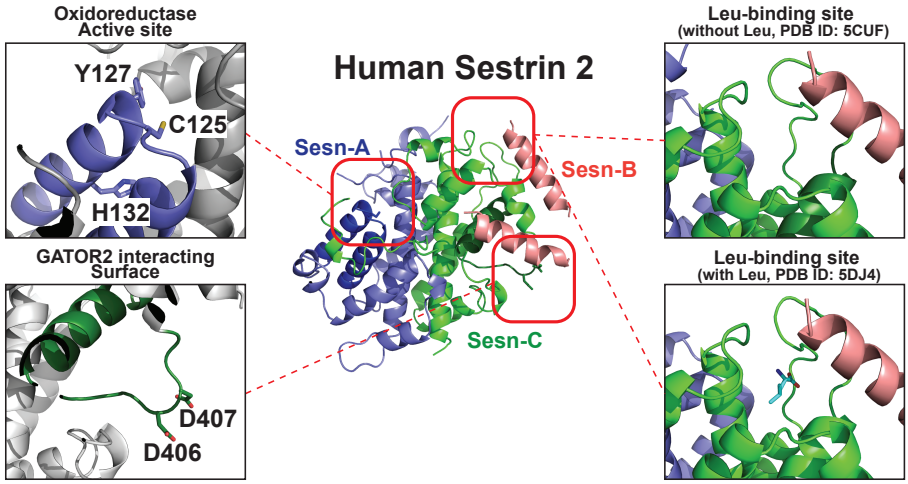

Figure 1.1 Structure of hSesn2 with highlighted functional domains. Ribbon diagram of full-length hSesn2 (PDB ID: 5CUF (10)). Sesn-A, Sesn-B and Sesn-C domains, which were originally predicted through a phylogenetic analysis (19), are represented in blue, pink and green, respectively. The oxidoreductase active site of Sesn-A is magnified in the top left, and the catalytic cysteine (C125) and conserved residues of the proton relay system (Y127 and H132) are indicated. These residues were found to be critical for the antioxidant function of hSesn2. The GATOR2-interacting surface of the Sesn-C domain is magnified on the bottom left with the critical residues (D406 and D407; the 'DD motif') labeled. This DD motif is required for the interaction between hSesn2 and GATOR2, and for subsequent control of AMPK and mTORC1 signaling. Finally, the leucine-binding site of the Sesn-C domain is magnified on the right. The top representation is the crystallized structure without added leucine (PDB ID: 5CUF (10)), and the bottom representation is the structure with leucine (PDB ID: 5DJ4 (20)). No significant conformational change was observed between these two structures. Illustrations of the protein structure were generated with PYMOL (Delano Scientific, LLC).

worms (21), flies (22) and mice (11,16,17,23-25), has led to the accelerated progression of diverse age- and obesity-associated pathological disorders including fat accumulation, insulin resistance, muscle degeneration, cardiac dysfunction, mitochondrial pathologies and tumorigenesis, which could be relieved by treatments that suppressed ROS or mTORC1 signaling. However, the biochemical mechanisms underlying how this small, 55kDa protein performs such versatile physiological functions and prevents the progression of diverse age-associated pathologies have remained elusive. Recently, our understanding of Sestrin protein biochemistry has dramatically improved. Major recent findings include identifying GAP activity towards Rags 2 (GATOR2), a heteropentameric protein complex that consists of WDR59, WDR24, Mios, Seh1L, and Sec13, as a direct physical target of Sestrin (13-15), acquiring an in-depth understanding of the antioxidant activity of Sestrin (10,11,26), identifying Sestrin as an amino acid sensor (18,20,27,28), and determining the three-dimensional molecular structure of Sestrin (10,20). The Sestrin structure revealed three functional sites for each of its identified activities: mTOR regulation, ROS suppression and leucine binding (Figure 1.1) (10,20). In this review, we discuss the current findings related to Sestrin function and signaling while highlighting questions elicited by these discoveries.

Sestrin suppresses oxidative damage

Sestrins are transcriptionally induced upon oxidative damage through diverse transcription factors including p53, Nrf2, AP-1 and FoxOs (6,29). Cells overexpressing Sestrin are protected from oxidative damage (7,9,29), while Sestrin deficiency renders cells and tissues hypersensitive to oxidative stress (7,11,22,30). Therefore, Sestrin is considered an important component of

antioxidant defense, and many different theories have been proposed to explain its antioxidant activity.

Sestrin as a Prx reductase

Sestrin exhibits a remote sequence similarity to AhpD, an antioxidant protein in *Mycobacterium tuberculosis* (7). AhpD has two known redox functions: detoxification of alkylhydroperoxides (a group of hydrophobic ROS (31)), and reduction of the cysteine disulfides (Cys-S-S-Cys) of AhpC (32), a peroxiredoxin (Prx)-family peroxidase in *M. tuberculosis*.

Mutation of Cys125 in Sestrin ($Sestrin^{CS}$), which corresponds to one of the two catalytic cysteines in AhpD, abolished the ability of Sestrin to protect cells from oxidative stress (7). Based on this functional similarity, it was originally proposed that Sestrin acts as a reductase for Prx. However, unlike AhpD, which can reduce the cysteine disulfides of AhpC (32), Sestrin2 was suggested to function as a reductase for cysteine sulfinic acids (Cys-SO_2H), an overoxidized form of Prx (7). Supporting this argument, induction of Sestrin expression significantly reduced the level of overoxidized Prx in two independent studies (7,33).

Although the role of Sestrin as a Prx reductase can explain its antioxidant function, another study rebuked this hypothesis; purified Sestrin did not exhibit any intrinsic cysteine sulfinic acid reductase activity toward Prx, while sulfiredoxin (Srx) did (34). A genetic study in *Caenorhabditis elegans* further demonstrated that Sestrin is not genetically required for recycling overoxidized Prx (35). Therefore, it is now widely agreed that Sestrin is not a stand-alone sulfinic acid reductase for Prx (6,26). Nevertheless, it seems clear that the induction of Sestrin can promote recycling of overoxidized Prx (7,33) and reduce oxidative damage in cells (7,9,29). These effects likely occur

through an indirect transcriptional upregulation of Srx or direct detoxification of ROS, mechanisms that will be discussed in more detail below.

Sestrin as an autophagy regulator

Autophagic degradation of dysfunctional mitochondria, known as mitophagy, is critical for redox homeostasis because the accumulation of damaged mitochondria results in excessive ROS production that can lead to diverse degenerative pathologies (36). Sestrin can upregulate autophagy through AMP-activated Protein Kinase (AMPK) activation and mTORC1 inhibition. Correspondingly, Sestrin was found to induce autophagy during diverse environmental stresses that provoke mitochondrial dysfunction (11,37-40).

A genetic study in *Drosophila* also supported the importance of autophagy in mediating the antioxidant activity of Sestrin because the loss of Sestrin led to autophagy impairment, resulting in accumulation of damaged mitochondria and subsequent elevation of ROS in skeletal muscle (22). Similar muscle phenotypes were also observed in Sestrin-deficient *C. elegans* (21). These phenotypes were dependent on AMPK/mTORC1 misregulation and autophagy abrogation because (i) pharmacological AMPK activation or mTORC1 inhibition restored mitochondrial homeostasis in Sestrin-deficient flies, (ii) Sestrin^{CS}, a redox-inactive Sestrin that can still regulate AMPK/mTORC1 signaling (8), also restored mitochondrial homeostasis, and (iii) RNAi-mediated downregulation of *Ampk* or *Atg1*, the fly homolog of ULK1, resulted in mitochondrial phenotypes like those seen in Sestrin-deficient flies (22).

Even though the mitophagy-regulating function of Sestrin is important for redox homeostasis, Sestrin also contributes to redox biology through additional mechanisms. First, in several non-muscle cell types, Sestrin^{CS} was less effective than Sestrin^{WT} in suppressing ROS

accumulation (7,41). Second, Sestrin suppressed ROS in physiological contexts that do not involve mitochondrial damage, including neuronal synaptic stimulation (42), replicative senescence (30), macrophage peroxide signaling (33), brown adipocyte thermogenesis (41) and renal dopamine signaling (43). Thus, Sestrin-mediated redox regulation is not narrowly confined to the control of mitophagy and autophagy but must involve additional mechanisms.

Sestrin as an Nrf2 regulator

Nrf2 is a transcription factor that upregulates the expression of a wide range of antioxidant genes including Prx, Srx, glutathione-S-transferase (GST) and thioredoxin (Trx) (44). In normal environments, kelch-like ECH-associated protein 1 (Keap1) binds to Nrf2 and targets it for proteasomal degradation (Figure 1.2A). Keap1 inactivation occurs through oxidation of its several cysteine residues (44) or by autophagic elimination mediated by an autophagy adapter p62/sequestosome-1 (SQSTM1) (45,46).

Sestrin2 was found to associate with both Keap1 and SQSTM1 (11), as well as autophagy-initiator ULK1 (47). Sestrin2 promotes ULK1-induced phosphorylation of SQSTM1 (47), which facilitates Keap1 degradation and Nrf2 activation (48). This pathway can explain how Sestrin2 functions as an antioxidant through upregulation of Nrf2 and its antioxidant targets (Figure 1.2B) (26). Indeed, the Sestrin2-Keap1-Nrf2 pathway was shown to be physiologically important for the antioxidant defense of hepatocytes against nutritional (11) and chemical (49) stress.

Another intriguing point is that both Sestrin2 and SQSTM1, which contribute to the degradation of Keap1, are direct transcriptional targets of Nrf2 (50,51). Therefore, Nrf2-dependent induction of Sestrin2 and SQSTM1 can generate a positive feedback loop that guarantees the maximal activation of the antioxidant activity of Nrf2 upon oxidative stress.

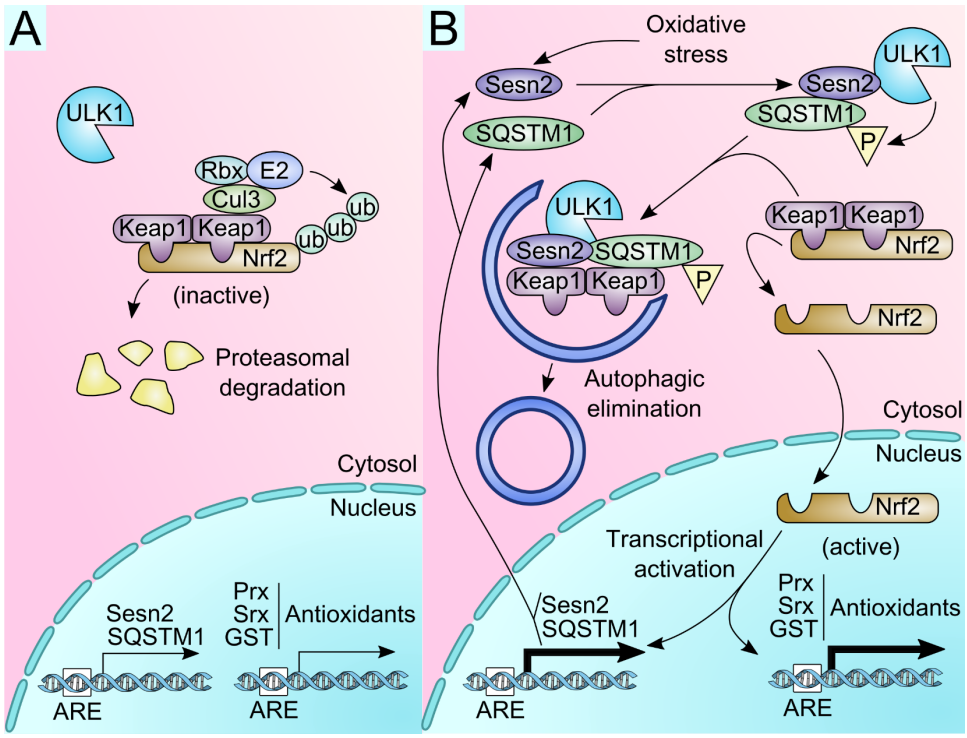

Figure 1.2. Sestrin-mediated regulation of Nrf2. (A) Under normal environmental conditions, Nrf2 is inactivated when Keap1 binds and targets it for proteasomal degradation through the Cul3-based E3 ligase (Cul3) and associated RING box protein (Rbx), which recruits an E2 ligase to tag Nrf2 with ubiquitin (ub). **(B)** Under conditions of oxidative stress, Sestrin2 (Sesn2) and SQSTM1 are expressed. Sesn2 binds ULK1, an initiator of autophagy, and SQSTM1, an autophagy adaptor protein. This interaction between the three proteins promotes ULK1-dependent phosphorylation of SQSTM1, which then specifically targets Keap1 for autophagic elimination. Now, Nrf2 is freed from Keap1, translocates to the nucleus, and promotes transcriptional activation of genes controlled by the antioxidant response element (ARE), including *Sesn2*, *SQSTM1* and antioxidant enzymes such as *Prx*, *Srx*, and *GST*.

Although this Nrf2-dependent mechanism provides a convincing explanation of the antioxidant role of Sestrin2, several questions still remain: (i) is the physical interaction between Sestrin2, Keap1, SQSTM1 and ULK1 supported by structural studies, (ii) can Sestrin2, in conjunction with Keap1, regulate Nrf2 activity in a redox-sensitive manner, and (iii) does Sestrin regulation of AMPK and mTORC1 signaling also contribute to the autophagic regulation of Keap1 and Nrf2. Assessing the effect of specific mutations that block the peroxidase activity of Sestrin or mTORC1-regulating function (Table 1.2) may provide some clues about its regulation of the Keap1-Nrf2 pathway.

Sestrin as a peroxidase

Recent determination of the human Sestrin2 (hSesn2) structure by X-ray crystallography allowed us to gain novel insights into its antioxidant function. The crystal structure revealed that hSesn2 contains two structurally similar subdomains, Sesn-A and Sesn-C. Both subdomains share significant structural homology with the *Ralstonia eutropha* protein YP_296737.1, which belongs to a family of alkylhydroperoxidases, including the *M. tuberculosis* AhpD (10,20). Moreover, the Sesn-A domain of hSesn2 contains the helix–turn–helix oxidoreductase motif (Figure 1.1) that has an intact proton relay system with the catalytic cysteine (Cys125) and other key residues (Tyr127 and His132) conserved in AhpD and YP_296737.1 (10).

Subsequent biochemical studies demonstrated that hSesn2 is indeed an active alkylhydroperoxidase (10). This conclusion was based on the observations that (i) recombinant hSesn2 catalyzed the reduction of cumene hydroperoxide, an alkylhydroperoxide, at an efficiency comparable to *M. tuberculosis* AhpC and AhpD; (ii) substitutions of the key catalytic residues of Sesn-A, including Cys125, Tyr127 and His132 (Figure 1.1), abolished the alkylhydroperoxidase

Table 1.2. Point mutations of hSesn2 that significantly affect its molecular function

Point Mutation	Inhibits ROS in cells	In vitro [a]Ahp activity	Binds to Keap1	Inhibits mTORC1 in cells	Binds to GATOR2	Activates AMPK in cells	Binds to leucine	References
WT	O	O	O	O	O	O	O	(7,8,10,11,13,14, 18,20,27)
Mutations in Sesn-A domain								
H86A	-	-	-	-	O	-	X	(20)
C125S	X	X	O	O	O	-	-	(7,8,10,11)
Y127F	-	X	-	O	-	-	-	(10)
H132A	-	X	-	O	-	-	-	(10)
S190W	-	-	-	X	X	-	O	(18)
Mutations in Sesn-B domain								
L261A	-	-	-	O	O	-	X	(18)
Mutations in Sesn-C domain								
T374A	-	-	-	-	-	-	X	(20)
Y375F	-	-	-	-	O	-	X	(20)
T386A	-	-	-	-	O	-	X	(20)
R390A	-	-	-	-	O	-	X	(20)
R404A/ D406A/ D407A	-	-	-	X	X	-	-	(10)
D406A	-	O	-	X	X	X	-	(10)
D407A	-	O	-	X	X	X	-	(10)
D406A/ D407A	-	-	-	-	X	-	O	(20)
R419A	-	-	-	OX	-	-	-	(10,27)
R419A/ K422A/ K426A	-	-	-	OX	-	-	-	(10,27)
W444E	-	-	-	-	O	-	X	(20)
W444L	-	-	-	-	O	-	▲	(20)
E451A	-	-	-	O	O	-	X	(18)
E451Q	-	-	-	-	O	-	X	(20)

[a]alkylhydroperoxidase
O = Functional
▲ = Partially functional
OX = Conflicting results
X = Non-functional
- = Undetermined

activity of hSesn2; and (iii) the proposed reaction intermediate form—cysteine sulfenic acid (Cys-SOH)—of hSesn2 was detectable in wild-type hSesn2 but not Cys125-substituted hSesn2 ($hSesn2^{CS}$).

Although the structural and biochemical evidence demonstrates that hSesn2 has intrinsic peroxidase activity, the physiological ROS substrate of hSesn2 still needs to be identified. Hydrogen peroxide, which is among the most abundant and biologically significant ROS in cells, is not efficiently reduced by hSesn2 (10). The only known substrate for hSesn2 is cumene hydroperoxide (10), which is not a physiological ROS in any known cell type. Because hSesn2 is expected to be specific for hydrophobic alkylhydroperoxides (10), lipid hydroperoxides may be a physiologically relevant substrate for Sestrin as they are implicated in diverse age- and obesity-associated diseases (52-54). It is also possible that hSesn2 acts as a redox sensor, if the reversible oxidation of Cys125 in hSesn2 is found to affect its function in promoting autophagy or regulating Nrf2.

Sestrin regulates the mTOR signaling network

Independent of redox regulation, Sestrin is also involved in stress-dependent mTOR regulation. mTOR is present in two different protein kinase complexes, mTORC1 and mTORC2. Sestrin specifically inhibits mTORC1 by inhibiting Rheb and RagA/B, the two GTPases essential for mTORC1 activation. The AMPK-TSC2 pathway mediates the effects of Sestrin on Rheb, while the GATOR1-GATOR2 complexes are responsible for the effects of Sestrin on RagA/B (Figure 1.3). GATOR1 is a heterotrimeric protein complex that consists of DEPDC5, Nprl2, and Nprl3 with GAP activity towards RagA/B. Interestingly, although Sestrin strongly inhibits mTORC1, it activates mTORC2 through several independent mechanisms.

Sestrin as an AMPK regulator

The study that first described Sestrin-mediated mTORC1 control concluded that this regulation was dependent on AMPK (8). In this study, Sestrin was shown to associate with the TSC1:TSC2 complex and promote the activation of TSC2 by AMPK-mediated phosphorylation. Sestrin also increased AMPK phosphorylation at Thr172 (8), a marker of AMPK activation. As TSC2 is a GTPase-activating protein (GAP) for Rheb, Sestrin-dependent TSC2 activation inactivates Rheb and mTORC1 (Figure 1.3B). Supporting this model, pharmacological (via compound C) or shRNA-mediated inhibition of AMPK and TSC2 blunted the inhibition of mTORC1 by Sestrin (8). Importantly, Sestrin was necessary for DNA damage-induced inhibition of mTORC1 (8), which was also dependent on the activation of AMPK and TSC2 (55).

The AMPK-activating role of Sestrin was widely observed and shown to be important for mTORC1 control in diverse cellular contexts (23,24,40,56-58). Genetic studies in *Drosophila* also supported this model because the AMPK-TSC2 axis was critical for the effect of Sestrin in controlling tissue growth and attenuating age-associated pathologies (22,59). Metabolic phenotypes of Sestrin2-deficient mice, including insulin resistance and steatohepatitis, were also strongly suppressed by pharmacological (via AICAR) or viral (via Ad-AMPK^{CA}) activation of AMPK (17,23), further supporting the idea that AMPK is the critical downstream target of Sestrin controlling metabolic homeostasis.

Although this evidence indicates that AMPK is physiologically important for mediating Sestrin activity, Sestrin was recently found to inhibit mTORC1 in *AMPK*-null mouse embryonic fibroblasts (MEF) (14,15,27), suggesting that AMPK is not the only target of Sestrin in the mTORC1 pathway. In addition, the molecular mechanism of Sestrin-induced AMPK activation is still unknown. Some studies suggested that Sestrin functions as a signaling scaffold between

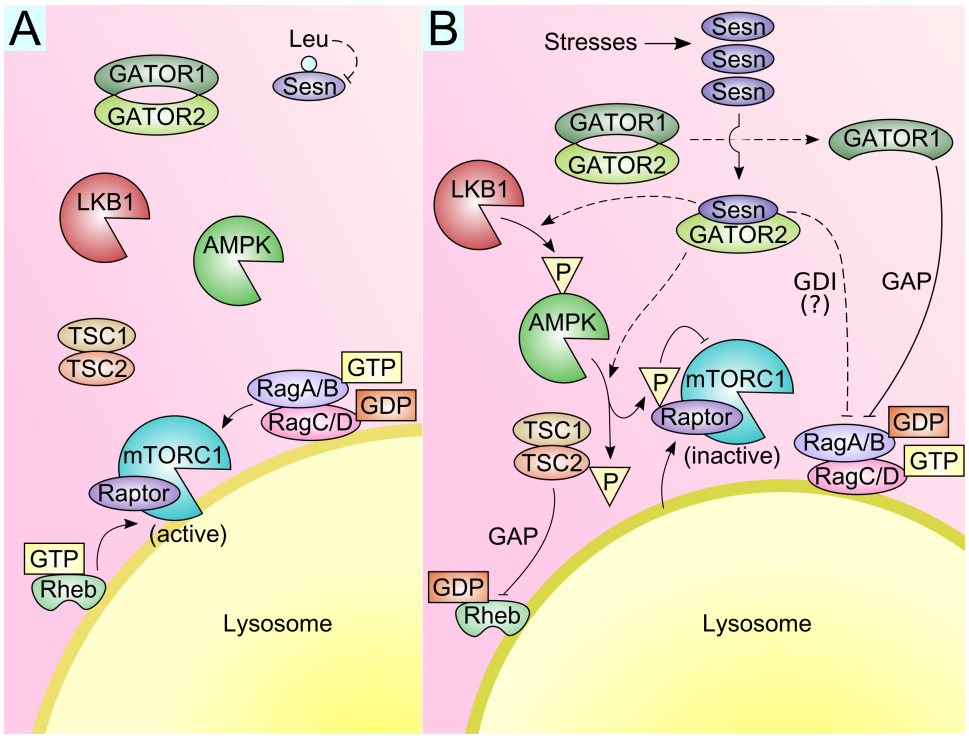

Figure 1.3. Sestrin-mediated regulation of mTORC1. (A) Under unstressed conditions, Sestrin expression and activity is low, and GATOR1 and GATOR2 form a supercomplex. mTORC1 is fully activated; activated RagA/B:RagC/D localizes mTORC1 to the lysosomal membrane, and GTP-loaded Rheb activates mTORC1's kinase activity. **(B)** Under conditions of stress, Sestrin is upregulated and binds GATOR2. This then frees GATOR1 from GATOR2 inhibition, and GATOR1 subsequently acts as a GAP for RagA/B. Inactivated RagA/B:RagC/D is then unable to localize mTORC1 to the lysosome, and mTORC1 disperses to the cytosol. In addition, the Sestrin-GATOR2 interaction also promotes AMPK activation through unclear biochemical mechanisms possibly involving LKB1, the major kinase upstream of AMPK. Activated AMPK then phosphorylates TSC2, a GAP for Rheb, leaving Rheb now in its inactive GDP-loaded form. AMPK also phosphorylates Raptor, a regulatory subunit of mTORC1, and this phosphorylation inhibits the kinase activity of mTORC1 (60). Sestrin may also regulate RagA/B proteins as a GDI. Solid lines indicate established mechanisms, while dashed lines indicate models that require further biochemical clarification.

AMPK and LKB1 (24,61) and that Sestrin induces the expression of AMPK regulatory subunits to achieve maximal AMPK activation (61). Although these models do explain a mechanism for Sestrin-induced AMPK activation, more robust experimental evidence is needed to clarify the exact biochemical role of Sestrin in AMPK signaling.

Sestrin as a Rag GDI

In search of alternative mechanisms to account for Sestrin regulation of mTORC1 in an AMPK-independent manner, Sestrin was suggested to act as a GDP dissociation inhibitor (GDI) to inhibit RagA/B (27). This model was based on the following observations: (i) Sestrin could not inhibit mTORC1 when constitutively active RagB was expressed, (ii) Sestrin exhibited physical interaction with the RagA/B:RagC/D complex, (iii) Sestrin inhibited GTP loading on the RagA/B proteins in an *in vitro* assay, and (iv) Sestrin shows limited sequence homology to human and mouse GDI1 proteins (27).

Although this model could explain the observations that Sestrin-mediated mTORC1 inhibition is dependent on RagA/B (13-15,27), several findings contradict this model. Crystal structures of hSesn2 show no structural homology between Sestrin and GDI proteins (10,20) and actually indicate that the proposed GDI motif in Sestrin has a very different conformation from GDI1. Indeed, mutations of the putative GDI motif did not prevent Sestrin from inhibiting mTORC1 (10). In addition, although the initial study reported that hSesn2 immunostaining overlaps with the Rag complex on the lysosomal membrane (27), subsequent studies with higher immunofluorescence resolution demonstrated that hSesn2 is actually excluded from the lysosomal surface (14,15), indicating that hSesn2 does not directly control RagA/B activity on the lysosomal membrane. Finally, the direct physical interaction between Sestrin and RagA/B

was undetectable in several subsequent experiments (15). These observations suggest that Sestrin-mediated control of RagA/B could occur through indirect mechanisms involving additional signaling components.

Sestrin as a GATOR modulator

In several independent labs, proteomic studies identified a strong physical interaction between Sestrin and GATOR2 (13-15), a RagA/B-regulating hetero-pentameric protein complex (62). GATOR2 is known to suppress GATOR1, a heterotrimeric complex that functions as a GAP for RagA/B (63). Therefore, Sestrin was postulated to bind GATOR2, liberating GATOR1 from GATOR2-mediated inhibition, and thereby promote the RagA/B-inhibiting activity of GATOR1 (Figure 1.3) (13-15). Supporting this model, silencing or knocking out GATOR1 components abolished inhibition of mTORC1 by Sestrin (13-15). The genetic relationship between Sestrin, GATOR1 and GATOR2 was also conserved in *Drosophila*; silencing GATOR1 inhibited suppression of wing growth by Sestrin, and mutations of GATOR2 restored autophagy defects in *Sestrin*-null flies (15). These results suggest that Sestrin inhibits RagA/B-dependent mTORC1 activation through modulation of the GATOR complexes.

Even though these results implicate a functional relationship between Sestrin, GATOR2, GATOR1 and RagA/B, the biochemical mechanisms of how Sestrin modulates the GATOR complexes are still elusive with noticeable inconsistencies between the reports. Two papers indicated that Sestrin does not affect the association between GATOR1 and GATOR2 (13,14), while another study demonstrated that high levels of Sestrin expression destabilized the GATOR1:GATOR2 supercomplex (15). One paper indicated that Sestrin does not affect the GTP loading status of RagB (14), while the other two papers showed that GTP loading of RagB was

altered by Sestrin overexpression (15,27). This confusion is in part because the molecular natures of the GATOR1 and GATOR2 complexes are not yet biochemically defined. For example, the biochemical mechanism of how GATOR2 suppresses GATOR1 is also unknown.

Despite these unanswered questions, the recently determined crystal structure of hSesn2 led to the discovery of a structural motif that mediates the hSesn2-GATOR2 interaction. As previously mentioned, hSesn2 has two-fold pseudosymmetrical subdomains, Sesn-A and Sesn-C (Figure 1.1), each of which is structurally homologous to an alkylhydroperoxidase (10,20). Whereas the helix–turn–helix oxidoreductase motif was found to be well-conserved and functional in Sesn-A, the corresponding structural motif was absent in Sesn-C and replaced with a long loop structure containing two surface-exposed aspartates (Asp406 and Asp407, the DD motif) (Figure 1.1) (10). Mutations in the DD motif almost completely abolished the binding between hSesn2 and GATOR2 (10,20), suggesting that the DD motif constitutes a key protein-protein interaction site. Importantly, mutations in the DD motif abolished both AMPK-activating and mTORC1-inhibiting functions of hSesn2 (10), signifying the importance of the DD motif and GATOR2 in Sestrin signaling.

Sestrin as an amino acid sensor

Sestrin-null MEF or HEK293 cells, generated by triple knockout or knockdown of *Sestrin1-3* genes, failed to downregulate mTORC1 activity after amino acid starvation (13,27). These observations implicated Sestrin in the amino acid-dependent control of mTORC1. Recently, two papers further suggested that hSesn2 acts as a direct sensor of leucine, based on the following observations: (i) hSesn2 physically binds to leucine at a K_d of 20μM (18), which is lower than that of leucyl tRNA synthetase (45μM) (64), (ii) leucine binding to hSesn2 changes

its melting temperature and prevents its binding to GATOR2 (18), (iii) crystal structure of hSesn2 was determined in the presence of added leucine, and leucine was found in a binding pocket in the crystal structure of hSesn2 (20), and (iv) wild-type hSesn2, but not leucine-binding defective hSesn2 mutants, restored the leucine sensitivity of mTORC1 signaling in *Sestrin*-null HEK293 cells (18,20). According to this model, hSesn2 cannot inhibit mTORC1 in the presence of leucine because leucine binding prohibits hSesn2 from interacting with its effector, GATOR2.

In addition to leucine, hSesn2 can also bind to other hydrophobic amino acids such as methionine, isoleucine and valine, although with a lower binding affinity (18). hSesn1 can also strongly bind to leucine while the binding between hSesn3 and leucine was found to be weak (Table 1.1) (18). On the other hand, all three Sestrin isoforms, hSesn1-3, can strongly bind to GATOR2 and inhibit mTORC1 (13-15). Although leucine was reported to disrupt the hSesn1-GATOR2 and hSesn2-GATOR2 interactions, the hSesn3-GATOR2 interaction was not disrupted by the in vitro addition of leucine (18).

Although these are potentially important findings in the field of amino acid signaling, there are several caveats that need to be addressed before considering hSesn2 as an established leucine sensor. First, in contrast to the prediction that Sestrin2 is inactivated by leucine above 20μM, numerous studies (8,10,12-15,22,23,27,61,65) indicated that hSesn2 is still able to suppress mTORC1 signaling in conditions rich with leucine. These conditions include conventional cell culture media such as RPMI and DMEM that contains 380μM and 800μM of leucine, respectively, and the intracellular amino acid concentration can be higher due to the presence of active transporters (66,67). Therefore, the effect of leucine on Sestrin2 function could be variable depending on the biological context. Second, in contrast to the theory that the hSesn2-GATOR2 interaction is completely disrupted by leucine (18,20), the physical interaction

between hSesn2 and GATOR2 was detectable in various cell lines cultured in leucine-rich conditions (13-15). Finally, although the leucine sensor model predicted that leucine binding and dissociation would induce large conformational changes in hSesn2 (18,20), the crystal structures determined in the presence or absence of leucine were actually quite similar (Figure 1.1) (10,20). Thus, whether hSesn2 is indeed inactivated by leucine binding under physiological conditions needs further clarification.

More recently, several additional mechanisms were suggested to explain the role of Sestrin2 in amino acid sensing. First, GCN2, an established sensor of amino acids (68), was shown to induce hSesn2 transcription through upregulation of the ATF4 transcription factor (28). The GCN2-dependent hSesn2 induction was important for mTORC1 regulation in response to amino acid availability, including leucine and glutamine (28). Second, it was also shown that Sestrin2 is phosphorylated by ULK1 in response to leucine starvation (69). Because phosphorylation may affect the leucine-binding or mTORC1-regulating activities of Sestrin2, further studies may clarify why different studies contradict each other in regards to whether physiological leucine concentrations can inhibit Sestrin2 function and/or Sestrin2-GATOR2 binding. It is also worth noting that, in addition to being phosphorylated by ULK1, Sestrin2 can potentiate ULK1-dependent phosphorylation (47) and degradation (11) of SQSTM1. Considering that SQSTM1 was recently characterized as an important mTORC1 regulator that is involved in amino acid sensing (70-72), future studies are necessary to understand how Sestrin2, ULK1, SQSTM1 and GATOR2 are functionally connected with each other in the context of amino acid sensing.

Sestrin as an mTORC2 regulator

Even though Sestrin strongly suppresses mTORC1 signaling, Sestrin upregulated mTORC2-dependent AKT phosphorylation in cultured cells as well as in mouse and *Drosophila* tissues (16,17). Because chronic activation of mTORC1 and S6K signaling is known to cause insulin resistance (73), Sestrin-mediated mTORC2-AKT activation could be dependent on the mTORC1-suppressive activity of Sestrin. However, Sestrin-induced activation of the TSC1:TSC2 complex can also contribute to mTORC2 upregulation through an mTORC1-independent mechanism (74). Recently, Sestrin2 and Sestrin3 were shown to physically bind to mTORC2 through Rictor, one of its regulatory subunits, and directly promote the catalytic activity of mTORC2 (16). Thus, it seems that Sestrin can upregulate mTORC2-AKT signaling through multiple mechanisms. The AKT-upregulating activities of Sestrin could be critical for its protection against insulin resistance and diabetic progression (16,17). Further investigation should be targeted towards defining a clear molecular mechanism for Sestrin-mediated AKT upregulation and defining the context-dependent contributions of the multiple signaling pathways.

Concluding Remarks

In recent years, significant progress has been made towards understanding the biochemical mechanisms behind the actions of Sestrin; however, many questions still remain. Sestrin is a versatile protein that can single-handedly control a variety of anti-aging functions, which can be roughly classified into its ROS-reducing and mTOR-regulating functions. The recently determined crystal structure of hSesn2 supported this dual role by revealing two subdomains responsible for each of these functions. In addition, structure-guided mutagenesis studies generated a list of point

mutations that specifically ablate the redox-controlling or mTORC1-modulating functions of Sestrin (Table 1.2), which constitutes an essential toolkit for the molecular dissection of Sestrin function in diverse physiological contexts. Considering the important physiological functions of Sestrin in regulating metabolic homeostasis and attenuating age-associated pathologies, further investigation into the biochemical functions of Sestrin may generate novel insight into developing a new class of anti-aging therapeutics that harness the beneficial activities of Sestrin.

References

1. Lopez-Otin, C., Blasco, M. A., Partridge, L., Serrano, M., and Kroemer, G. (2013) The hallmarks of aging. *Cell* **153**, 1194-1217

2. Hekimi, S., Lapointe, J., and Wen, Y. (2011) Taking a "good" look at free radicals in the aging process. *Trends in cell biology* **21**, 569-576

3. Johnson, S. C., Rabinovitch, P. S., and Kaeberlein, M. (2013) mTOR is a key modulator of ageing and age-related disease. *Nature* **493**, 338-345

4. Wu, J. J., Liu, J., Chen, E. B., Wang, J. J., Cao, L., Narayan, N., Fergusson, M. M., Rovira, II, Allen, M., Springer, D. A., Lago, C. U., Zhang, S., DuBois, W., Ward, T., deCabo, R., Gavrilova, O., Mock, B., and Finkel, T. (2013) Increased mammalian lifespan and a segmental and tissue-specific slowing of aging after genetic reduction of mTOR expression. *Cell reports* **4**, 913-920

5. Harrison, D. E., Strong, R., Sharp, Z. D., Nelson, J. F., Astle, C. M., Flurkey, K., Nadon, N. L., Wilkinson, J. E., Frenkel, K., Carter, C. S., Pahor, M., Javors, M. A., Fernandez, E., and Miller, R. A. (2009) Rapamycin fed late in life extends lifespan in genetically heterogeneous mice. *Nature* **460**, 392-395

6. Lee, J. H., Budanov, A. V., and Karin, M. (2013) Sestrins orchestrate cellular metabolism to attenuate aging. *Cell metabolism* **18**, 792-801

7. Budanov, A. V., Sablina, A. A., Feinstein, E., Koonin, E. V., and Chumakov, P. M. (2004) Regeneration of peroxiredoxins by p53-regulated sestrins, homologs of bacterial AhpD. *Science* **304**, 596-600

8. Budanov, A. V., and Karin, M. (2008) p53 target genes sestrin1 and sestrin2 connect genotoxic stress and mTOR signaling. *Cell* **134**, 451-460

9. Kopnin, P. B., Agapova, L. S., Kopnin, B. P., and Chumakov, P. M. (2007) Repression of sestrin family genes contributes to oncogenic Ras-induced reactive oxygen species up-regulation and genetic instability. *Cancer Res* **67**, 4671-4678

10. Kim, H., An, S., Ro, S. H., Teixeira, F., Jin Park, G., Kim, C., Cho, C. S., Kim, J. S., Jakob, U., Hee Lee, J., and Cho, U. S. (2015) Janus-faced Sestrin2 controls ROS and mTOR signalling through two separate functional domains. *Nat Commun* **6**, 10025

11. Bae, S. H., Sung, S. H., Oh, S. Y., Lim, J. M., Lee, S. K., Park, Y. N., Lee, H. E., Kang, D., and Rhee, S. G. (2013) Sestrins activate Nrf2 by promoting p62-dependent autophagic degradation of Keap1 and prevent oxidative liver damage. *Cell metabolism* **17**, 73-84

12. Chen, C. C., Jeon, S. M., Bhaskar, P. T., Nogueira, V., Sundararajan, D., Tonic, I., Park, Y., and Hay, N. (2010) FoxOs inhibit mTORC1 and activate Akt by inducing the expression of Sestrin3 and Rictor. *Dev Cell* **18**, 592-604

13. Chantranupong, L., Wolfson, R. L., Orozco, J. M., Saxton, R. A., Scaria, S. M., Bar-Peled, L., Spooner, E., Isasa, M., Gygi, S. P., and Sabatini, D. M. (2014) The Sestrins interact with GATOR2 to negatively regulate the amino-acid-sensing pathway upstream of mTORC1. *Cell reports* **9**, 1-8

14. Parmigiani, A., Nourbakhsh, A., Ding, B., Wang, W., Kim, Y. C., Akopiants, K., Guan, K. L., Karin, M., and Budanov, A. V. (2014) Sestrins inhibit mTORC1 kinase activation through the GATOR complex. *Cell reports* **9**, 1281-1291

15. Kim, J. S., Ro, S. H., Kim, M., Park, H. W., Semple, I. A., Park, H., Cho, U. S., Wang, W., Guan, K. L., Karin, M., and Lee, J. H. (2015) Sestrin2 inhibits mTORC1 through modulation of GATOR complexes. *Scientific reports* **5**, 9502

16. Tao, R., Xiong, X., Liangpunsakul, S., and Dong, X. C. (2015) Sestrin 3 protein enhances hepatic insulin sensitivity by direct activation of the mTORC2-Akt signaling. *Diabetes* **64**, 1211-1223

17. Lee, J. H., Budanov, A. V., Talukdar, S., Park, E. J., Park, H. L., Park, H. W., Bandyopadhyay, G., Li, N., Aghajan, M., Jang, I., Wolfe, A. M., Perkins, G. A., Ellisman, M. H., Bier, E., Scadeng, M., Foretz, M., Viollet, B., Olefsky, J., and Karin, M. (2012) Maintenance of metabolic homeostasis by Sestrin2 and Sestrin3. *Cell metabolism* **16**, 311-321

18. Wolfson, R. L., Chantranupong, L., Saxton, R. A., Shen, K., Scaria, S. M., Cantor, J. R., and Sabatini, D. M. (2016) Sestrin2 is a leucine sensor for the mTORC1 pathway. *Science* **351**, 43-48

19. Budanov, A. V., Lee, J. H., and Karin, M. (2010) Stressin' Sestrins take an aging fight. *EMBO molecular medicine* **2**, 388-400

20. Saxton, R. A., Knockenhauer, K. E., Wolfson, R. L., Chantranupong, L., Pacold, M. E., Wang, T., Schwartz, T. U., and Sabatini, D. M. (2016) Structural basis for leucine sensing by the Sestrin2-mTORC1 pathway. *Science* **351**, 53-58

21. Yang, Y. L., Loh, K. S., Liou, B. Y., Chu, I. H., Kuo, C. J., Chen, H. D., and Chen, C. S. (2013) SESN-1 is a positive regulator of lifespan in Caenorhabditis elegans. *Experimental gerontology* **48**, 371-379

22. Lee, J. H., Budanov, A. V., Park, E. J., Birse, R., Kim, T. E., Perkins, G. A., Ocorr, K., Ellisman, M. H., Bodmer, R., Bier, E., and Karin, M. (2010) Sestrin as a feedback inhibitor of TOR that prevents age-related pathologies. *Science* **327**, 1223-1228

23. Park, H. W., Park, H., Ro, S. H., Jang, I., Semple, I. A., Kim, D. N., Kim, M., Nam, M., Zhang, D., Yin, L., and Lee, J. H. (2014) Hepatoprotective role of Sestrin2 against chronic ER stress. *Nat Commun* **5**, 4233

24. Morrison, A., Chen, L., Wang, J., Zhang, M., Yang, H., Ma, Y., Budanov, A., Lee, J. H., Karin, M., and Li, J. (2015) Sestrin2 promotes LKB1-mediated AMPK activation in the ischemic heart. *FASEB journal : official publication of the Federation of American Societies for Experimental Biology* **29**, 408-417

25. Ro, S. H., Xue, X., Ramakrishnan, S. K., Cho, C. S., Namkoong, S., Jang, I., Semple, I. A., Ho, A., Park, H. W., Shah, Y. M., and Lee, J. H. (2016) Tumor suppressive role of sestrin2 during colitis and colon carcinogenesis. *eLife* **5**, 12204

26. Rhee, S. G., and Bae, S. H. (2015) The antioxidant function of sestrins is mediated by promotion of autophagic degradation of Keap1 and Nrf2 activation and by inhibition of mTORC1. *Free radical biology & medicine* **88**, 205-211

27. Peng, M., Yin, N., and Li, M. O. (2014) Sestrins Function as Guanine Nucleotide Dissociation Inhibitors for Rag GTPases to Control mTORC1 Signaling. *Cell* **159**, 122-133

28. Ye, J., Palm, W., Peng, M., King, B., Lindsten, T., Li, M. O., Koumenis, C., and Thompson, C. B. (2015) GCN2 sustains mTORC1 suppression upon amino acid deprivation by inducing Sestrin2. *Genes & development* **29**, 2331-2336

29. Budanov, A. V., Shoshani, T., Faerman, A., Zelin, E., Kamer, I., Kalinski, H., Gorodin, S., Fishman, A., Chajut, A., Einat, P., Skaliter, R., Gudkov, A. V., Chumakov, P. M., and Feinstein, E. (2002) Identification of a novel stress-responsive gene Hi95 involved in regulation of cell viability. *Oncogene* **21**, 6017-6031

30. Nogueira, V., Park, Y., Chen, C. C., Xu, P. Z., Chen, M. L., Tonic, I., Unterman, T., and Hay, N. (2008) Akt determines replicative senescence and oxidative or oncogenic premature senescence and sensitizes cells to oxidative apoptosis. *Cancer cell* **14**, 458-470

31. Hillas, P. J., del Alba, F. S., Oyarzabal, J., Wilks, A., and Ortiz De Montellano, P. R. (2000) The AhpC and AhpD antioxidant defense system of Mycobacterium tuberculosis. *The Journal of biological chemistry* **275**, 18801-18809

32. Bryk, R., Lima, C. D., Erdjument-Bromage, H., Tempst, P., and Nathan, C. (2002) Metabolic enzymes of mycobacteria linked to antioxidant defense by a thioredoxin-like protein. *Science* **295**, 1073-1077

33. Essler, S., Dehne, N., and Brune, B. (2009) Role of sestrin2 in peroxide signaling in macrophages. *FEBS letters* **583**, 3531-3535

34. Woo, H. A., Bae, S. H., Park, S., and Rhee, S. G. (2009) Sestrin 2 is not a reductase for cysteine sulfinic acid of peroxiredoxins. *Antioxidants & redox signaling* **11**, 739-745

35. Thamsen, M., Kumsta, C., Li, F., and Jakob, U. (2011) Is overoxidation of peroxiredoxin physiologically significant? *Antioxidants & redox signaling* **14**, 725-730

36. Zhang, J. (2015) Teaching the basics of autophagy and mitophagy to redox biologists--mechanisms and experimental approaches. *Redox biology* **4**, 242-259

37. Maiuri, M. C., Malik, S. A., Morselli, E., Kepp, O., Criollo, A., Mouchel, P. L., Carnuccio, R., and Kroemer, G. (2009) Stimulation of autophagy by the p53 target gene Sestrin2. *Cell Cycle* **8**, 1571-1576

38. Ishihara, M., Urushido, M., Hamada, K., Matsumoto, T., Shimamura, Y., Ogata, K., Inoue, K., Taniguchi, Y., Horino, T., Fujieda, M., Fujimoto, S., and Terada, Y. (2013) Sestrin-2 and BNIP3 regulate autophagy and mitophagy in renal tubular cells in acute kidney injury. *American journal of physiology. Renal physiology* **305**, F495-509

39. Chen, Y. S., Chen, S. D., Wu, C. L., Huang, S. S., and Yang, D. I. (2014) Induction of sestrin2 as an endogenous protective mechanism against amyloid beta-peptide neurotoxicity in primary cortical culture. *Experimental neurology* **253**, 63-71

40. Hou, Y. S., Guan, J. J., Xu, H. D., Wu, F., Sheng, R., and Qin, Z. H. (2015) Sestrin2 Protects Dopaminergic Cells against Rotenone Toxicity through AMPK-Dependent Autophagy Activation. *Molecular and cellular biology* **35**, 2740-2751

41. Ro, S. H., Nam, M., Jang, I., Park, H. W., Park, H., Semple, I. A., Kim, M., Kim, J. S., Park, H., Einat, P., Damari, G., Golikov, M., Feinstein, E., and Lee, J. H. (2014) Sestrin2 inhibits uncoupling protein 1 expression through suppressing reactive oxygen species. *Proceedings of the National Academy of Sciences of the United States of America* **111**, 7849-7854

42. Papadia, S., Soriano, F. X., Leveille, F., Martel, M. A., Dakin, K. A., Hansen, H. H., Kaindl, A., Sifringer, M., Fowler, J., Stefovska, V., McKenzie, G., Craigon, M., Corriveau, R., Ghazal, P., Horsburgh, K., Yankner, B. A., Wyllie, D. J., Ikonomidou, C., and Hardingham, G. E. (2008) Synaptic NMDA receptor activity boosts intrinsic antioxidant defenses. *Nature neuroscience* **11**, 476-487

43. Yang, Y., Cuevas, S., Yang, S., Villar, V. A., Escano, C., Asico, L., Yu, P., Jiang, X., Weinman, E. J., Armando, I., and Jose, P. A. (2014) Sestrin2 decreases renal oxidative stress, lowers blood pressure, and mediates dopamine D2 receptor-induced inhibition of reactive oxygen species production. *Hypertension* **64**, 825-832

44. Suzuki, T., Motohashi, H., and Yamamoto, M. (2013) Toward clinical application of the Keap1-Nrf2 pathway. *Trends in pharmacological sciences* **34**, 340-346

45. Komatsu, M., Kurokawa, H., Waguri, S., Taguchi, K., Kobayashi, A., Ichimura, Y., Sou, Y. S., Ueno, I., Sakamoto, A., Tong, K. I., Kim, M., Nishito, Y., Iemura, S., Natsume, T., Ueno, T., Kominami, E., Motohashi, H., Tanaka, K., and Yamamoto, M. (2010) The selective autophagy substrate p62 activates the stress responsive transcription factor Nrf2 through inactivation of Keap1. *Nat Cell Biol* **12**, 213-223

46. Lau, A., Wang, X. J., Zhao, F., Villeneuve, N. F., Wu, T., Jiang, T., Sun, Z., White, E., and Zhang, D. D. (2010) A noncanonical mechanism of Nrf2 activation by autophagy deficiency: direct interaction between Keap1 and p62. *Molecular and cellular biology* **30**, 3275-3285

47. Ro, S. H., Semple, I. A., Park, H., Park, H., Park, H. W., Kim, M., Kim, J. S., and Lee, J. H. (2014) Sestrin2 promotes Unc-51-like kinase 1 mediated phosphorylation of p62/sequestosome-1. *The FEBS journal* **281**, 3816-3827

48. Ichimura, Y., Waguri, S., Sou, Y. S., Kageyama, S., Hasegawa, J., Ishimura, R., Saito, T., Yang, Y., Kouno, T., Fukutomi, T., Hoshii, T., Hirao, A., Takagi, K., Mizushima, T., Motohashi, H., Lee, M. S., Yoshimori, T., Tanaka, K., Yamamoto, M., and Komatsu, M. (2013) Phosphorylation of p62 activates the Keap1-Nrf2 pathway during selective autophagy. *Mol Cell* **51**, 618-631

49. Buitrago-Molina, L. E., Marhenke, S., Longerich, T., Sharma, A. D., Boukouris, A. E., Geffers, R., Guigas, B., Manns, M. P., and Vogel, A. (2013) The degree of liver injury determines the role of p21 in liver regeneration and hepatocarcinogenesis in mice. *Hepatology* **58**, 1143-1152

50. Jain, A., Lamark, T., Sjottem, E., Larsen, K. B., Awuh, J. A., Overvatn, A., McMahon, M., Hayes, J. D., and Johansen, T. (2010) p62/SQSTM1 is a target gene for transcription factor NRF2 and creates a positive feedback loop by inducing antioxidant response element-driven gene transcription. *The Journal of biological chemistry* **285**, 22576-22591

51. Shin, B. Y., Jin, S. H., Cho, I. J., and Ki, S. H. (2012) Nrf2-ARE pathway regulates induction of Sestrin-2 expression. *Free radical biology & medicine* **53**, 834-841

52. Reed, T. T. (2011) Lipid peroxidation and neurodegenerative disease. *Free radical biology & medicine* **51**, 1302-1319

53. Davi, G., Falco, A., and Patrono, C. (2005) Lipid peroxidation in diabetes mellitus. *Antioxidants & redox signaling* **7**, 256-268

54. Zhang, P. Y., Xu, X., and Li, X. C. (2014) Cardiovascular diseases: oxidative damage and antioxidant protection. *European review for medical and pharmacological sciences* **18**, 3091-3096

55. Feng, Z., Zhang, H., Levine, A. J., and Jin, S. (2005) The coordinate regulation of the p53 and mTOR pathways in cells. *Proceedings of the National Academy of Sciences of the United States of America* **102**, 8204-8209

56. Ben-Sahra, I., Dirat, B., Laurent, K., Puissant, A., Auberger, P., Budanov, A., Tanti, J. F., and Bost, F. (2013) Sestrin2 integrates Akt and mTOR signaling to protect cells against energetic stress-induced death. *Cell Death Differ* **20**, 611-619

57. Hong-Brown, L. Q., Brown, C. R., Navaratnarajah, M., and Lang, C. H. (2015) Adamts1 mediates ethanol-induced alterations in collagen and elastin via a FoxO1-sestrin3-AMPK signaling cascade in myocytes. *Journal of cellular biochemistry* **116**, 91-101

58. Eid, A. A., Lee, D. Y., Roman, L. J., Khazim, K., and Gorin, Y. (2013) Sestrin 2 and AMPK connect hyperglycemia to Nox4-dependent endothelial nitric oxide synthase uncoupling and matrix protein expression. *Molecular and cellular biology* **33**, 3439-3460

59. Kim, M., and Lee, J. H. (2015) Identification of an AMPK phosphorylation site in Drosophila TSC2 (gigas) that regulate cell growth. *International journal of molecular sciences* **16**, 7015-7026

60. Gwinn, D. M., Shackelford, D. B., Egan, D. F., Mihaylova, M. M., Mery, A., Vasquez, D. S., Turk, B. E., and Shaw, R. J. (2008) AMPK phosphorylation of raptor mediates a metabolic checkpoint. *Mol Cell* **30**, 214-226

61. Sanli, T., Linher-Melville, K., Tsakiridis, T., and Singh, G. (2012) Sestrin2 modulates AMPK subunit expression and its response to ionizing radiation in breast cancer cells. *PloS one* **7**, e32035

62. Dokudovskaya, S., and Rout, M. P. (2015) SEA you later alli-GATOR--a dynamic regulator of the TORC1 stress response pathway. *Journal of cell science* **128**, 2219-2228

63. Bar-Peled, L., Chantranupong, L., Cherniack, A. D., Chen, W. W., Ottina, K. A., Grabiner, B. C., Spear, E. D., Carter, S. L., Meyerson, M., and Sabatini, D. M. (2013) A Tumor suppressor complex with GAP activity for the Rag GTPases that signal amino acid sufficiency to mTORC1. *Science* **340**, 1100-1106

64. Chen, X., Ma, J. J., Tan, M., Yao, P., Hu, Q. H., Eriani, G., and Wang, E. D. (2011) Modular pathways for editing non-cognate amino acids by human cytoplasmic leucyl-tRNA synthetase. *Nucleic acids research* **39**, 235-247

65. Bruning, A., Rahmeh, M., and Friese, K. (2013) Nelfinavir and bortezomib inhibit mTOR activity via ATF4-mediated sestrin-2 regulation. *Mol Oncol* **7**, 1012-1018

66. Eagle, H., Piez, K. A., and Levy, M. (1961) The intracellular amino acid concentrations required for protein synthesis in cultured human cells. *The Journal of biological chemistry* **236**, 2039-2042

67. Baydoun, A. R., Emery, P. W., Pearson, J. D., and Mann, G. E. (1990) Substrate-dependent regulation of intracellular amino acid concentrations in cultured bovine aortic endothelial cells. *Biochemical and biophysical research communications* **173**, 940-948

68. Gallinetti, J., Harputlugil, E., and Mitchell, J. R. (2013) Amino acid sensing in dietary-restriction-mediated longevity: roles of signal-transducing kinases GCN2 and TOR. *The Biochemical journal* **449**, 1-10

69. Kimball, S. R., Gordon, B. S., Moyer, J. E., Dennis, M. D., and Jefferson, L. S. (2016) Leucine induced dephosphorylation of Sestrin2 promotes mTORC1 activation. *Cellular signalling* **28**, 896-906

70. Linares, J. F., Duran, A., Reina-Campos, M., Aza-Blanc, P., Campos, A., Moscat, J., and Diaz-Meco, M. T. (2015) Amino Acid Activation of mTORC1 by a PB1-Domain-Driven Kinase Complex Cascade. *Cell reports* **12**, 1339-1352

71. Moscat, J., and Diaz-Meco, M. T. (2011) Feedback on fat: p62-mTORC1-autophagy connections. *Cell* **147**, 724-727

72. Duran, A., Amanchy, R., Linares, J. F., Joshi, J., Abu-Baker, S., Porollo, A., Hansen, M., Moscat, J., and Diaz-Meco, M. T. (2011) p62 is a key regulator of nutrient sensing in the mTORC1 pathway. *Mol Cell* **44**, 134-146

73. Dann, S. G., Selvaraj, A., and Thomas, G. (2007) mTOR Complex1-S6K1 signaling: at the crossroads of obesity, diabetes and cancer. *Trends Mol Med* **13**, 252-259

74. Huang, J., Dibble, C. C., Matsuzaki, M., and Manning, B. D. (2008) The TSC1-TSC2 complex is required for proper activation of mTOR complex 2. *Molecular and cellular biology* **28**, 4104-4115

CHAPTER II[2]

The GATOR2-mTORC2 Axis Mediates Sestrin2-induced AKT Ser/Thr Kinase Activation

Abstract

Sestrins represent a family of stress-inducible proteins that prevent the progression of many age- and obesity-associated disorders. Endogenous Sestrins maintain insulin-dependent AKT Ser/Thr kinase (AKT) activation during high-fat diet (HFD)-induced obesity, and overexpressed Sestrins activate AKT in various cell types, including liver and skeletal muscle cells. Although Sestrin-mediated AKT activation improves metabolic parameters, the mechanistic details underlying such improvement remain elusive. Here, we investigated how Sestrin2, the Sestrin homolog highly expressed in liver, induces strong AKT activation. We found that two known targets of Sestrin2, mTOR complex 1 (mTORC1) and AMP-activated protein kinase (AMPK), are not required for Sestrin2-induced AKT activation. Rather, phosphoinositol-3-kinase (PI3K) and mTORC2, kinases upstream of AKT, were essential for Sestrin2-induced AKT activation. Among these kinases, mTORC2 catalytic activity was strongly upregulated upon Sestrin2 overexpression in an *in vitro* kinase assay, indicating that mTORC2 may represent the major link between Sestrin2 and AKT. As reported previously, Sestrin2 interacted with mTORC2; however, we found here that this interaction occurs indirectly through GATOR2, a pentameric protein complex that directly interacts with Sestrin2. Deleting or silencing WD repeat domain 24 (WDR24), the GATOR2

[2] This chapter represents a published manuscript: Kowalsky AH*, Namkoong S*, Mettetal E, Park HW, Kazyken D, Fingar DC, Lee JH. The GATOR2-mTORC2 axis mediates Sestrin2-induced AKT Ser/Thr kinase activation. *Journal of Biological Chemistry* (2020)

component essential for the Sestrin2–GATOR2 interaction, or WDR59, the GATOR2 component essential for the GATOR2–mTORC2 interaction, completely ablated Sestrin2-induced AKT activation. We also noted that Sestrin2 directly binds to the pleckstrin homology (PH) domain of AKT and induces AKT translocation to the plasma membrane. These results uncover a signaling mechanism whereby Sestrin2 activates AKT through GATOR2 and mTORC2.

Introduction

Sestrins are highly conserved, stress-induced proteins with anti-aging properties in model organisms such as worms and flies (1,2). In the mammalian genome, three Sestrin paralogs (Sestrin1-3) exist (3). Sestrin proteins have two important functions: reducing reactive oxygen species (ROS) (4,5) and inhibiting mammalian target of rapamycin complex 1 (mTORC1) (1,6). Many studies have also shown that Sestrin2 is important for metabolic homeostasis, especially during nutritional overload. For example, Sestrin2 was required to maintain insulin sensitivity in the liver upon high fat diet (HFD)-induced dietary obesity and *Lep*^{ob} mutation-induced genetic obesity (7). Under lipotoxic conditions, Sestrin2 was selectively upregulated in the liver to alleviate endoplasmic reticulum (ER) stress by inhibiting mTORC1, thereby attenuating the development of steatohepatitis (8). Likewise, Sestrin3, another Sestrin paralog, is also expressed in the liver and upregulates the insulin-AKT signaling pathway during HFD and obesity (9). These metabolic studies revealed that, in addition to oxidative stress reduction and mTORC1 downregulation, Sestrins also upregulate AKT signaling (7,9). Sestrin-induced AKT activation was also observed in Drosophila (7).

The molecular structure of Sestrin2 revealed a structural basis for Sestrin2's formerly characterized biochemical functions (5,10). A helix-turn-helix motif, composed of a proton relay

system and reactive Cys125, mediates the oxidoreductase function of Sestrin2 in reducing alkylhydroperoxides (5). The DD motif, composed of two adjacent Asp406 and Asp407 residues in a loop, was important for the interaction between Sestrin2 and GATOR2, a pentameric protein complex regulating mTORC1 signaling (5,10). Mutation in either of these two Asp residues nullifies Sestrin2's ability to downregulate mTORC1 (5). Through the DD motif, Sestrin2 directly interacts with GATOR2 and releases it from inhibiting GATOR1, a trimeric protein complex with GTPase activity on the mTORC1-activating Rag proteins (5,11-13). Therefore, Sestrin2 inhibits mTORC1 by inhibiting GATOR2 and allowing GATOR1 to inhibit the Rag proteins (11-13). Although the detailed mechanism is yet to be elucidated, the Sestrin2-GATOR2 interaction was also critical for AMPK activation (5), which is also critical for Sestrin2-mediated mTORC1 downregulation in many different cell types and physiological contexts (1,6,14-18). Therefore, it is possible that GATOR2 has functions outside of mTORC1 regulation, mediating Sestrin2 output to other effector molecules and target pathways. GATOR2 consists of five proteins: WDR24, WDR59, MIOS, SEH1L, and SEC13 (19). Among these components, WDR24 and SEH1L are critical for physically interacting with Sestrin2 (12).

AKT is a major regulatory protein downstream of the insulin receptor that is responsible for many glucose and lipid regulating functions (20). Upon insulin stimulation, AKT is activated and phosphorylates a wide range of protein substrates to inhibit gluconeogenesis and upregulate glycogenesis and lipogenesis. In addition to its metabolic regulation, AKT also promotes cell growth and proliferation and is implicated in many cancers. AKT has two active phosphorylation sites, Thr308 and Ser473, which are phosphorylated by phosphoinositide-dependent kinase 1 (PDK1) and mTORC2, respectively. Upon activation of the insulin signaling cascade leading to phosphoinositol-3-kinase (PI3K) activation, a second messenger phosphatidylinositol 3, 4, 5-

triphosphate (PI(3,4,5)P) accumulates in the plasma membrane, which recruits PDK1, mTORC2 and AKT and induces PDK1 and mTORC2 to phosphorylate and activate AKT (20).

Sestrin-induced AKT activation was observed in a variety of cellular and physiological contexts, in addition to the insulin resistance and obesity contexts (7,9). For instance, Sestrins have been shown to positively regulate AKT in cancer cells to protect against environmental stress, such as UV irradiation, energetic stress and chemical stress (21-25). Sestrins are also important for muscle AKT activation, and the Sestrin-dependent AKT regulation is critical for producing exercise benefits and preventing age- and disuse-associated atrophy (26,27). There have been several mechanisms proposed to explain Sestrin-induced AKT activation. The first is that Sestrin-induced mTORC1 inhibition releases the insulin receptor signaling pathway from mTORC1/S6K-mediated negative feedback inhibition (28). In this model, chronic mTORC1 activation induces S6K-dependent insulin receptor substrate (IRS) serine phosphorylation, which attenuates signal transduction from the insulin receptor to PI3K (29). Therefore, Sestrin-mediated mTORC1 inhibition can indirectly upregulate PI3K-AKT signaling (28). Consistent with this model, loss of Sestrin2 upregulated S6K-mediated inhibitory serine phosphorylation of IRS while downregulating insulin receptor-mediated activatory tyrosine phosphorylation (7). In addition to the S6K-mediated feedback, Sestrin may also downregulate additional pathways that lead to insulin resistance, such as ER stress (8) and inflammation pathways (30). Furthermore, several recent studies also suggested that Sestrin-dependent AKT activation could be independent of mTORC1 and directly through mTORC2 (9,23). Still, the mechanistic details of how Sestrin2 regulates AKT remain incompletely understood.

In this study, we investigated the molecular mechanism by which Sestrin2 induces AKT activation in liver cells. We found that GATOR2 and mTORC2 link Sestrin2 to AKT activation.

This new mechanism explains, at least in part, how Sestrin2 promotes metabolic homeostasis through increased AKT activity.

Results

Sestrin2 overexpression improves glucose and lipid regulation in HFD mice

Extensive studies have established that endogenous Sestrins protect against obesity-associated fatty liver and insulin resistance (7-9,28). Based on these findings, we tested if Sestrin2 overexpression could improve metabolic regulation in obese WT mice under HFD conditions. For this, adenoviruses expressing GFP (Ad-GFP) or Sestrin2 (Ad-SESN2) were administered to weight and age-matched mice through tail vein injections. Strikingly, after adenoviral expression of Sestrin2, both basal and insulin-reduced blood glucose levels were strongly decreased (Figure 2.1A), and HFD-induced lipid accumulation in the liver tissue was also strongly decreased (Figure 2.1B). Nevertheless, Ad-SESN2 transduction did not substantially change overall body weight (Figure 2.1C). Consistent with reduction in blood glucose (Figure 2.1A) and liver fat levels (Figure 2.1B), mRNA expression of gluconeogenic and lipogenic genes were strongly decreased by Sestrin2 overexpression (Figure 2.1D). Therefore, the evidence suggests that Sestrin2 overexpression in liver was sufficient to alter hepatic transcription of metabolic genes and subsequently restore glucose and lipid homeostasis in obese, insulin-resistant mice.

Sestrin2 overexpression induces strong AKT activation in mouse liver and HepG2 cells

Upon examining liver lysates obtained from HFD-fed mice, we found that overexpression of Sestrin2 increased AKT phosphorylation on both the PDK1-mediated activation loop site (T308) and the mTORC2-mediated hydrophobic motif site (S473) relative to control livers, indicating

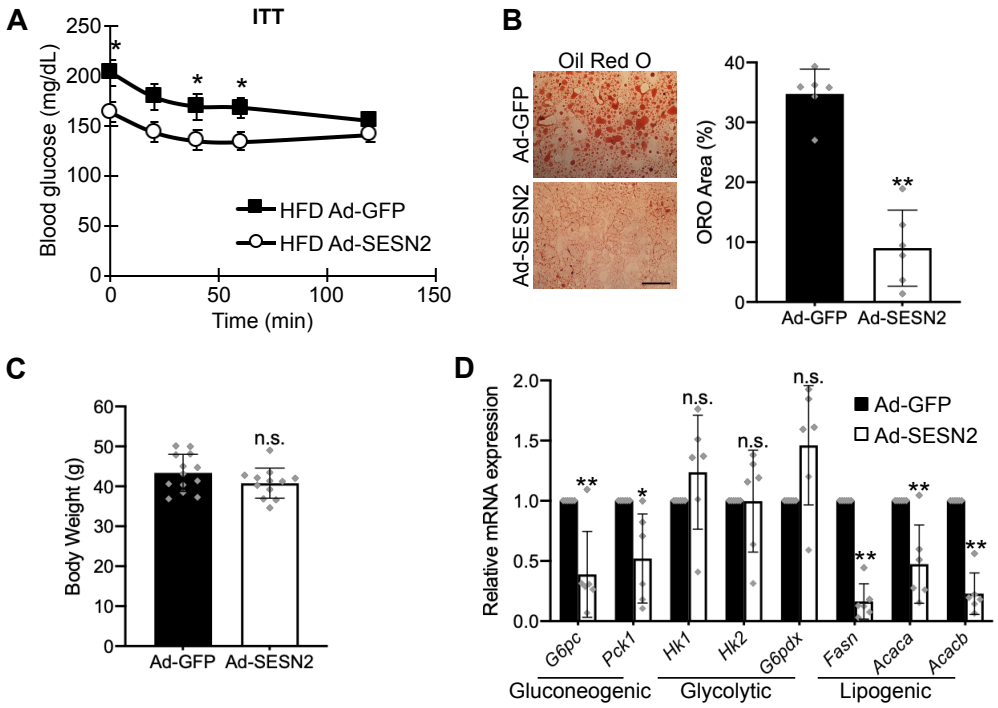

Figure 2.1. Sestrin2 overexpression improves glucose and lipid homeostasis in HFD mice. Two-month-old C57BL/6J mice were fed a high fat diet (HFD) for at least two additional months. Mice were then administered tail vein injections of adenoviruses (10^9 pfu) that express GFP (Ad-GFP; n=13) or Sestrin2 (Ad-SESN2; n=12). **(A)** Four to ten days after adenovirus administration, mice were fasted for six hours then subjected to insulin tolerance tests (ITT, 0.65U/kg). **(B)** Fresh frozen liver sections were stained with Oil Red O (ORO) and quantified (n=6) to determine fat accumulation in liver tissue. Scale bar, 200 μm **(C)** Body weights of animals at ten days after adenovirus administration. **(D)** Liver lysates were analyzed by quantitative RT-PCR to examine expression of metabolism-regulating genes in the liver tissue (n=6). Data are presented as mean ± SEM. P-values were calculated between Ad-GFP and Ad-SESN2 groups from a two-tailed student's t-test: *p<0.05, **p<0.01.

strong AKT activation. In fact, Sestrin2 increased phosphorylation on these sites to a level higher than that mediated by acute insulin treatment of control mice (Figure 2.2A). Moreover, Sestrin2 overexpression increased basal liver AKT phosphorylation strongly in HFD-fed mice (Figure 2.2A) and consistently increased AKT phosphorylation in HepG2 cells (Figure 2.2B). However, unlike in the liver where the effect of Sestrin2 on AKT phosphorylation was stronger than insulin (Figure 2.2A), the effects of Sestrin2 and insulin on AKT phosphorylation were additive in HepG2 cells (Figure 2.2B). Sestrin2 overexpression also rescued AKT phosphorylation in the presence of inhibitory palmitic acid (PA) treatment, a saturated fatty acid that produces strong cellular insulin resistance (31) (Figure 2.2B, 2.2C). Conversely, silencing Sestrin2 in HepG2 cells decreased AKT phosphorylation in both normal and PA-treated conditions (Figure 2.2C).

Sestrin2 overexpression upregulates AKT independently of mTORC1 and AMPK

Because Sestrin2 inhibits mTORC1 and thus suppresses mTORC1/S6K1-meditated negative feedback on insulin signaling and PI3K flux, it was possible that Sestrin2 activates AKT indirectly through this negative feedback mechanism (29) (Figure 2.2D). To test whether mTORC1 inhibition mediates Sestrin2-induced AKT activation, we transduced HepG2 cells with increasing dosages of Sestrin2 and co-treated the cells with rapamycin, an mTORC1-specific inhibitor. As expected, Sestrin2 dose-dependently activated AKT in HepG2 cells (Figure 2.2E). Interestingly, Sestrin2-induced AKT activation was still observed in rapamycin-treated cells, in which mTORC1-dependent S6K1 phosphorylation was completely blocked (Figure 2.2E), indicating that Sestrin2 activates AKT independently of the mTORC1/S6K1-mediated negative

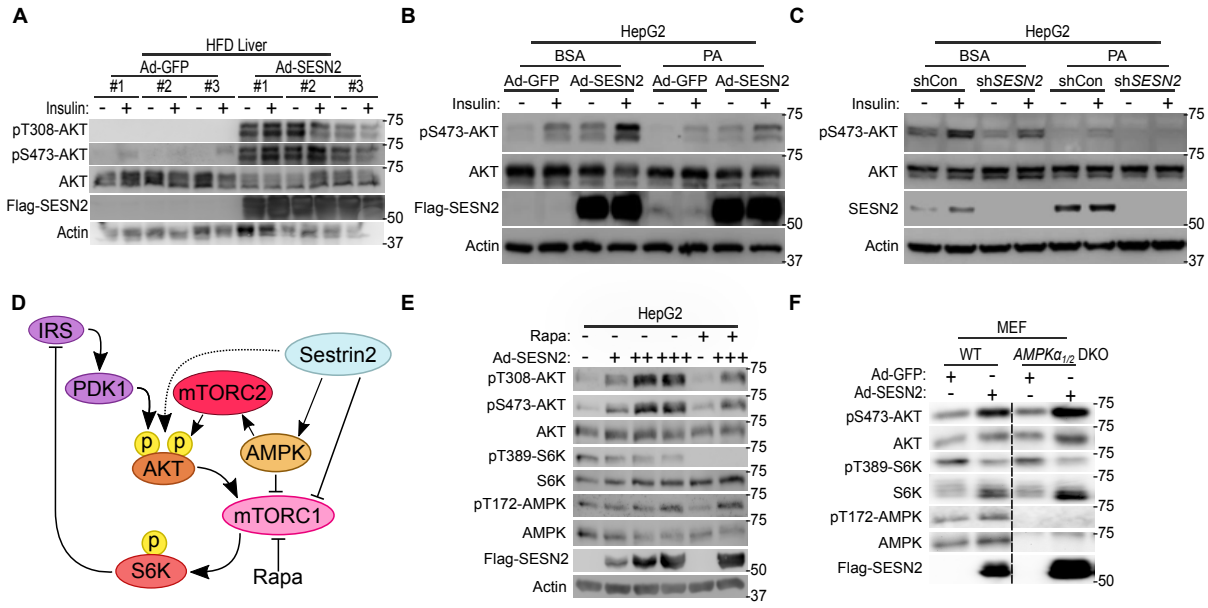

Figure 2.2. Sestrin2 activates AKT independently of mTORC1 and AMPK. (A) At 10 days after Ad-GFP or Ad-SESN2 administration, mouse livers were collected before (-) and 10 min after (+) an injection of insulin (0.8U/kg). Liver lysates were analyzed by immunoblotting. **(B-C)** HepG2 cells were treated with bovine serum albumin (BSA) loaded with palmitic acid (PA, 500μM) for 9 hours, then treated with insulin (+, 50 nmol) for 20 min. BSA-only and water-only (-) samples were used as controls. **(B)** HepG2 cells were acutely infected with control or Sestrin2-overexpressing adenoviruses before BSA and PA treatments. **(C)** HepG2 cells were stably infected with control (shRNA-Luciferase) and shRNA-SESN2 lentiviruses before BSA and PA treatments. All samples were analyzed by immunoblotting. **(D)** Schematic of potential molecular mechanisms that can account for Sestrin2-induced AKT activation. **(E)** HepG2 cells were infected with Ad-GFP or Ad-SESN2 for 12 hours, serum starved with or without rapamycin (Rapa, 10nM) for 24 hours, and subjected to immunoblotting. **(F)** WT and *Ampkα1*$^{-/-}$/*Ampkα2*$^{-/-}$ mouse embryonic fibroblasts (MEFs) were serum starved in DMEM with 0.1% FBS and treated with Ad-GFP or Ad-SESN2 overnight, then analyzed by immunoblotting.

feedback loop (Figure 2.2D). More recently, it was reported that AMPK promotes mTORC2 signaling in response to acute energetic stress through phosphorylation of mTOR and mTORC2 partner proteins (32). As Sestrin2 activates AMPK, it was possible that Sestrin2 increases mTORC2-mediated AKT phosphorylation and activation through AMPK (Figure 2.2D). To determine if Sestrin2-induced AKT activation was occurring through AMPK, we treated wild-type and *AMPK*-null mouse embryonic fibroblasts (WT and $Ampk\alpha_1^{-/-}/Ampk\alpha_2^{-/-}$ DKO MEFs) with Ad-SESN2. As observed in HepG2 cells, Sestrin2 still activated AKT in both WT and $AMPK\alpha_{1/2}$ DKO MEFs, indicating that this regulation was independent of AMPK (Figure 2.2F). These results reveal a novel mechanism by which Sestrin2 induces AKT activation independently of mTORC1 and AMPK, two established effectors of Sestrin2.

PI3K and mTORC2 are required for Sestrin2-induced AKT activation

To further investigate the mechanism by which Sestrin2 activates AKT, we treated HepG2 cells with a panel of chemical inhibitors specific for signaling components that regulate AKT (Figure 2.3A). BYL719, a PI3K-specific inhibitor, and Torin1, an active site mTOR inhibitor (inhibits both mTORC1 and mTORC2), completely ablated Sestrin2-induced AKT activation (Figure 2.3B), indicating that both PI3K and mTOR, specifically mTORC2, are required for Sestrin2-induced AKT activation. Consistent with this, LY294002, an inhibitor of both PI3K and mTOR, and PP242, another active site mTOR inhibitor, also blocked Sestrin2-induced AKT activation (Figure 2.3C). Therefore, these data suggest that both PI3K and mTORC2 activities are required for Sestrin2-induced AKT activation.

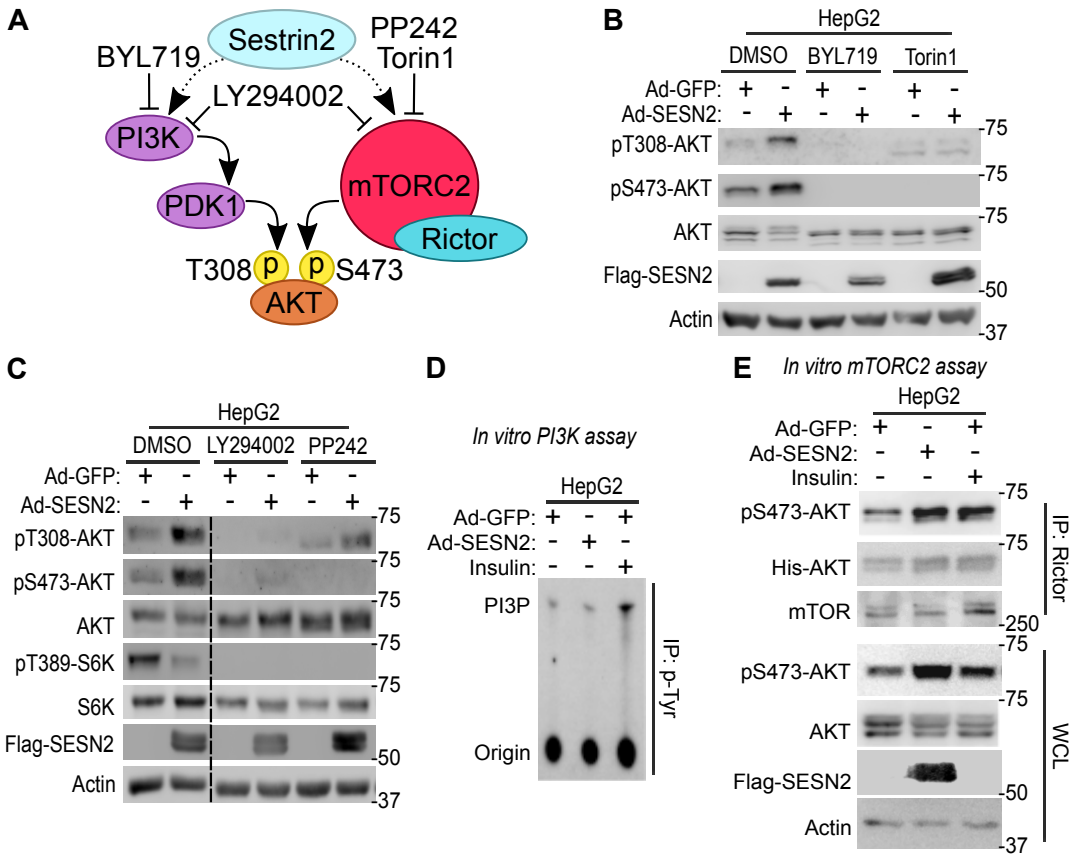

Figure 2.3. Sestrin2 upregulates mTORC2. (A) Schematic of AKT-regulating pathways and drugs targeting the pathway. **(B-C)** HepG2 cells were treated with Ad-GFP or Ad-SESN2, serum starved and treated with DMSO (Con), BYL719 (10nM), Torin1 (200nM), LY294002 (20μM), or PP242 (5μM), then analyzed by immunoblotting. **(D-E)** HepG2 cells infected with Ad-GFP or Ad-SESN2 were stimulated with or without insulin (100nM). **(D)** Lysates were subjected to phosphotyrosine (p-Tyr) immunoprecipitation, and subjected to a lipid kinase assay with γ-^{32}P-ATP and phosphotidylinositol, then subjected to thin layer chromatography and autoradiography to visualize radiolabeled PI3P. **(E)** Lysates were subjected to anti-Rictor immunoprecipitation, and subjected to an in vitro kinase assay using ATP and recombinant full-length inactive His-AKT. The reaction mixtures, as well as original whole cell lysates (WCL) were subjected to subsequent immunoblot analyses for examining protein amount and phosphorylation.

Sestrin2 upregulates the catalytic activity of mTORC2 but not PI3K

Because both PI3K and mTORC2 were required for Sestrin2-induced AKT activation, we assessed the effect of Sestrin2 on these signaling components through in vitro kinase assays. Although the established PI3K activator insulin was able to prominently increase the lipid kinase activity of PI3K, Sestrin2 did not have a measurable effect on PI3K activity in basal serum-starved conditions (Figure 2.3D). In contrast, both insulin and Sestrin2 had a strong positive effect on the catalytic activity of mTORC2 in phosphorylating AKT (Figure 2.3E). Sestrin2-induced mTORC2 activation can lead to AKT S473 phosphorylation, which can subsequently facilitate PDK1-mediated AKT T308 phosphorylation (33). Therefore, our data suggest that Sestrin2 acts through mTORC2 to activate AKT.

The GATOR2-binding function of Sestrin2 is required for AKT activation

We next investigated the biochemical basis of how Sestrin2 upregulates mTORC2 and AKT. To address this problem, we utilized point mutants of Sestrin2 that specifically eliminate either its redox-regulating or GATOR2-binding functions (34). Like wild-type Sestrin2, Cys125-mutated Sestrin2 with no oxidoreductase activity (5) strongly upregulated mTORC2-dependent AKT phosphorylation as well as AKT-dependent phosphorylation of its substrates FOXO1 and SIN1 (Figure 2.4A). In contrast, Asp406- and Asp407-mutated Sestrin2, which cannot bind to the GATOR2 complex (5), was unable to upregulate the AKT signaling pathway (Figure 2.4A). These results suggest that the GATOR2-binding motif of Sestrin2, but not the redox-regulating motif, is critical for activating AKT.

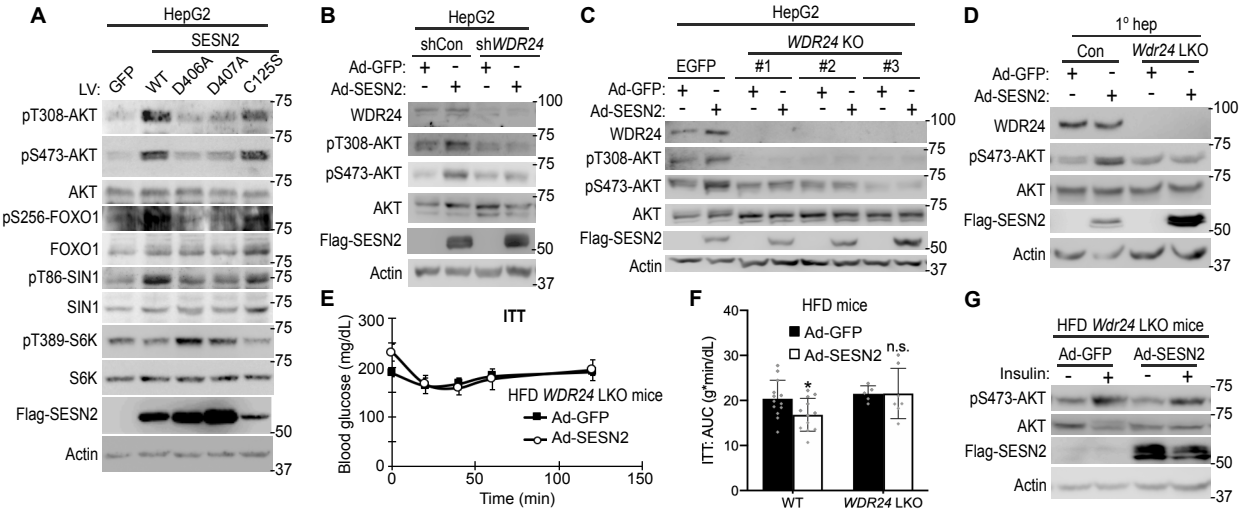

Figure 2.4. Sestrin2 requires GATOR2 to activate AKT. (A) HepG2 cells were infected with lentiviruses (LV) that express control (GFP), wild-type (WT), or single residue mutant forms of Sestrin2 (D406A, D407A, C125S), serum starved and subjected to immunoblotting. **(B)** HepG2 cells expressing control (pLKO-Con) or WDR24 (pLKO-WDR24) shRNA were treated with Ad-GFP or Ad-SESN2, serum starved, then subjected to immunoblotting. **(C)** HepG2 cells were subjected to control (EGFP) or *WDR24* gene knockout targeting using CRISPR/Cas9. Cells with confirmed knockouts were then treated with Ad-GFP or Ad-SESN2, serum starved, then subjected to immunoblotting. **(D)** Primary hepatocytes were isolated from Con (*Wdr24*$^{f/f}$) or liver-specific *Wdr24*-knockout (*Wdr24* LKO; *Wdr24*$^{f/f}$*/Alb-Cre*) livers, treated with Ad-GFP or Ad-SESN2, serum starved for 3 hours, then subjected to immunoblotting. **(E-G)** Two-month-old *Wdr24* LKO mice were fed a HFD for two additional months, administered tail vein injections of Ad-GFP (n=5) or Ad-SESN2 (n=7). (E) *Wdr24* LKO mice were subjected to an ITT 7 days after adenovirus administration. **(F)** Area under curve (AUC) was calculated for the ITT. WT data are from Figure 1A. **(G)** Livers were collected before (-) or 5 min after (+) an injection of insulin (0.8U/kg), and their lysates were analyzed by immunoblotting. Data are presented as mean ± SEM. P-values were calculated between control (Ad-GFP) and Sestrin2 overexpressing (Ad-SESN2) groups from a two-tailed student's t-test: not significant (n.s.), *p<0.05.

GATOR2 is required for Sestrin2-induced AKT activation

WDR24 is a GATOR2 component that is essential for the Sestrin2-GATOR2 interaction (12). To directly assess the requirement of GATOR2 in Sestrin2-induced AKT activation, we ablated WDR24 function through both gene silencing and knockout methods. In HepG2 cells, shRNA-mediated *WDR24* silencing (Figure 2.4B) and CRISPR/Cas9-mediated *WDR24* knockout (Figure 2.4C) eliminated Sestrin2-induced AKT activation. Likewise, hepatocytes isolated from liver-specific *Wdr24*-knockout (*Wdr24* LKO) mice failed to increase AKT activation after Sestrin2 overexpression (Figure 2.4D). Consistent with the requirement for WDR24 in Sestrin2-induced AKT activation, HFD-fed obese *Wdr24* LKO mice did not reduce blood glucose levels (Figure 2.4E, 2.4F) or increase hepatic AKT signaling (Figure 2.4G) in response to Ad-SESN2 transduction, unlike HFD-fed obese wild-type mice (Figure 2.1A, 2.2A, 2.4G). Notably, *Wdr24* LKO mice retained insulin-induced AKT upregulation (Figure 2.4G), indicating that WDR24 is not required for insulin signaling to AKT but is required for Sestrin2-induced AKT activation. Taken together, these data indicate that Sestrin2 requires GATOR2 to activate AKT and improve metabolic phenotypes in HFD mice.

GATOR2 physically bridges Sestrin2 and mTORC2

To identify Sestrin2 targets in HepG2 cells, we performed proteomic analysis of Sestrin2-interacting proteins in HepG2 cells. Consistent with previous studies of the Sestrin2 interactome analyzed from MCF10A cells (12,13) and HEK293T cells (11), the GATOR2 components appeared among the top Sestrin2 interacting proteins in HepG2 cells (Table 2.1). Based on the genetic requirement of GATOR2 in Sestrin2-induced AKT activation (Figure 2.4), and the physical association between Sestrin2 and GATOR2 in HepG2 cells (Table 2.1), we hypothesized

that GATOR2 may be the molecular conduit for Sestrin2-mediated upregulation of mTORC2 and subsequent AKT activation. Recent reports showed that Sestrin2 physically associates with mTORC2 (9,23), and consistent with this, we were able to replicate the interaction between Sestrin2 and Rictor, an mTORC2-specific protein (Figure 2.5A). Interestingly however, Sestrin2 mutants that cannot bind GATOR2 (e.g. Asp406Ala and Asp407Ala) lost the ability to bind Rictor (Figure 2.5A). In contrast, the Cys125-mutated Sestrin2 fully retained Rictor-binding, indicating that the redox-regulating function of Sestrin2 is not required for the Sestrin2-mTORC2 interaction.

These findings raised the possibility that GATOR2 bridges Sestrin2 and mTORC2. We therefore examined whether mTORC2 associates with GATOR2 through co-immunoprecipitation assays between Rictor and GATOR2 components. In addition to testing the interaction with the full complex, we systematically deleted subcomponents of GATOR2 or systematically expressed single components of GATOR2, to identify the GATOR2 subcomponent(s) that are responsible for the GATOR2-Rictor interaction. Interestingly, we found that GATOR2 and Rictor interact (Figure 2.5B, blue boxes), and moreover, the WDR59 subcomponent of GATOR2 was critical and sufficient for this interaction. When WDR59 was not expressed, the interaction between Rictor and GATOR2 was very weak (Figure 2.5B, red box in left panel), and WDR59 alone pulled down Rictor (Figure 2.5B, red box in right panel). Previous work showed that WDR24 is critical for the Sestrin2-GATOR2 interaction (12), and our current work identifies WDR59 as a critical component for the GATOR2-Rictor interaction (Figure 2.5C). These data suggest that Sestrin2 and Rictor interact through GATOR2, containing both WDR24 and WDR59. Indeed, like WDR24, WDR59 was also required for Sestrin2-induced AKT activation; Sestrin2 failed to upregulate AKT in *WDR59* knockout (KO) HepG2 cells generated through CRISPR targeting (Figure 2.5D). In addition, we confirmed the GATOR2-mTORC2 interaction through showing that Sin1, another

Table 2.1. Sestrin2-interacting proteins from HepG2 cells

Protein Name	Isolated Peptides	Unique Peptides	AA Coverage	Uniprot Accession #
SESN2	59	54	85.00%	P58004
TJAP1	14	14	31.80%	Q5JTD0-1
MIOS	13	13	21.11%	Q9NXC5-1
GMPPB	12	12	47.55%	Q9Y5P6-2
ASB1	6	6	25.07%	Q9Y576
SEH1L	6	6	20.43%	Q96EE3-1
WDR59	4	4	7.39%	Q6PJI9-1
RMDN1	4	4	12.10%	Q96DB5
AMMECR1	4	4	15.62%	Q9Y4X0
LGALS3	3	3	14.40%	P17931
WDR24	3	3	4.57%	Q96S15-1

The number of peptide hits for Sestrin2 and its ten strongest interacting partners, among which four are GATOR2 components (shaded in grey). The full mass-spectrometry proteomics data is available in the PRIDE archive (PXD015824) at: https://www.ebi.ac.uk/pride/archive/projects/PXD015824.

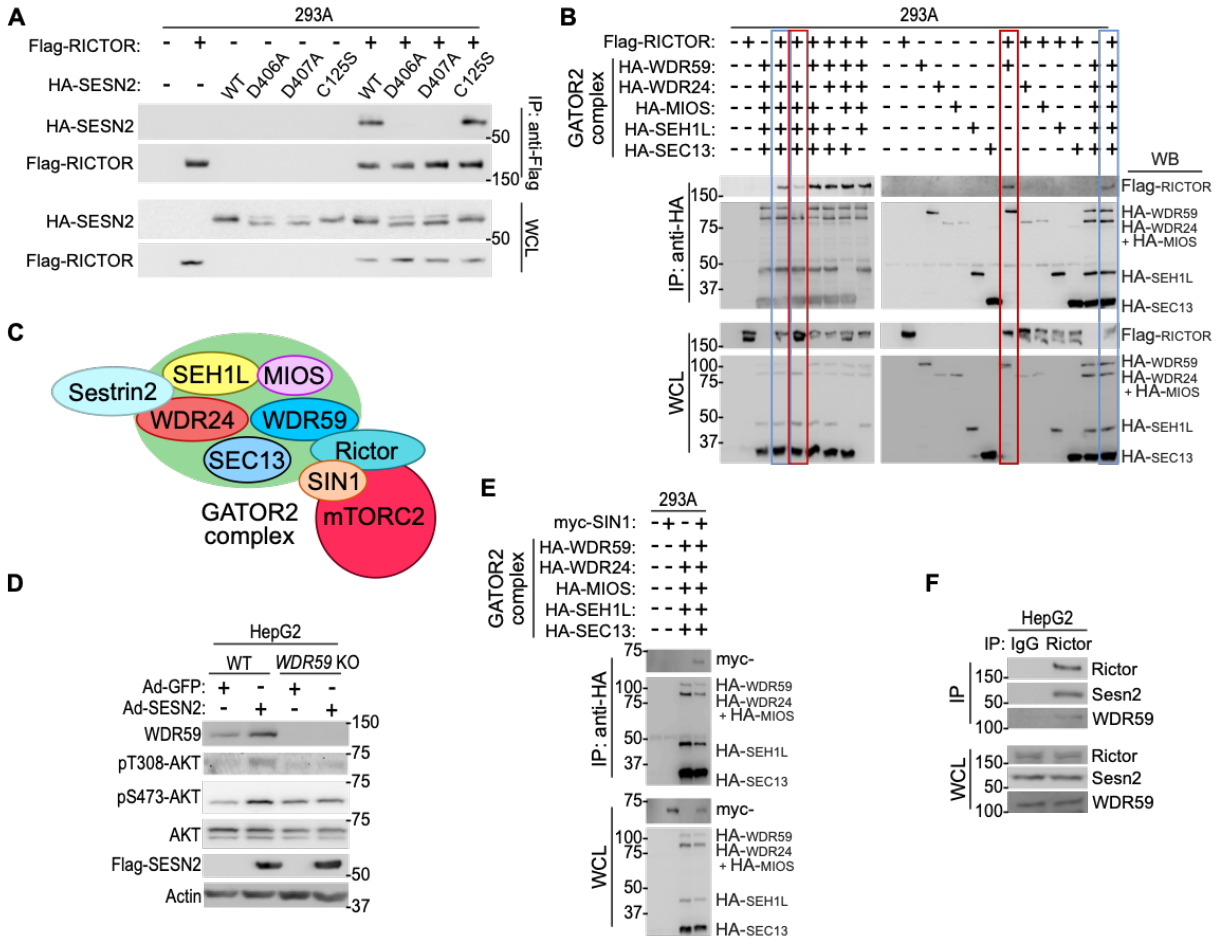

Figure 2.5. GATOR2 physically bridges Sestrin2 and mTORC2. (A-B) HEK293 cells were transfected with indicated constructs for 48 hours then subjected to co-immunoprecipitation (IP) with indicated antibodies. IP complexes and whole cell lysates (WCL) were examined through immunoblotting. **(C)** Schematic of how GATOR2 interacts with Sestrin2 and mTORC2. WDR24 was critical for the Sestrin2-GATOR2 interaction, while WDR59 was critical for the GATOR2-Rictor interaction. **(D)** HepG2 cells stably expressing control (WT) or *WDR59*-targeting CRISPR/Cas9 constructs were infected with Ad-GFP or Ad-SESN2, serum starved overnight, then subjected to immunoblotting. **(E)** HEK293 cells were transfected with indicated constructs for 48 hours then subjected to IP with indicated antibodies. IP complexes and WCL were examined through immunoblotting. **(F)** HepG2 cells were subjected to anti-IgG or anti-Rictor IP overnight. IP complexes and WCL were examined through immunoblotting of endogenous proteins.

critical mTORC2-specific subcomponent, also interacted with the full GATOR2 complex (Figure 2.5E). Finally, we also observed Rictor-Sestrin2 and Rictor-WDR59 interactions at the endogenous level in HepG2 cells (Figure 2.5F). These data collectively suggest that GATOR2 bridges Sestrin2 and mTORC2 to enable Sestrin2-mediated activation of mTORC2 and AKT (Figure 2.5C).

Sestrin2 directly binds to the PH domain of AKT

While examining the physical interaction between Sestrin2 and other proteins, we serendipitously found that overexpressed Flag-tagged Sestrin2 pulls down endogenous AKT in liver tissue (Figure 2.6A). The Sestrin2-interacting AKT proteins were phosphorylated at both Thr308 and Ser473 (Figure 2.6A), suggesting that these are active AKT proteins. The Sestrin2-AKT interaction was also observable in HEK293A cells (Figure 2.6B); interestingly, Sestrin2 mutants that cannot bind GATOR2 were still able to interact with AKT (Figure 2.6B). Therefore, it seems that the Sestrin2-AKT interaction is independent of the interactions we observed above for the Sestrin2-GATOR2-mTORC2 complexes.

To dissect the interaction between Sestrin2 and AKT further, we transfected Sestrin2 with three different forms of AKT: full-length, PH domain only (F-AKT_PH: residues 1-149), or kinase domain only (F-AKT_KD: residues 150-480) truncated forms (Figure 2.6C). Using an immunoprecipitation assay, we confirmed that Sestrin2 physically interacted with full-length AKT. Sestrin2 also slightly interacted with AKT_KD, but we found the strongest association with AKT_PH, the truncated form of AKT that includes the PH domain only (Figure 2.6C). Therefore, independently of GATOR2 and mTORC2, Sestrin2 binds the AKT PH domain, a domain

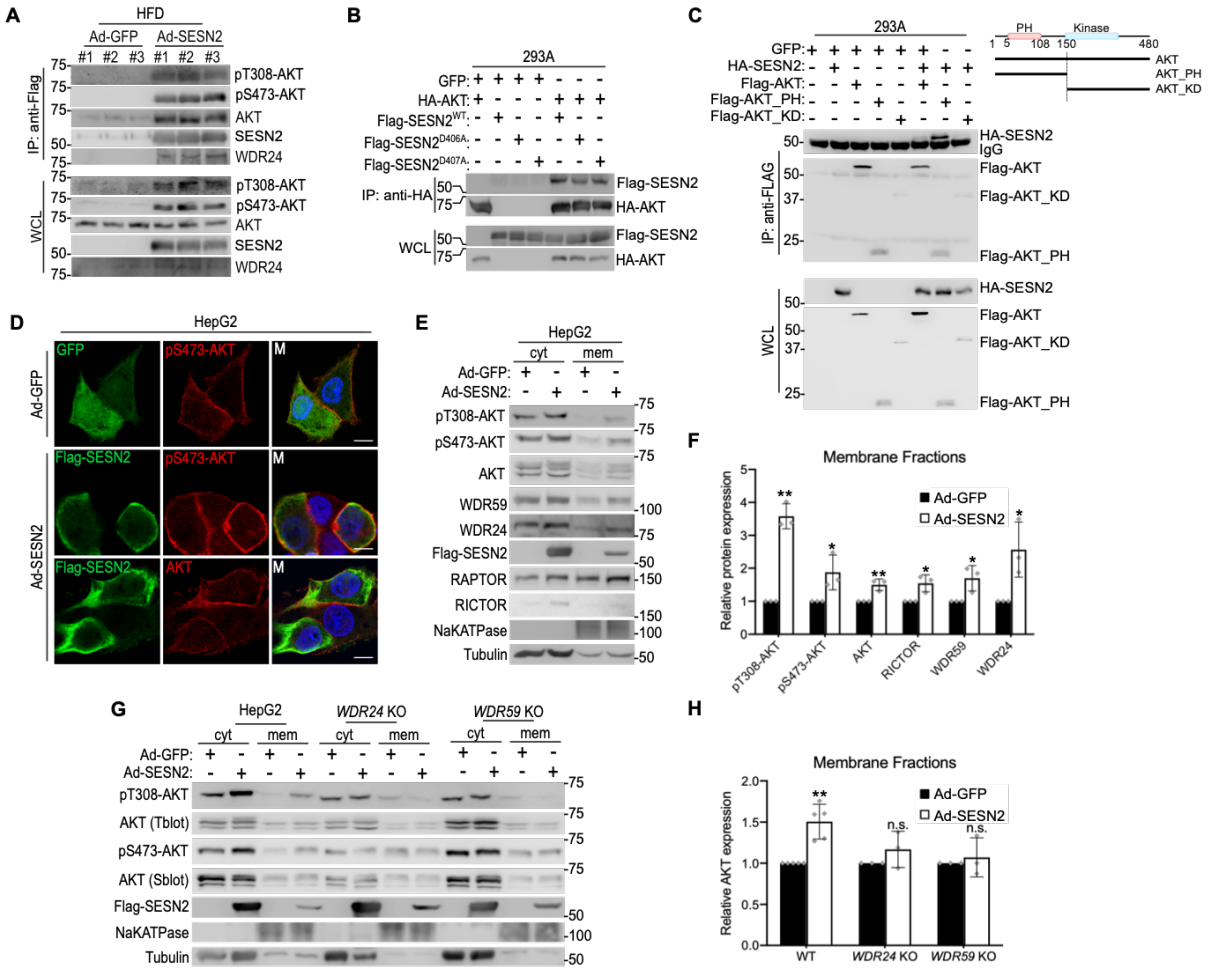

Figure 2.6. Sestrin2 induces AKT translocation to the plasma membrane. (A) Liver lysates from Ad-GFP and Ad-SESN2 infected mice, described in Figure 1, were subjected to anti-Flag immunoprecipitation (IP). IP complexes and whole cell lysates (WCL) were examined through immunoblotting. **(B-C)** HEK293 cells were transfected with indicated constructs for 24 hours then subjected to IP with indicated antibodies. IP complexes and WCL were examined through immunoblotting. **(D)** HepG2 cells were infected with Ad-GFP or Ad-SESN2, serum starved overnight, then analyzed by immunocytochemistry using indicated antibodies. **(E-H)** HepG2 cells were infected with Ad-GFP or Ad-SESN2, serum starved overnight, then subjected to membrane fractionation experiments and subsequent immunoblotting. **(F)** Membrane fractions for indicated proteins were quantified by densitometry (n=3). (G) *WDR24* and *WDR59* were targeted using CRISPR/Cas9 in HepG2 cells. Cells with confirmed knockouts were subjected to indicated treatments, membrane fractionation then immunoblotting. **(H)** Relative AKT protein expression was quantified by densitometry for membrane fractions (n≥3). P-values were calculated between control (Ad-GFP) and Sestrin2 overexpressing (Ad-SESN2) membrane fractions from a two-tailed student's t-test: *p<0.05, **p<0.01.

important for AKT translocation to the plasma membrane through binding 3' phosphorylated phosphoinositide lipids generated by PI3K (20).

Sestrin2 induces AKT plasma membrane translocation through GATOR2

We were curious if the interaction between Sestrin2 and the PH domain of AKT could alter the subcellular localization of AKT. In serum-starved HepG2 cells, Sestrin2 overexpression through adenoviral transduction induced strong AKT activation at the plasma membrane (Figure 2.6D). Total AKT was also generally translocated to the plasma membrane in Sestrin2 overexpressing cells (Figure 2.6D). The Sestrin2-induced membrane localization of AKT also occurred in cell fractionation experiments; Sestrin2 overexpression increased the presence of both p-AKT and AKT in total membrane fractions (Figure 2.6E, 2.6F). Interestingly, the GATOR2 components WDR24 and WDR59 were also targeted to the membrane fraction upon Sestrin2 overexpression (Figure 2.6E, 2.6F). Therefore, we tested if Sestrin2-induced AKT membrane translocation required GATOR2. *WDR24* KO and *WDR59* KO HepG2 cells, in which GATOR2 function is compromised, did not target AKT to the membrane fraction in response to Sestrin2 overexpression (Figure 2.6G, 2.6H). Therefore, even though Sestrin2 binding to AKT may not require GATOR2, GATOR2 is required for Sestrin2-induced AKT activation and its translocation to the plasma membrane.

Discussion

Insulin resistance represents one of the most prominent phenotypes exhibited by Sestrin-deficient animals (28). *Sesn2*-knockout mice (7) and *Sesn3*-knockout mice (9,35), as well as *dSesn*-null flies (7), are all prone to developing insulin resistance and subsequent dysregulation of blood

glucose homeostasis. Hypoactivity of insulin receptor-AKT signaling is commonly observed in these models, while mTORC1 signaling was aberrantly activated through a mechanism independent of insulin signaling regulation. As Sestrins downregulate mTORC1, it was thought that mTORC1 inhibition was the major cause of AKT upregulation (28). However, Sestrin-induced AKT activation was observed when mTORC1 components were silenced or ablated (9,23), suggesting that Sestrins may regulate AKT independently of mTORC1. Consistent with these reports, we confirmed that Sestrin2-induced AKT activation did not require mTORC1. Instead, Sestrin2 activated AKT by upregulating mTORC2, a kinase upstream of AKT. Therefore, our results indicate that Sestrin2 not only suppresses mTORC1 but concurrently activates mTORC2, a finding that aligns with other work indicating that tuberous sclerosis complex (TSC) and AMPK inhibit mTORC1 but activate mTORC2 (32,36,37).

We also defined the molecular mechanism by which Sestrin2 upregulates mTORC2. AMPK was recently shown to upregulate mTORC2 activity and signaling independently of mTORC1/S6K1-mediated negative feedback through direct phosphorylation of mTORC2 subunits (32). Since Sestrin2 represents an established AMPK activator (3), it was possible that Sestrin2/AMPK signaling mediates Sestrin2-induced mTORC2 activation. However, we found that Sestrin2 activated mTORC2 and AKT similarly in wild type and *Ampk*-null cells, indicating that Sestrin2-induced mTORC2 activation could occur independently of AMPK.

Utilizing mutational studies, we showed that Sestrin2's GATOR2-binding residues were required for its activation of mTORC2 and AKT. Consistent with former studies reporting a direct interaction between Sestrin2 and mTORC2 (9,23), we found a physical association between Sestrin2 and Rictor, an mTORC2-specific subunit. However, Sestrin2 mutants that lost GATOR2 binding were not able to interact with Rictor. Subsequent experiments suggested that GATOR2

acted as a bridge between Sestrin2 and mTORC2; GATOR2 interacts with Sestrin2 through WDR24 (12) and with mTORC2 through WDR59. Indeed, Sestrin2 was unable to upregulate mTORC2 and AKT in cells with genetic deletion of either WDR24 or WDR59. These experiments showed that GATOR2 mediates Sestrin2-induced activation of mTORC2 and AKT. Finally, our data suggested that Sestrin2 affects AKT subcellular localization. Through both immunocytochemistry and fractionation experiments, we found that Sestrin2 overexpression enriched both pAKT and AKT at the membrane. Since Sestrin2, WDR24/WDR59 and AKT are all enriched in the membrane fraction in conditions of Sestrin2 overexpression, it is possible that Sestrin2-GATOR2 complexes somehow physically direct AKT translocation. However, it is also possible that Ser473 phosphorylation, which is dependent on GATOR2-mTORC2, somehow promotes membrane translocation and further activation of AKT. The exact mechanism of how Sestrin2-GATOR2 induces membrane translocation and activation of AKT needs to be further clarified in future studies.

Importantly, the unique ability of Sestrin2 to inhibit mTORC1, activate AMPK, and activate mTORC2 makes it an ideal candidate for extending an organism's life and health span. While the mTORC1 inhibitor rapamycin extended lifespan in multiple animal models (38), it also coincided with serious side effects such as insulin resistance caused by suppression of mTORC2 assembly and thus function (39). Although chronic mTORC1 upregulation is detrimental and accelerates aging, mTORC2 activity is required to maintain metabolic homeostasis because it is essential for insulin-dependent signal transduction. Therefore, many aging researchers have searched for genetic and pharmacological agents that specifically inhibit mTORC1 while preserving mTORC2 activity (40). Sestrin2 or its chemical mimetics may be candidates for such agents.

In addition, unlike other pathways that activate AKT (i.e. insulin), Sestrin2-induced AKT activation did not concurrently activate mTORC1. AKT typically upregulates mTORC1 through inhibitory phosphorylation of the mTORC1 inhibitors TSC2 (41) and PRAS40 (42,43). Therefore, although forced AKT activation in the liver through PTEN inactivation (44) or constitutively active AKT (myr-AKT) expression (45) upregulated insulin signaling, it also detrimentally hyperactivated mTORC1, resulting in hepatomegaly and hepatic fat accumulation. Even though Sestrin2 activated AKT, it did not upregulate mTORC1 because it has an independent inhibitory function on mTORC1. Therefore, unlike other models of AKT activation, Sestrin2 reduced liver fat accumulation while upregulating insulin signaling. Consistent with these functional outcomes, Sestrin2 inhibited mRNA expression of both gluconeogenic and lipogenic genes.

In summary, we show that Sestrin2 upregulates the mTORC2/AKT pathway through a novel mechanism involving the GATOR2 complex. Further investigation into this signaling axis may reveal a novel mechanism for improving insulin signaling and normalizing metabolism during obesity and insulin resistance.

Experimental Procedures

Mice and Diets

Wdr24$^{f/f}$ (*Wdr24*^{tm1c})/*Alb-Cre* strain was generated from the *Wdr24*$^{tm1a(KOMP)Mbp}$ mouse line obtained from the UC Davis Mouse Biology program by breeding with the FLPo strain, backcrossed into the C57BL/6J background, and then crossed with the *Alb-Cre* line. Two-month-old WT or *Wdr24*$^{f/f}$*/Alb-Cre* mice of the C57BL/6J background were kept on a high fat diet (HFD, Bioserv S3282) for two additional months. Insulin tolerance tests were performed on 25 WT mice and 12 *Wdr24*$^{f/f}$*/Alb-Cre* mice. In each cohort, littermate mice were divided into two groups and

injected with adenoviruses through the tail vein. The insulin tolerance test (ITT) was performed at 4-10 days after adenoviral injection. For the ITT, mice were fasted for 4-6 hours in the morning, then injected with insulin (0.65 U/kg body weight i.p.). Blood glucose was measured 0, 20, 40, 60, and 120 min after insulin injection using a OneTouch Ultra glucose meter. At 10 days after adenoviral injection, livers were harvested under a surgical plane of isoflurane anesthesia before and after an injection of insulin (0.8 U/kg) through the inferior vena cava. All mice were housed at the Unit for Laboratory Animal Medicine (ULAM), and all procedures were approved by the Institutional Animal Care & Use Committee (IACUC) at the University of Michigan.

Oil Red O Staining

Optimum cutting temperature compound (OCT)-embedded frozen liver sections were air dried and rinsed with 60% isopropanol, followed by staining with fresh 0.5% Oil Red Solution for 15 min. After staining, slides were rinsed with 60% isopropanol, washed with distilled water, mounted and analyzed under a light microscope (Olympus). For quantification, 10 randomly chosen fields were used for each mouse liver.

Quantitative reverse-transcription PCR

Total RNA was extracted from tissues using Trizol (Invitrogen), and cDNA was made using MMLV-RT (Thermo fisher 28025013) and random hexamers (Invitrogen). Quantitative PCR was performed in a Real-Time PCR detection system (Applied Biosystems) with iQ SYBR Green Supermix (Bio-Rad) and primers listed in Table 2.2. Relative mRNA expression was calculated from the comparative threshold cycle (Ct) values normalized to β-actin and expressed as fold change over control values.

Table 2.2. Chapter 2 qPCR Primers

Gene	Primer sequence
G6pc F	CTGCAAGGGAGAACTCAGCAA
G6pc R	GAGGACCAAGGAAGCCACAAT
Pck1 F	GTGTCATCCGCAAGCTGAAG
Pck1 R	CTTTCGATCCTGGCCACATC
Hk1 F	CACCGGCAGATTGAGGAAAC
Hk1 R	CTCAGCCCCATTTCCATCTCT
Hk2 F	GGAACCCAGCTGTTTGACCA
Hk2 R	CAGGGGAACGAGAAGGTGAAA
G6pdx F	GGCAAGCTCCTCAAAACTTG
G6pdx R	AGAGCCCCCAAAATATTGCT
Fasn F	GGCATCATTGGGCACTCCTT
Fasn R	GCTGCAAGCACAGCCTCTCT
Acaca F	GCCATTGGTATTGGGGCTTAC
Acaca R	CCCGACCAAGGACTTTGTTG
Acacb F	CATACACAGAGCTGGTGTTGGACT
Acacb R	CACCATGCCCACCTCGTTAC
Actb F	CAAAAGCCACCCCCACTCCTAAGA
Actb R	GCCCTGGCTGCCTCAACACCTC

Antibodies and Reagents

Sestrin2 (10795) is from Proteintech. pT308-Akt (4056), pS473-Akt (4060), Akt (4691), pT389-S6K (9234), pT172-AMPK (2535), AMPKα (2532), mTOR (2983), Rictor (2114), WDR59 (53385), pS256-FOXO1 (9461), FOXO1 (2880), pT86-Sin1 (14716), Sin1 (12860), NaKATPase (23565), and Raptor (2280) are from Cell Signaling Technology. MAPKAP-1 (393166), WDR24 (244614), p70S6 kinase α (8418), and Rictor (271081) are from Santa Cruz Biotechnology. Flag (M2) is from Sigma. HA (3F10) is from Roche. Actin (JLA20), His (P5A11), Tubulin (E7), and c-Myc (9E10) are from Developmental Studies Hybridoma Bank (DSHB). Chemical inhibitors used in this study include rapamycin (LC Labs), BYL719 (Selleck), PP242 (Chemdea), Torin1 (Adooq), and LY294002 (LC Labs).

Western Blotting

Cells or tissues were lysed in cell lysis buffer (20mM Tris-Cl, pH 7.5, 150mM NaCl, 1mM EDTA, 1mM EGTA, 2.5mM sodium pyrophosphate, 1mM ß-glycerophosphate, 1mM Na_3VO_4, 1% Triton-X-100 or 1% NP-40 or 0.3% Chaps) containing protease inhibitor cocktail (Roche). After clarification by centrifugation, lysates were boiled in SDS sample buffer, separated by SDS-PAGE, transferred to polyvinylidene difluoride membranes and probed with indicated antibodies. Primary antibody dilution factors were 1:200 for Santa Cruz antibodies and 1:1000 for all others. After incubation with secondary antibodies conjugated with HRP at 1:2000, chemiluminescence was detected using LAS4000 (GE) system. All protein loading was normalized to total protein concentration determined using Biorad Protein Assay (Biorad 5000006). Protein expression in membrane fractions were normalized by the level of NaKATPase. Primary antibodies were

incubated in western blocking reagent (11921681001, Sigma Aldrich) for phospho-specific antibodies or 5% blotting grade blocker (Bio-Rad 1706404) for all other antibodies.

Cell Culture and Transfection

All cells were maintained in Dulbecco's modified Eagle's medium (DMEM, Invitrogen) containing 10% fetal bovine serum (Sigma), 20 U/ml penicillin and 50 mg/ml streptomycin. HepG2 is from ATCC. *WDR24*- and *WDR59*-knockout HepG2 cell lines were made from HepG2 using the LentiCRISPR v2 system (Addgene, originated from Feng Zhang lab (46)) using the gRNA-encoding primers. hWDR24 F: CACCG TCA GGG TTG GCG CGC TCG AC, hWDR24 R: AAAC GTC GAG CGC GCC AAC CCT GA C, hWDR59 F: CACCG ACC CGC GCA AAC GTC GGT AA, and hWDR59 R: AAAC TTA CCG ACG TTT GCG CGG GT C. After LentiCRISPR infection, multiple HepG2 cell clones with stable loss of targeted proteins were isolated through immunoblotting and used for the experiments. Primary hepatocytes were isolated from two-month-old control (*Wdr24*$^{f/f}$) and liver-specific *Wdr24*-knockout (*Alb-Cre*/*Wdr24*$^{f/f}$) mice as previously described (8). WT and *AMPKa1/2* KO MEFs were gifts from the Ken Inoki lab. Palmitic acid treatment was done as previously described (8,47). HEK293A cells (Invitrogen) were transfected with plasmids expressing indicated proteins using the polyethylenimine (PEI, Sigma) method as previously described (48). Sestrin constructs of wild-type and mutant forms are described in our previous work (5). GATOR2 constructs were originated from the David Sabatini lab (19) and obtained through Addgene. AKT and Rictor constructs were made by PCR amplification of corresponding cDNA and subsequent subcloning into pLU-CMV/Flag or HA expression vectors. The Sin1 plasmid was a gift from the Do-Hyung Kim lab at the University of Minnesota.

Adenoviral and Lentiviral Production

Adenoviruses and lentiviruses were produced at the University of Michigan Vector Core. For adenoviral production, full-length human Sestrin2 coding sequence, attached to an N-terminal Flag tag, was cloned into the pACCMV shuttle vector and incorporated into the Adenoviral backbone at the Vector Core, to generate Ad-SESN2. Ad-GFP was used as the control. For lentiviral production, pLU-CMV-SESN2 lentiviruses expressing wild-type and mutant Sestrin2 were formerly described (5). Lentiviruses expressing shRNA-Sestrin2 were also formerly described (8). Lentiviruses expressing shRNA-WDR24 is pLKO-shWDR24 obtained from Sigma (130142).

Immunoprecipitation

Cells were lysed in cell lysis buffer with 0.3% chaps, clarified by centrifugation, then incubated with Flag-bead (A2220, Sigma), HA-bead (A2095, Sigma), Mouse IgG sepharose bead conjugate (3420, Cell Signaling), or Rictor sepharose bead conjugate (5379, Cell Signaling) on a rotisserie at 4°C for 2 hours or overnight. The immunocomplexes were washed 6 times with the lysis buffer, samples were boiled with SDS sample buffer for 5 min at 95°C and analyzed by immunoblotting.

In vitro PI3K assay

The assay was performed as previously described (49). In brief, HepG2 cells were incubated with Ad-GFP or Ad-SESN2 for 48 hours and replaced with serum free DMEM. After 12 hours, cells were treated with water (control) or 100nM insulin for 3 min, then harvested. Lysates were immunoprecipitated with p-Tyr antibodies (9411, Cell Signaling) conjugated to a

protein G/A bead, subjected to a lipid kinase assay with γ-^{32}P-ATP and phosphotidylinositol, then subjected to thin layer chromatography and autoradiography to visualize PI3P.

In vitro mTORC2 kinase assay

HepG2 cells were treated with Ad-GFP or Ad-SESN2 and serum starved overnight. Lysates were immunoprecipitated with anti-Rictor antibodies conjugated to a protein G/A bead, subjected to a kinase assay with ATP and recombinant full-length inactive His-AKT substrate (Millipore 14-279), then analyzed by immunoblotting, as previously described (50).

Protein Identification by LC-Tandem MS

HepG2 cells were infected with Ad-GFP or Ad-SESN2 for 24 hours. Lysates were then immunoprecipitated with anti-Flag bead on a rotisserie at 4°C for 2 hours then washed 7 times in cell lysis buffer (20mM Tris pH 7.6, 150mM NaCl, 1mM EDTA, 1mM EGTA, 2.5mM sodium pyrophosphate, 1mM ß-glycerophosphate, 1mM Na_3VO_4, 0.3% Chaps), then 2 times in PBS. Samples were sent to the University of Michigan Proteomics Resource Facility and subjected to the protein identification service plus 3-hour LC-MS/MS analysis, according to their standardized procedure as described below.

The beads were resuspended in 50 µl of 0.1M ammonium bicarbonate buffer (pH~8). Cysteines were reduced by adding 50 µl of 10 mM DTT and incubating at 45° C for 30 min. Samples were cooled to room temperature and alkylation of cysteines was achieved by incubating with 65 mM 2-Chloroacetamide, under darkness, for 30 min at room temperature. An overnight digestion with 1 µg sequencing grade, modified trypsin was carried out at 37 °C with constant shaking in a Thermomixer. Digestion was stopped by acidification, and peptides were desalted

using SepPak C18 cartridges, using the manufacturer's protocol (Waters). Samples were completely dried using vacufuge. Resulting peptides were dissolved in 8 µl of 0.1% formic acid/2% acetonitrile solution, and 2 µls of the peptide solution were resolved on a nano-capillary reverse phase column (Acclaim PepMap C18, 2 micron, 50 cm, ThermoScientific), using a 0.1% formic acid/2% acetonitrile (Buffer A) and 0.1% formic acid/95% acetonitrile (Buffer B) gradient at 300 nl/min over a period of 180 min (2-22% buffer B in 110 min, 22-40% in 25 min, 40-90% in 5 min, followed by holding at 90% buffer B for 5 min and re-equilibration with Buffer A for 25 min). Eluent was directly introduced into Orbitrap Fusion tribrid mass spectrometer (Thermo Scientific, San Jose CA), using an EasySpray source. MS1 scans were acquired at 120K resolution (AGC target=$1x10^6$; max IT=50 ms). Data-dependent collision induced dissociation MS/MS spectra were acquired using Top speed method (3 seconds), following each MS1 scan (NCE ~32%; AGC target $1x10^5$; max IT 45 ms).

Proteins were identified by searching the MS/MS data against *H. Sapiens* database (UniProt; 2016-11-30 download, 42054 entries) using Proteome Discoverer (v2.1, Thermo Scientific). Search parameters included MS1 mass tolerance of 10 ppm and fragment tolerance of 0.2 Da; two missed cleavages were allowed; carbamidimethylation of cysteine was considered fixed modification and oxidation of methionine, deamidation of asparagine and glutamine were considered as potential modifications. False discovery rate (FDR) was determined using Percolator and proteins/peptides with an FDR of ≤1% were retained for further analysis.

Immunocytochemistry

Ad-GFP or Ad-SESN2 treated HepG2 were grown on coverslips overnight. After incubation with serum free DMEM overnight, cells were fixed with 4% paraformaldehyde and

permeabilized with 0.2% Triton X-100. Cells were incubated with 3% BSA, and then with primary antibodies (1:1000) in PBS for 2 hrs. After washing, cells were incubated with Alexa fluor-conjugated secondary antibodies (1:1000) for 1 hr, washed with PBS, counterstained with DAPI (Invitrogen), and mounted in Vectashield anti-fade mounting media (H-1000). Images were captured under a Leica SP5X confocal microscope.

Cell Fractionation

Cytosol and membrane protein fractions were isolated using the Mem-PER Plus Membrane Protein Extraction Kit (Thermo Scientific, Rockford, IL), according to the manufacturer's recommendation.

Statistical Analyses

Results are presented as mean ± SEM for line graphs and mean ± SD for bar graphs. Significance between two groups was calculated using a two-tailed student's t-test.

References

1. Lee, J. H., Budanov, A. V., Park, E. J., Birse, R., Kim, T. E., Perkins, G. A., Ocorr, K., Ellisman, M. H., Bodmer, R., Bier, E., and Karin, M. (2010) Sestrin as a feedback inhibitor of TOR that prevents age-related pathologies. *Science* **327**, 1223-1228

2. Yang, Y. L., Loh, K. S., Liou, B. Y., Chu, I. H., Kuo, C. J., Chen, H. D., and Chen, C. S. (2013) SESN-1 is a positive regulator of lifespan in Caenorhabditis elegans. *Experimental gerontology* **48**, 371-379

3. Budanov, A. V., Lee, J. H., and Karin, M. (2010) Stressin' Sestrins take an aging fight. *EMBO molecular medicine* **2**, 388-400

4. Budanov, A. V., Sablina, A. A., Feinstein, E., Koonin, E. V., and Chumakov, P. M. (2004) Regeneration of peroxiredoxins by p53-regulated sestrins, homologs of bacterial AhpD. *Science* **304**, 596-600

5. Kim, H., An, S., Ro, S. H., Teixeira, F., Park, G. J., Kim, C., Cho, C. S., Kim, J. S., Jakob, U., Lee, J. H., and Cho, U. S. (2015) Janus-faced Sestrin2 controls ROS and mTOR signalling through two separate functional domains. *Nat Commun* **6**, 10025

6. Budanov, A. V., and Karin, M. (2008) p53 target genes sestrin1 and sestrin2 connect genotoxic stress and mTOR signaling. *Cell* **134**, 451-460

7. Lee, J. H., Budanov, A. V., Talukdar, S., Park, E. J., Park, H. L., Park, H. W., Bandyopadhyay, G., Li, N., Aghajan, M., Jang, I., Wolfe, A. M., Perkins, G. A., Ellisman, M. H., Bier, E., Scadeng, M., Foretz, M., Viollet, B., Olefsky, J., and Karin, M. (2012) Maintenance of metabolic homeostasis by Sestrin2 and Sestrin3. *Cell metabolism* **16**, 311-321

8. Park, H. W., Park, H., Ro, S. H., Jang, I., Semple, I. A., Kim, D. N., Kim, M., Nam, M., Zhang, D., Yin, L., and Lee, J. H. (2014) Hepatoprotective role of Sestrin2 against chronic ER stress. *Nat Commun* **5**, 4233

9. Tao, R., Xiong, X., Liangpunsakul, S., and Dong, X. C. (2015) Sestrin 3 protein enhances hepatic insulin sensitivity by direct activation of the mTORC2-Akt signaling. *Diabetes* **64**, 1211-1223

10. Saxton, R. A., Knockenhauer, K. E., Wolfson, R. L., Chantranupong, L., Pacold, M. E., Wang, T., Schwartz, T. U., and Sabatini, D. M. (2016) Structural basis for leucine sensing by the Sestrin2-mTORC1 pathway. *Science* **351**, 53-58

11. Chantranupong, L., Wolfson, R. L., Orozco, J. M., Saxton, R. A., Scaria, S. M., Bar-Peled, L., Spooner, E., Isasa, M., Gygi, S. P., and Sabatini, D. M. (2014) The Sestrins interact with GATOR2 to negatively regulate the amino-acid-sensing pathway upstream of mTORC1. *Cell reports* **9**, 1-8

12. Parmigiani, A., Nourbakhsh, A., Ding, B., Wang, W., Kim, Y. C., Akopiants, K., Guan, K. L., Karin, M., and Budanov, A. V. (2014) Sestrins inhibit mTORC1 kinase activation through the GATOR complex. *Cell reports* **9**, 1281-1291

13. Kim, J. S., Ro, S. H., Kim, M., Park, H. W., Semple, I. A., Park, H., Cho, U. S., Wang, W., Guan, K. L., Karin, M., and Lee, J. H. (2015) Sestrin2 inhibits mTORC1 through modulation of GATOR complexes. *Scientific reports* **5**, 9502

14. Sanli, T., Linher-Melville, K., Tsakiridis, T., and Singh, G. (2012) Sestrin2 modulates AMPK subunit expression and its response to ionizing radiation in breast cancer cells. *PloS one* **7**, e32035

15. Eid, A. A., Lee, D. Y., Roman, L. J., Khazim, K., and Gorin, Y. (2013) Sestrin 2 and AMPK connect hyperglycemia to Nox4-dependent endothelial nitric oxide synthase uncoupling and matrix protein expression. *Molecular and cellular biology* **33**, 3439-3460

16. Morrison, A., Chen, L., Wang, J., Zhang, M., Yang, H., Ma, Y., Budanov, A., Lee, J. H., Karin, M., and Li, J. (2015) Sestrin2 promotes LKB1-mediated AMPK activation in the ischemic heart. *FASEB journal : official publication of the Federation of American Societies for Experimental Biology* **29**, 408-417

17. Deng, W., Cha, J., Yuan, J., Haraguchi, H., Bartos, A., Leishman, E., Viollet, B., Bradshaw, H. B., Hirota, Y., and Dey, S. K. (2016) p53 coordinates decidual sestrin 2/AMPK/mTORC1 signaling to govern parturition timing. *J Clin Invest* **126**, 2941-2954

18. Kim, M., and Lee, J. H. (2015) Identification of an AMPK phosphorylation site in Drosophila TSC2 (gigas) that regulate cell growth. *International journal of molecular sciences* **16**, 7015-7026

19. Bar-Peled, L., Chantranupong, L., Cherniack, A. D., Chen, W. W., Ottina, K. A., Grabiner, B. C., Spear, E. D., Carter, S. L., Meyerson, M., and Sabatini, D. M. (2013) A Tumor suppressor complex with GAP activity for the Rag GTPases that signal amino acid sufficiency to mTORC1. *Science* **340**, 1100-1106

20. Manning, B. D., and Toker, A. (2017) AKT/PKB Signaling: Navigating the Network. *Cell* **169**, 381-405

21. Zhao, B., Shah, P., Budanov, A. V., Qiang, L., Ming, M., Aplin, A., Sims, D. M., and He, Y. Y. (2014) Sestrin2 protein positively regulates AKT enzyme signaling and survival in human squamous cell carcinoma and melanoma cells. *J Biol Chem* **289**, 35806-35814

22. Ben-Sahra, I., Dirat, B., Laurent, K., Puissant, A., Auberger, P., Budanov, A., Tanti, J. F., and Bost, F. (2013) Sestrin2 integrates Akt and mTOR signaling to protect cells against energetic stress-induced death. *Cell Death Differ* **20**, 611-619

23. Byun, J. K., Choi, Y. K., Kim, J. H., Jeong, J. Y., Jeon, H. J., Kim, M. K., Hwang, I., Lee, S. Y., Lee, Y. M., Lee, I. K., and Park, K. G. (2017) A Positive Feedback Loop between Sestrin2 and mTORC2 Is Required for the Survival of Glutamine-Depleted Lung Cancer Cells. *Cell Rep* **20**, 586-599

24. Dai, J., Huang, Q., Niu, K., Wang, B., Li, Y., Dai, C., Chen, Z., Tao, K., and Dai, J. (2018) Sestrin 2 confers primary resistance to sorafenib by simultaneously activating AKT and AMPK in hepatocellular carcinoma. *Cancer Med* **7**, 5691-5703

25. Chen, C. C., Jeon, S. M., Bhaskar, P. T., Nogueira, V., Sundararajan, D., Tonic, I., Park, Y., and Hay, N. (2010) FoxOs inhibit mTORC1 and activate Akt by inducing the expression of Sestrin3 and Rictor. *Dev Cell* **18**, 592-604

26. Kim, M., Sujkowski, A., Namkoong, S., Gu, B., Cobb, T., Kim, B., Kowalsky, A. H., Cho, C. S., Semple, I., Ro, S. H., Davis, C., Brooks, S. V., Karin, M., Wessells, R. J., and Lee, J. H. (2020) Sestrins are evolutionarily conserved mediators of exercise benefits. *Nat Commun* **11**, 190

27. Segales, J., Perdiguero, E., Serrano, A. L., Sousa-Victor, P., Ortet, L., Jardi, M., Budanov, A. V., Garcia-Prat, L., Sandri, M., Thomson, D. M., Karin, M., Hee Lee, J., and Munoz-Canoves, P. (2020) Sestrin prevents atrophy of disused and aging muscles by integrating anabolic and catabolic signals. *Nat Commun* **11**, 189

28. Lee, J. H., Budanov, A. V., and Karin, M. (2013) Sestrins orchestrate cellular metabolism to attenuate aging. *Cell metabolism* **18**, 792-801

29. Um, S. H., D'Alessio, D., and Thomas, G. (2006) Nutrient overload, insulin resistance, and ribosomal protein S6 kinase 1, S6K1. *Cell Metab* **3**, 393-402

30. Kim, M. J., Bae, S. H., Ryu, J. C., Kwon, Y., Oh, J. H., Kwon, J., Moon, J. S., Kim, K., Miyawaki, A., Lee, M. G., Shin, J., Kim, Y. S., Kim, C. H., Ryter, S. W., Choi, A. M., Rhee, S. G., Ryu, J. H., and Yoon, J. H. (2016) SESN2/sestrin2 suppresses sepsis by inducing mitophagy and inhibiting NLRP3 activation in macrophages. *Autophagy* **12**, 1272-1291

31. Gao, D., Nong, S., Huang, X., Lu, Y., Zhao, H., Lin, Y., Man, Y., Wang, S., Yang, J., and Li, J. (2010) The effects of palmitate on hepatic insulin resistance are mediated by NADPH Oxidase 3-derived reactive oxygen species through JNK and p38MAPK pathways. *J Biol Chem* **285**, 29965-29973

32. Kazyken, D., Magnuson, B., Bodur, C., Acosta-Jaquez, H. A., Zhang, D., Tong, X., Barnes, T. M., Steinl, G. K., Patterson, N. E., Altheim, C. H., Sharma, N., Inoki, K., Cartee, G. D., Bridges, D., Yin, L., Riddle, S. M., and Fingar, D. C. (2019) AMPK directly activates mTORC2 to promote cell survival during acute energetic stress. *Sci Signal* **12**

33. Sarbassov, D. D., Guertin, D. A., Ali, S. M., and Sabatini, D. M. (2005) Phosphorylation and regulation of Akt/PKB by the rictor-mTOR complex. *Science* **307**, 1098-1101

34. Ho, A., Cho, C. S., Namkoong, S., Cho, U. S., and Lee, J. H. (2016) Biochemical Basis of Sestrin Physiological Activities. *Trends Biochem Sci* **41**, 621-632

35. Huang, M., Kim, H. G., Zhong, X., Dong, C., Zhang, B., Fang, Z., Zhang, Y., Lu, X., Saxena, R., Liu, Y., Zhang, C., Liangpunsakul, S., and Dong, X. C. (2019) Sesn3 protects against diet-induced nonalcoholic steatohepatitis in mice via suppression of the TGFbeta signal transduction. *Hepatology* **71**, 76-92

36. Huang, J., and Manning, B. D. (2009) A complex interplay between Akt, TSC2 and the two mTOR complexes. *Biochem Soc Trans* **37**, 217-222

37. Huang, J., and Manning, B. D. (2008) The TSC1-TSC2 complex: a molecular switchboard controlling cell growth. *Biochem J* **412**, 179-190

38. Ehninger, D., Neff, F., and Xie, K. (2014) Longevity, aging and rapamycin. *Cell Mol Life Sci* **71**, 4325-4346

39. Lamming, D. W., Ye, L., Katajisto, P., Goncalves, M. D., Saitoh, M., Stevens, D. M., Davis, J. G., Salmon, A. B., Richardson, A., Ahima, R. S., Guertin, D. A., Sabatini, D. M., and Baur, J. A. (2012) Rapamycin-induced insulin resistance is mediated by mTORC2 loss and uncoupled from longevity. *Science* **335**, 1638-1643

40. Kennedy, B. K., and Lamming, D. W. (2016) The Mechanistic Target of Rapamycin: The Grand ConducTOR of Metabolism and Aging. *Cell Metab* **23**, 990-1003

41. Inoki, K., Li, Y., Zhu, T., Wu, J., and Guan, K. L. (2002) TSC2 is phosphorylated and inhibited by Akt and suppresses mTOR signalling. *Nat Cell Biol* **4**, 648-657

42. Vander Haar, E., Lee, S. I., Bandhakavi, S., Griffin, T. J., and Kim, D. H. (2007) Insulin signalling to mTOR mediated by the Akt/PKB substrate PRAS40. *Nat Cell Biol* **9**, 316-323

43. Sancak, Y., Thoreen, C. C., Peterson, T. R., Lindquist, R. A., Kang, S. A., Spooner, E., Carr, S. A., and Sabatini, D. M. (2007) PRAS40 is an insulin-regulated inhibitor of the mTORC1 protein kinase. *Mol Cell* **25**, 903-915

44. Stiles, B., Wang, Y., Stahl, A., Bassilian, S., Lee, W. P., Kim, Y. J., Sherwin, R., Devaskar, S., Lesche, R., Magnuson, M. A., and Wu, H. (2004) Liver-specific deletion of negative regulator Pten results in fatty liver and insulin hypersensitivity [corrected]. *Proc Natl Acad Sci U S A* **101**, 2082-2087

45. Ono, H., Shimano, H., Katagiri, H., Yahagi, N., Sakoda, H., Onishi, Y., Anai, M., Ogihara, T., Fujishiro, M., Viana, A. Y., Fukushima, Y., Abe, M., Shojima, N., Kikuchi, M.,

Yamada, N., Oka, Y., and Asano, T. (2003) Hepatic Akt activation induces marked hypoglycemia, hepatomegaly, and hypertriglyceridemia with sterol regulatory element binding protein involvement. *Diabetes* **52**, 2905-2913

46. Ran, F. A., Hsu, P. D., Wright, J., Agarwala, V., Scott, D. A., and Zhang, F. (2013) Genome engineering using the CRISPR-Cas9 system. *Nat Protoc* **8**, 2281-2308

47. Park, H. W., Park, H., Semple, I. A., Jang, I., Ro, S. H., Kim, M., Cazares, V. A., Stuenkel, E. L., Kim, J. J., Kim, J. S., and Lee, J. H. (2014) Pharmacological correction of obesity-induced autophagy arrest using calcium channel blockers. *Nat Commun* **5**, 4834

48. Horbinski, C., Stachowiak, M. K., Higgins, D., and Finnegan, S. G. (2001) Polyethyleneimine-mediated transfection of cultured postmitotic neurons from rat sympathetic ganglia and adult human retina. *BMC Neurosci* **2**, 2

49. Wang, L. P., and Summers, S. A. (2003) Measuring insulin-stimulated phosphatidyl-inositol 3-kinase activity. *Methods Mol Med* **83**, 127-136

50. Huang, J. (2012) An in vitro assay for the kinase activity of mTOR complex 2. *Methods Mol Biol* **821**, 75-86

CHAPTER III[3]

Concurrent Activation of Growth Factor and Nutrient Arms of mTORC1 Induces Oxidative Liver Injury

Abstract

mTORC1 is a protein kinase important for metabolism and is regulated by growth factor and nutrient signaling pathways, mediated by the Rheb and Rag GTPases, respectively. Here we provide the first animal model in which both pathways were upregulated through concurrent mutations in their GTPase-activating proteins, *Tsc1* and *Depdc5*. Unlike former models that induced limited mTORC1 upregulation, hepatic deletion of both *Tsc1* and *Depdc5* (DKO) produced strong, synergistic activation of the mTORC1 pathway and provoked pronounced and widespread hepatocyte damage, leading to externally visible liver failure phenotypes, such as jaundice and systemic growth defects. The transcriptome profile of DKO was different from single knockout mutants but similar to those of diseased human livers with severe hepatitis and mouse livers challenged with oxidative stress-inducing chemicals. In addition, DKO liver cells exhibited prominent molecular pathologies associated with excessive endoplasmic reticulum (ER) stress, oxidative stress, DNA damage and inflammation. Although DKO liver pathologies were ameliorated by mTORC1 inhibition, ER stress suppression unexpectedly aggravated them, suggesting that ER stress signaling is not the major conduit of how hyperactive mTORC1 produces

[3] This chapter represents a published manuscript: Cho CS*, Kowalsky AH*, Namkoong S, Park SR, Wu S, Kim B, James A, Gu B, Semple IA, Tohamy MA, Solanki S, Cho US, Greenson JK, Shah YM, Kim M, Lee JH. Concurrent activation of growth factor and nutrient arms of mTORC1 induces oxidative liver injury. *Cell Discovery* (2019)

liver damage. Interestingly, superoxide scavengers N-acetylcysteine (NAC) and Tempol, chemicals that reduce oxidative stress, were able to recover liver phenotypes, indicating that mTORC1 hyperactivation induced liver damage mainly through oxidative stress pathways. Our study provides a new model of unregulated mTORC1 activation through concomitant upregulation of growth factor and nutrient signaling axes and shows that mTORC1 hyperactivation alone can provoke oxidative tissue injury.

Introduction

Mammalian target of rapamycin complex 1 (mTORC1) is a protein kinase complex that promotes cellular anabolism in response to insulin/growth factor stimuli and nutrient abundance (1-4). Regulation of mTORC1 is believed to be mediated by two small G proteins, Rheb and Rag (4,5). The tuberous sclerosis complex (TSC) and the GAP activities Towards Rags 1 complex (GATOR1) are GTPase-activating proteins (GAPs) that regulate Rheb and Rag, respectively (4,5). TSC, consisting of the TSC1, TSC2, and TBC1D7 proteins, mediates growth factor and energy signals to mTORC1 (6,7), while GATOR1, consisting of DEPDC5, NPRL2 and NPRL3 proteins are essential for amino acid sensing (8,9) and stress response (10) of the mTORC1 pathway.

DEPDC5 is a component of GATOR1 that inhibits mTORC1 by binding and inhibiting Rag (8,9). DEPDC5 is also implicated in various human pathologies including brain and liver diseases (11-15). Genetic variations in the *DEPDC5* locus were associated with hepatitis C virus (HCV)-induced hepatocellular carcinoma in a Japanese population (13), HCV-induced fibrosis progression in a European population (14), and hepatitis B virus (HBV)-related hepatocarcinogenesis in a Chinese population (15). However, whether DEPDC5 regulates liver

homeostasis and how it affects liver disease progression has not been investigated in an intact animal model.

mTORC1, the DEPDC5 and TSC1 target, is an important metabolic regulator in the liver (2,3). mTORC1 activation is important for upregulating protein translation by phosphorylating two substrates: p70 ribosomal protein S6 kinase (S6K) and translation initiation factor 4E-binding protein 1 (4E-BP1) (1). mTORC1 also upregulates lipid and nucleic acid synthesis while downregulating autophagic catabolism through inhibition of unc-51-like autophagy activating kinase (ULK1) (1-4). Therefore, mTORC1 regulation is thought to be critical for maintaining metabolic homeostasis in the liver (2,3). Indeed, disrupting mTORC1 through liver-specific deletion of Raptor, an essential subunit, induced spontaneous liver damage associated with inflammation and fibrosis (16). This accelerated liver carcinogenesis upon administration of diethylnitrosamine (DEN), a chemical hepatocarcinogen (16). Activating mTORC1 through hepatocyte-specific deletion of *Tsc1* (*Tsc1*$^{\Delta hep}$) also produced liver inflammation and carcinogenesis in aged mice, but these pathologies were not obvious in young mice (17,18).

Given the importance of DEPDC5 in nutrient and stress-dependent mTORC1 regulation (8-10), DEPDC5 could be an important regulator of mTORC1 in hepatocytes. To understand the genetic role of DEPDC5 in the liver, we generated *Depdc5*$^{\Delta hep}$ mice, which have hepatocyte-specific deletion of the *Depdc5* gene. Similar to *Tsc1*$^{\Delta hep}$ mice, *Depdc5*$^{\Delta hep}$ mice showed slight elevation in mTORC1 activity and exhibited mild inflammation and fibrosis in advanced age. However, when *Depdc5*$^{\Delta hep}$ mice were crossed to *Tsc1*$^{\Delta hep}$ mice, a much more striking phenotype was observed. Although individual deletions of *Depdc5* or *Tsc1* in the liver only slightly upregulated mTORC1 with no gross phenotypes, hepatocyte-specific *Depdc5* and *Tsc1* double knockout (DKO) mice had robust mTORC1 activation that induced prominent hepatocyte damage.

Consequently, serious liver failure associated with jaundice, hepatomegaly, fur discoloration and growth suppression were observed by 8 weeks of age. Transcriptomic analyses with RNA-seq and subsequent protein analyses indicated that DKO livers suffer excessive ER stress and oxidative stress leading to metabolic dysregulation, DNA damage and inflammation. Among these outputs, oxidative damage was the most critical in producing DKO pathologies, while ER stress signaling protected hepatocytes by suppressing mTORC1 in a negative feedback mechanism.

Results

Hepatic loss of *Depdc5* induces hepatocellular hypertrophy in zone 3

Immunoblot analyses of two-month-old mouse liver indicated that *Alb-Cre*/*Depdc5*$^{F/F}$ (*Depdc5*$^{\Delta hep}$) mice lost hepatic Depdc5 expression and slightly upregulated the level of phosphorylated S6 (p-S6), a downstream marker of mTORC1 (Figure 3.1A). Hematoxylin and eosin (H&E) staining of liver sections revealed that two-month-old *Depdc5*$^{\Delta hep}$ mice had specific enlargement of pericentral zone 3 hepatocytes (Figure 3.1B and Supplementary Figure S3.1A), associated with locally elevated levels of p-S6 immunostaining (Figure 3.1C and Supplementary Figure S3.1A).

Consistent with impaired zone 3 homeostasis, *Depdc5*$^{\Delta hep}$ mice were more extensively damaged from a high dose of acetaminophen (APAP), which provokes hepatocellular death most prominently in zone 3, compared to littermate controls (Supplementary Figure S3.1B). APAP-induced hepatic mTORC1 activation (19-21) was also stronger in *Depdc5*$^{\Delta hep}$ mice (Supplementary Figure S3.1C). Therefore, Depdc5 appears to be critical for homeostatic regulation of zone 3 hepatocytes, suppressing hepatic mTORC1 activation and hepatocellular hypertrophy, and protecting from APAP injury.

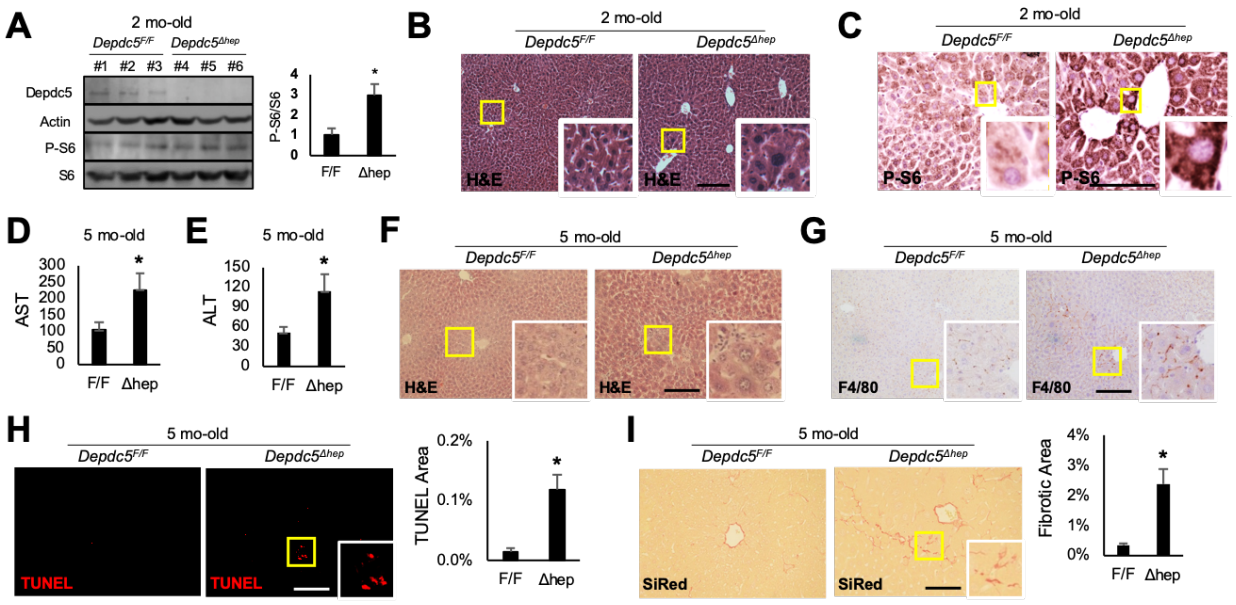

Figure 3.1: Liver-specific *Depdc5* deletion induces slight upregulation of mTORC1 and inflammation. Two-month-old **(A-C)** or five-month-old **(D-I)** littermates of Depdc5$^{\Delta hep}$ and Depdc5$^{F/F}$ male mice were subjected to the following analyses. **(A)** Liver lysates were subjected to immunoblotting with indicated antibodies (left). Band intensities were quantified (n=3; right). **(B, C)** Liver sections were subjected to H&E staining **(B)** and anti-phospho-S6 immunostaining (**c**). Boxed areas are magnified in the insets. **(D, E)** Serum AST (**D**) and ALT (**E**) assays (n≥6). **(F-I)** Liver sections were subjected to H&E **(F)**, F4/80 **(G)**, TUNEL **(H)** and Sirius Red (SiRed, **I**) staining. TUNEL and SiRed-positive areas were quantified (n=3). Data are shown as mean ± SEM. **P*<0.05 (Student's t-test). Scale bars, 200 μm.

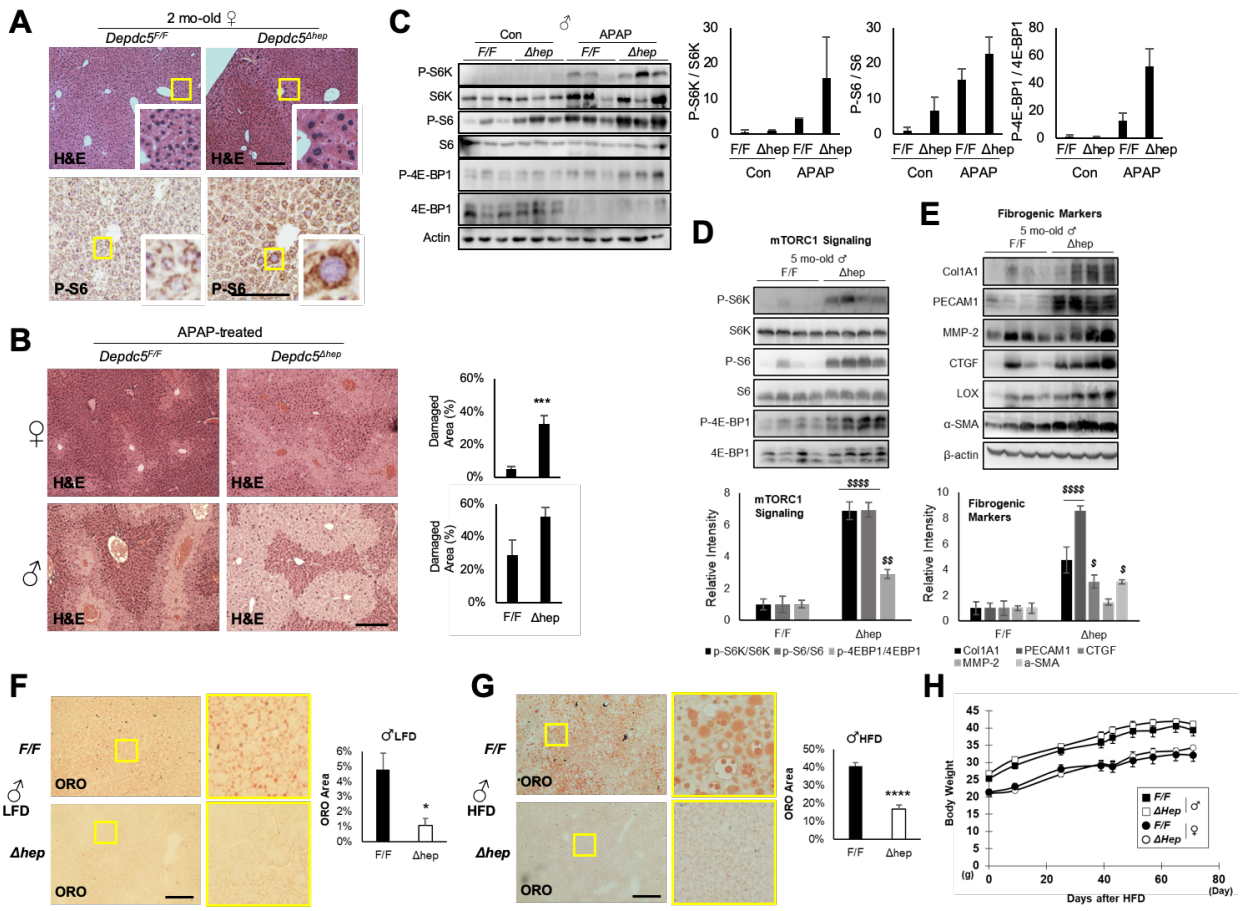

Figure S3.1: Liver phenotypes of *Depdc5*$^{\Delta hep}$ mice. (A) Liver sections were subjected to H&E staining and anti- phospho-S6 immunostaining for 2-month-old females of the Fig. 3.1 cohort. Boxed areas are magnified in the insets. **(B, C)** After 12 hours of fasting, 2-month-old *Depdc5*$^{F/F}$ and *Depdc5*$^{\Delta hep}$ littermate mice of indicated gender were injected with 400 mg/Kg of APAP. After 8 hours, livers were collected and analyzed by H&E staining **(B)** and immunoblotting **(C)**. Damaged areas (n≥8) and band intensities (n=3) were quantified. **(D, E)** Liver lysates from 5-month-old *Depdc5*$^{F/F}$ and *Depdc5*$^{\Delta hep}$ littermate male mice were subjected to immunoblotting (upper panels) and quantification (lower panels; n=4) to analyze mTORC1 signaling **(D)** and fibrogenic markers **(E)**. **(F,G)** Two-month-old *Depdc5*$^{F/F}$ and *Depdc5*$^{\Delta hep}$ littermate male mice were kept on normal chow (LFD) **(F)** or high fat diet (HFD) **(G)** for three additional months. Livers from the 5-month-old mice were subjected to Oil Red O (ORO) staining. ORO-positive areas were quantified (right panels, n=3). Boxed areas are magnified in right panels. **(H)** Body weight was monitored during HFD feeding (male, n=8; female, n≥4). Data are presented as mean ± SEM. **P* < 0.05; ****P* < 0.001; *****P* < 0.0001(Student's t-test). When multiple parameters were assessed, the Holm-Šídák method was used to compare groups ($, *P*<0.05; $$, *P*<0.01; $$$$, *P*<0.0001). Scale bars, 200 μm.

Depdc5$^{\Delta hep}$ mice exhibit mild zone 3 inflammation as they age

Five-month-old *Depdc5*$^{\Delta hep}$ mice demonstrated a slight but significant elevation in serum markers of liver damage: AST (Figure 3.1D) and ALT (Figure 3.1E). Although these values are still within normal clinical ranges, it is possible that there are subclinical levels of mild liver pathologies. Histological analyses indeed revealed occasional liver inflammation (Figure 3.1F, 3.1G), hepatocyte death (Figure 3.1H) and fibrosis (Figure 3.1I) in five-month-old *Depdc5*$^{\Delta hep}$ mice. Immunoblot analyses also confirmed mTORC1 signaling upregulation (Supplementary Figure S3.1D) and increased fibrogenic marker expression in five-month-old *Depdc5*$^{\Delta hep}$ mice (Supplementary Figure S3.1E). Therefore, similar to previously described *Tsc1*$^{\Delta hep}$ mice (18), *Depdc5*$^{\Delta hep}$ mice also exhibited age-dependent development of spontaneous liver pathologies.

Despite inflammatory phenotypes, *Tsc1*$^{\Delta hep}$ mice downregulated liver fat levels by blocking insulin-dependent lipogenic pathways (22). Likewise, *Depdc5*$^{\Delta hep}$ mice also exhibited reduced hepatic fat levels in both low fat diet (LFD, Supplementary Figure S3.1F) and high fat diet (HFD, Supplementary Figure S3.1G) conditions, without altering body weight gain (Supplementary Figure S3.1H). Therefore, the phenotypes exhibited by liver-specific *Depdc5* knockouts were generally similar to *Tsc1* knockouts.

Double deletion of *Tsc1* and *Depdc5* in liver suppresses systemic growth

Rag and Rheb are the two most important small GTPases directly regulating mTORC1 (4,5). Since Depdc5 and Tsc1 are critical for inhibiting Rag and Rheb, respectively, we hypothesized that mutations in these two genes may genetically interact (Figure 3.2A).

To test the genetic interaction, we crossed *Depdc5*$^{\Delta hep}$ mice with *Tsc1*$^{\Delta hep}$ mice. Although the *Depdc5*$^{\Delta hep}$/*Tsc1*$^{\Delta hep}$ double knockout (DKO) mice were born at the expected Mendelian ratios,

their growth was severely suppressed, and their fur was gray and patchy by two months old (Figure 3.2B, 3.2C and Supplementary Figure S3.2A). These phenotypes were not observed in littermates of any other genotype, including *Depdc5*$^{\Delta hep}$ and *Tsc1*$^{\Delta hep}$ single knockouts. Although body and adipose tissue weights were drastically reduced in DKO mice, the liver weights were similar to controls and single knockout mice, resulting in a dramatic increase of liver/body weight ratio (Figure 3.2C and Supplementary Figure S3.2A).

The body weight difference between control and DKO mice was not observed in 6 day-old mice (Supplementary Figure S3.2B), indicating that the DKO mice were not born with lower body weight and likely lose weight due to disease progression.

DKO mice experience severe liver injury and failure

Sera from the DKO mice were yellow, indicating bilirubin accumulation. All serum markers for liver damage and dysfunction were elevated prominently above normal clinical ranges (Figure 3.2D). Consistent with this, H&E staining revealed numerous necrotic lesions (arrows in Figure 3.2E and Supplementary Figure S3.2C) in DKO liver. The livers of DKO mice were extremely stiff, and Sirius Red staining revealed extensive pericellular fibrosis throughout the liver (Figure 3.2E, bottom). Fibrotic lesions were more intense around necrotic regions and often associated with proliferating bile ducts (Figure 3.2E, magnified images in blue and green boxes). All phenotypes were fully penetrant and prominently observed in both males (Figure 3.2) and females (Supplementary Figure S3.2A, C).

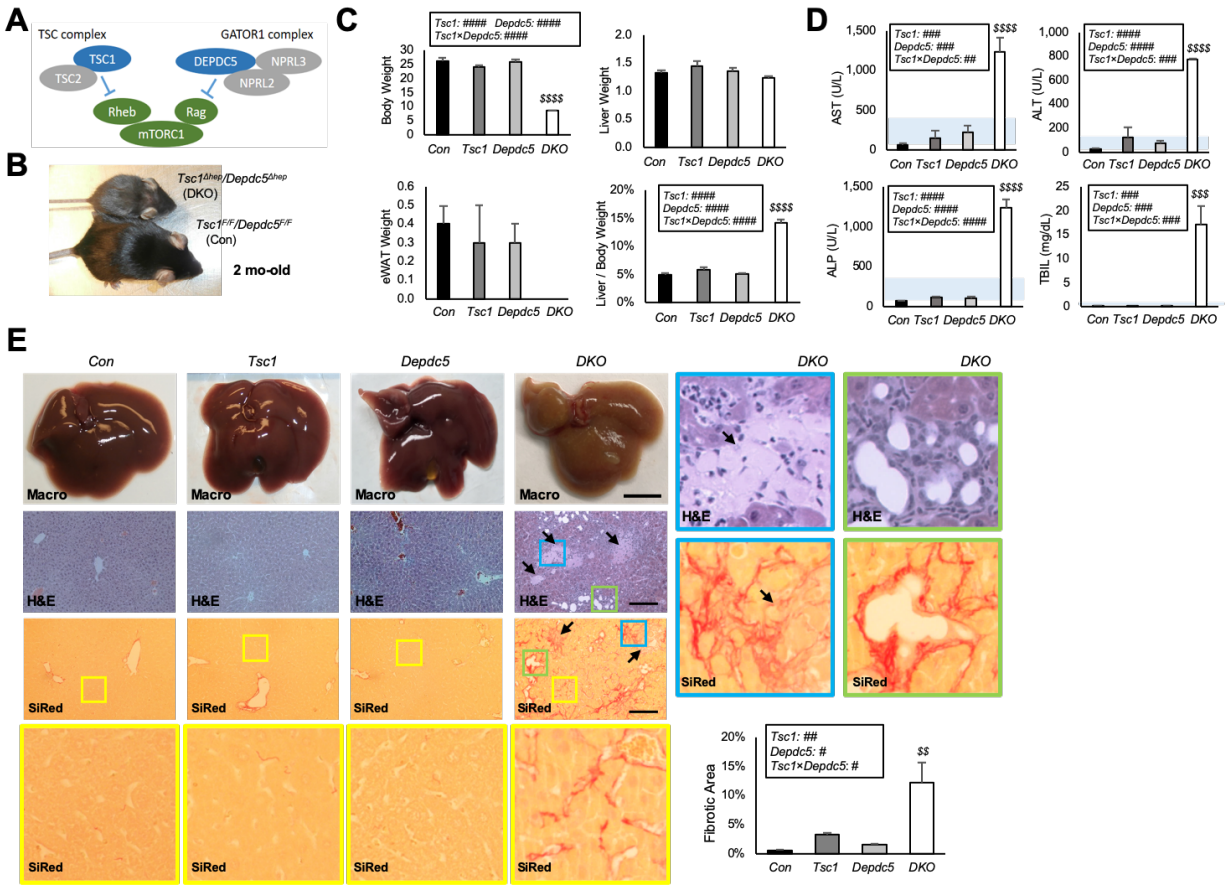

Figure 3.2: *Depdc5* and *Tsc1* mutations synergistically provoke liver injury and damage. Control (*Con*), *Tsc1*$^{\Delta hep}$ (*Tsc1*), *Depdc5*$^{\Delta hep}$ (*Depdc5*) and *Tsc1*$^{\Delta hep}$/*Depdc5*$^{\Delta hep}$ (*DKO*) male mice were generated as littermates and analyzed at two-months-old (n≥3). **(A)** Schematic of how the Rheb and Rag pathways regulate mTORC1. **(B)** Gross appearance of *Con* and *DKO* littermates. **(C)** Body weight, liver weight, epididymal white adipose tissue (eWAT) weight and liver/body weight ratios. **(D)** Serum liver panel assays. Blue shaded regions indicate clinically normal ranges. **(E)** Macroscopic view of liver (Macro), H&E staining and Sirius Red (SiRed) staining of liver sections. Arrows indicate necrotic lesions. Yellow boxed areas are magnified in the corresponding bottom row. Blue and green boxed areas are magnified in right panels. Sirius Red-positive fibrotic areas were quantified. Data are shown as mean ± SEM. Effects of *Tsc1* and *Depdc5* mutations and their interaction (*Tsc1*×*Depdc5*) were assessed through two-way ANOVA (#, P<0.05; ##, P<0.01; ###, P<0.001; ####, P<0.0001), and statistical significance between *Con* and indicated groups were assessed through Tukey's multiple comparison test (*$$*, P<0.01; *$$$*, P<0.001; *$$$$*, P<0.0001). Scale bars, 200 μm (histology) and 1 cm (whole liver).

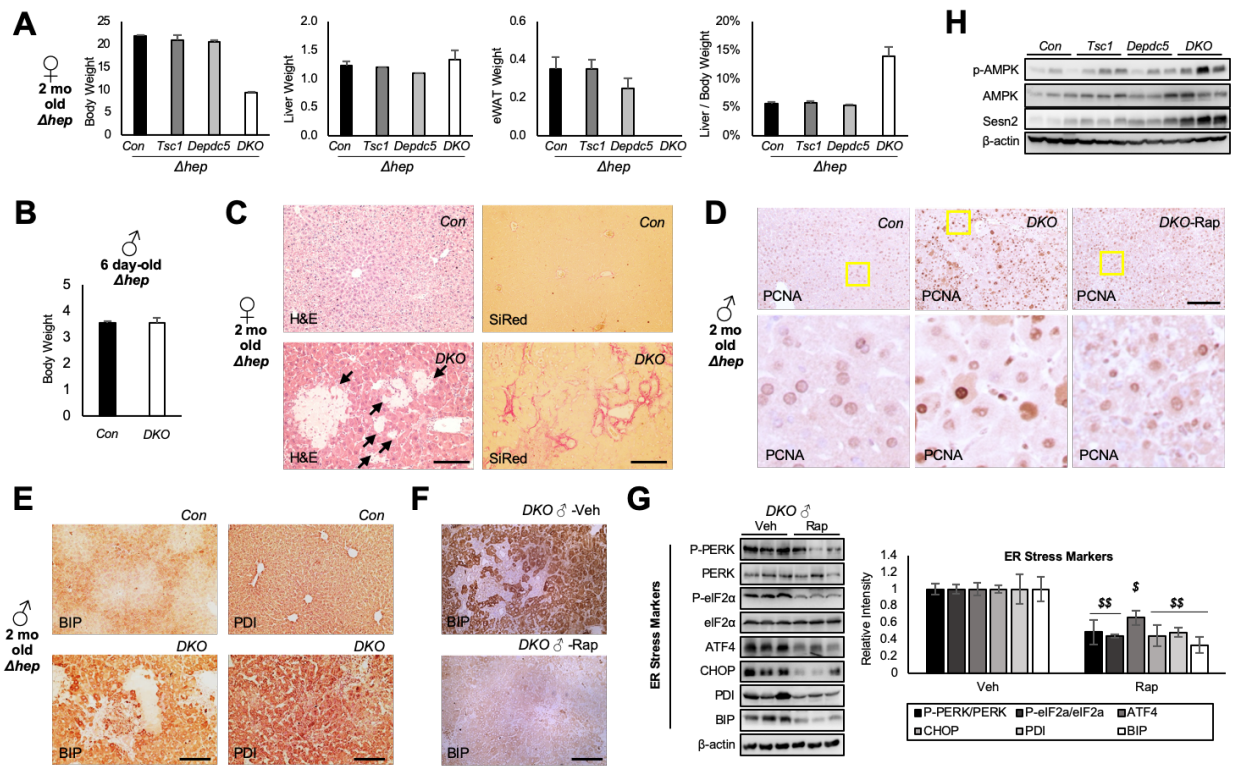

Figure S3.2: DKO mice exhibit mTORC1-dependent liver pathologies. (A) Body, liver, eWAT weights, and liver/body weight ratios were analyzed for females of the Fig. 3.2 cohort (n≥3 for Con and DKO; n=2 for single knockouts). **(B)** Body weights were analyzed for male pups at 6 days after birth (n≥3). **(C)** H&E and SiRed staining images from livers of the Fig. 3.2 female cohort. **(D, E)** PCNA **(D)**, BIP and PDI **(E)** immunostaining images from livers of the Fig. 3.2 male cohort. Boxed areas are magnified in bottom panels **(D)**. **(F)** BIP immunostaining images from livers of the Fig. 3.4 cohort. **(G)** Immunoblotting of ER stress markers (left panel) and quantification (right panel, n=3) for livers of the Fig. 3.4 cohort. β-actin image is the same as the one presented in Fig. 3.4f. **(H)** Immunoblotting of indicated proteins for livers of the Fig. 3.3 cohort. Data are presented as mean ± SEM. The Holm-Šídák method was used for multiple comparison tests ($, $P<0.05$; $$, $P<0.01$). Scale bars, 200 μm.

Further characterization of liver tissues with TUNEL staining revealed increased apoptotic cells in DKO liver (Figure 3.3a). In addition, both histology and immunoblot analyses confirmed that DKO livers had an increased expression of fibrogenic markers, significantly more than single knockouts (Figure 3.3B, 3.3C). Finally, we analyzed mTORC1 signaling by monitoring phosphorylation of its substrates, S6K and 4E-BP1. Although phosphorylation of these targets were upregulated in *Depdc5*$^{\Delta hep}$ and *Tsc1*$^{\Delta hep}$, DKO mouse liver exhibited synergistic activation, at levels far beyond the level achieved by single knockout littermates (Figure 3.3D). This was not a simple, additive effect as the level of synergism was robust and statistically supported through two-way ANOVA (Figure 3.3D). Therefore, concomitant activation of the Rheb and Rag pathways produced a strong genetic interaction and synergistically increased fibrosis and upregulated mTORC1 (Figure 3.3).

mTORC1 inhibition rescues DKO liver pathologies

To test whether the pathological synergy of *Tsc1* and *Depdc5* mutations was due solely to mTORC1 hyperactivation, we injected DKO mice with rapamycin, a chemical inhibitor of mTORC1. Interestingly, during the course of rapamycin administration, DKO mice resumed normal growth (Figure 3.4A). After 10 days of rapamycin administration, liver/body weight ratios (Figure 3.4B), as well as all serum markers of liver damage and dysfunction (Figure 3.4C), showed dramatic recovery, indicating that mTORC1 hyperactivation is indeed the major cause of liver pathologies observed in DKO mice. Further confirming these observations, liver histology (Figure 3.4D) and immunoblotting (Figure 3.4D-F) indicated that 10 days of rapamycin administration was sufficient to rescue all examined liver pathologies, including mTORC1 hyperactivation (Figure 3.4E), liver injury, inflammation and fibrosis (Figure 3.4D-F).

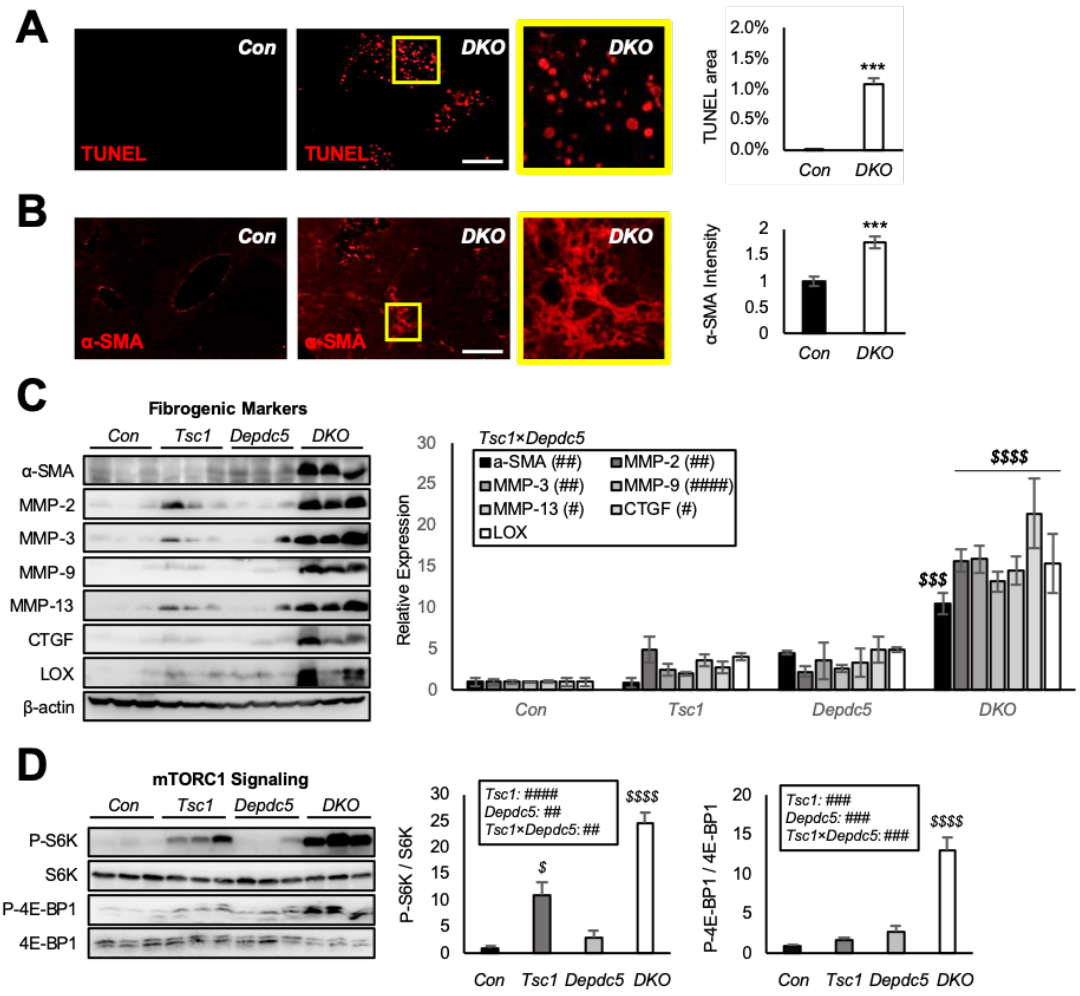

Figure 3.3: *Depdc5*/*Tsc1* double knockout (DKO) livers upregulate fibrosis and mTORC1 signaling. Mouse cohort described in Fig. 3.2 was subjected to histology **(A, B)** and immunoblotting **(C, D)** as outlined below. **(A)** TUNEL staining of liver sections. Boxed area is magnified in right panel. TUNEL-positive areas were quantified. **(B)** Liver sections were subjected to α-SMA staining. Boxed area was magnified in right panel. α-SMA staining intensities were quantified. **(C)** From the liver lysates, fibrogenic marker expression was analyzed through immunoblotting. Band intensities were quantified (n=3). **(D)** From the liver lysates, phosphorylation of mTORC1 substrates were analyzed through immunoblotting. Band intensities were quantified (n=3, mean ± SEM). Data are shown as mean ± SEM. ***$P < 0.001$ (Student's t-test). Effects of *Tsc1* and *Depdc5* mutations and their interaction (*Tsc1*×*Depdc5*) were assessed through two-way ANOVA (#, $P<0.05$; ##, $P<0.01$; ###, $P<0.001$; ####, $P<0.0001$), and statistical significance between *Con* and indicated groups were assessed through Tukey's multiple comparison test (*$*, $P<0.05$; *$$$*, $P<0.001$; *$$$$*, $P<0.0001$). Scale bars, 200 μm.

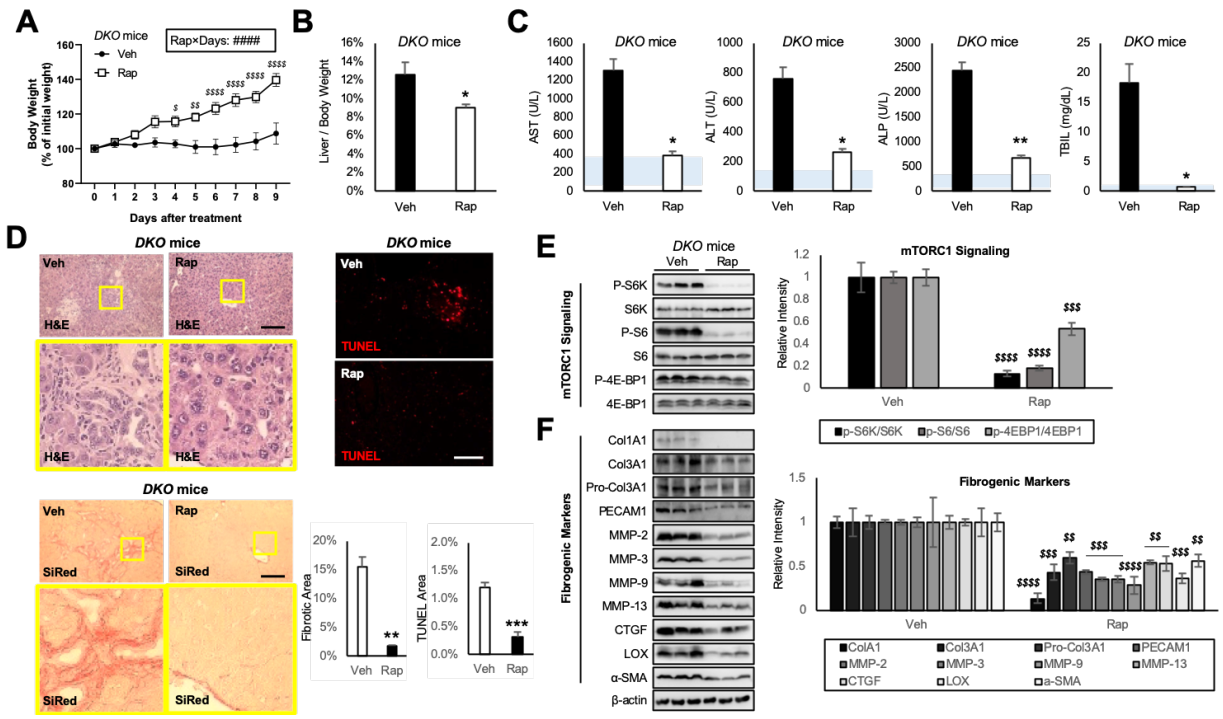

Figure 3.4: mTORC1 inhibition rescues DKO liver pathologies. Littermate cohorts of six-week-old DKO mice were injected daily with vehicle (Veh) or 10 mg/Kg rapamycin (Rap) for 10 days (n≥4). For drug treatment experiments, mice were gender-matched with both males and females. **(A)** Body weight was monitored throughout the course of the experiment. **(B)** Liver/body weight ratio was measured at the experimental endpoint. **(C)** Serum markers for liver damage were analyzed. Blue shaded regions indicate clinically normal ranges. **(D)** Liver sections were analyzed by H&E, SiRed, and TUNEL staining. Boxed areas are magnified in lower panels. Fibrotic area and TUNEL area were quantified (n=3). **(E, F)** Liver lysates were subjected to immunoblotting (left panels) and quantification (right panels) to examine mTORC1 signaling **(E)** and fibrogenic markers **(F)**. Data are shown as mean ± SEM. $*P < 0.05$; $**P < 0.01$; $***P < 0.001$ (Student's t-test). Interaction between rapamycin and treatment days (Rap×Days) were assessed through RM two-way ANOVA (####, P<0.0001), and differences in individual data points were assessed through Sidak's multiple comparison test ($, P<0.05; $$, P<0.01; $$$$, P<0.0001). For western blot quantification, the Holm-Šídák method was used to compare groups ($$, P<0.01; $$$, P<0.001; $$$$, P<0.0001). Scale bars, 200 μm.

DKO liver pathologies are associated with elevated PCNA staining (Supplementary Figure S3.2D), which reflects regenerative responses to injury and damage. Rapamycin did not further elevate the PCNA staining intensity (Supplementary Figure S3.2D), indicating that it relieves DKO pathologies mainly by restoring hepatocellular homeostasis, but not by promoting liver regeneration.

Relieving ER stress unexpectedly aggravated DKO liver pathologies

Upregulated mTORC1 is known to increase ER stress (23). Consistent with this, DKO livers exhibited prominent ER stress marker activation (Figure 3.5A and Supplementary Figure S3.2E), significantly stronger than *Tsc1* or *Depdc5* single knockouts (Figure 3.5A). ER stress marker activation was strongly suppressed by rapamycin treatment (Supplementary Figure S3.2F, G), indicating that mTORC1 hyperactivation in DKO livers provokes ER stress.

ER stress can be mitigated using chemical chaperones, such as tauroursodeoxycholic acid (TUDCA), which facilitates nascent protein folding in vivo (24,25). Therefore, we injected DKO mice with TUDCA to relieve ER stress. Unexpectedly, more than half of the mice died during the 10 days of TUDCA administration (Figure 3.5B). This was surprising because previous work showed that TUDCA injection was beneficial for WT mice, not lethal (24,25). In addition, the surviving mice exhibited even greater liver/body weight ratios (Figure 3.5C) and more severe liver histopathology associated with increased area of necrotic and fibrotic lesions (Figure 3.5D).

In light of these observations, we questioned if TUDCA actually relieved ER stress in DKO mice. Immunoblotting showed that despite aggravated phenotypes, TUDCA generally reduced hepatic ER stress (Figure 3.5E, top). Many ER stress markers, p-PERK, p-eIF2α, ATF4 and BIP,

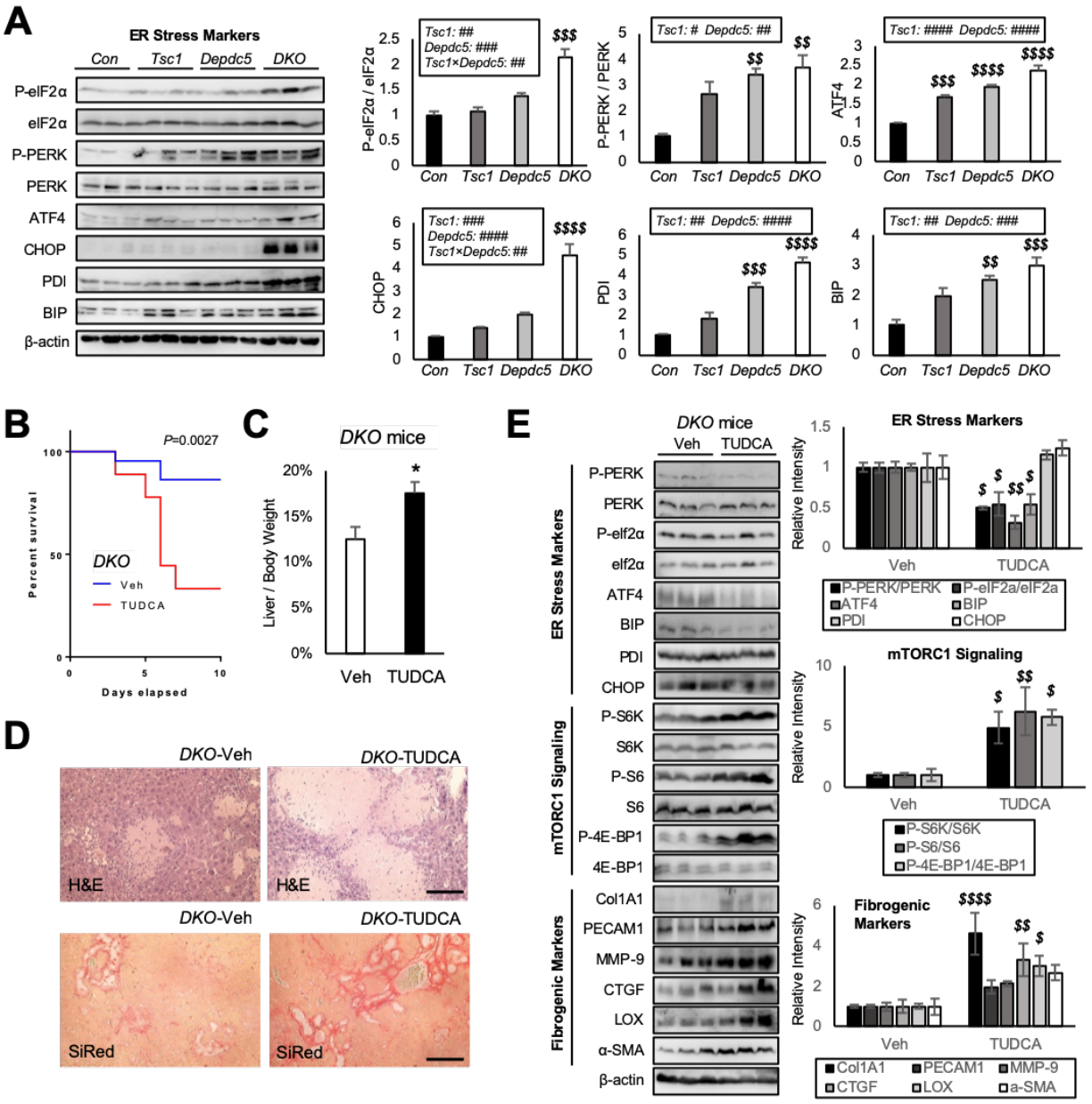

Figure 3.5: Relieving ER stress unexpectedly aggravated DKO liver pathologies. Mouse cohort described in Fig. 3.2 was subjected to immunoblotting **(A)**. Six-week-old DKO mice were injected daily with vehicle (Veh) or 500 mg/Kg TUDCA for 10 days (**B-E**; n≥9). For drug treatment experiments, mice were gender-matched with both males and females. **(A)** ER stress signaling markers were examined from the indicated liver lysates through immunoblotting (left panels) and quantification (right panels). **(B)** Mouse survival was monitored throughout the course of the experiment. The *P* value was calculated through a log-rank test. **(C)** Liver/body weight ratio was measured at the experimental endpoint. **(D)** Liver sections were analyzed through H&E and SiRed staining. **(E)** Liver lysates were subjected to immunoblotting (left panels) and quantification (right panels) to examine ER stress signaling (top), mTORC1 signaling (middle) and fibrogenic markers (bottom). Data are presented as mean ± SEM (n≥3) or actual values (**B**). **P*<0.05 (Student's t-test). Effects of *Tsc1* and *Depdc5* mutations and their interaction (*Tsc1*×*Depdc5*) were

assessed through two-way ANOVA (#, $P<0.05$; ##, $P<0.01$; ###, $P<0.001$; ####, $P<0.0001$), and statistical significance between *Con* and indicated groups were assessed through Tukey's multiple comparison test (*$$*, $P<0.01$; *$$$*, $P<0.001$; *$$$$*, $P<0.0001$). For western blot quantification, the Holm-Šídák method was used to compare groups (*$*, $P<0.05$; *$$*, $P<0.01$; *$$$$*, $P<0.0001$). Scale bars, 200 μm.

were significantly downregulated after TUDCA treatment; however, some markers, PDI and CHOP, did not change. Interestingly, mTORC1 signaling markers were all upregulated after TUDCA treatment (Figure 3.5E, middle), suggesting that the presence of ER stress signaling limited mTORC1 activation. Expression of fibrogenic genes increased after TUDCA treatment (Figure 3.5E, bottom), consistent with the observation that TUDCA and ER stress reduction actually worsened liver pathologies. These results indicate that ER stress is not a major conduit of DKO liver injury but may function as a negative feedback to limit mTORC1 activation.

The DKO transcriptomic profile is distinct from those of control and single knockouts

Due to the unexpected results from ER stress suppression, we tried to approach pathogenetic mechanisms underlying DKO phenotypes more systematically. Therefore, we determined the transcriptomic profiles of livers from control, *Tsc1*$^{\Delta hep}$, *Depdc5*$^{\Delta hep}$, and DKO mice through RNA sequencing (Supplementary Table S1, available at: https://doi.org/10.1038/s41421-019-0131-9). Although *Tsc1*$^{\Delta hep}$ and *Depdc5*$^{\Delta hep}$ mice showed modest transcriptomic changes from control mice, DKO mice showed stronger deviations from the control liver transcriptomic profile (Figure 3.6A). Heat map analysis of the correlations between individual datasets further demonstrated that DKO livers have a unique transcriptome profile that are most strongly correlated with each other, but not as strongly with controls or single knockouts (Supplementary Figure S3.3A). Principal component analysis of all experimental replicates also indicated that *Con*, *Tsc1*$^{\Delta hep}$ and *Depdc5*$^{\Delta hep}$ samples exhibited relatively similar transcriptomic profiles, while DKO samples displayed a highly distinct profile (Figure 3.6B). Likewise, although transcriptomic changes induced by single deletion of *Tsc1* or *Depdc5* correlated relatively well, DKO-induced changes had lower correlations with either single knockout-induced changes (Supplementary

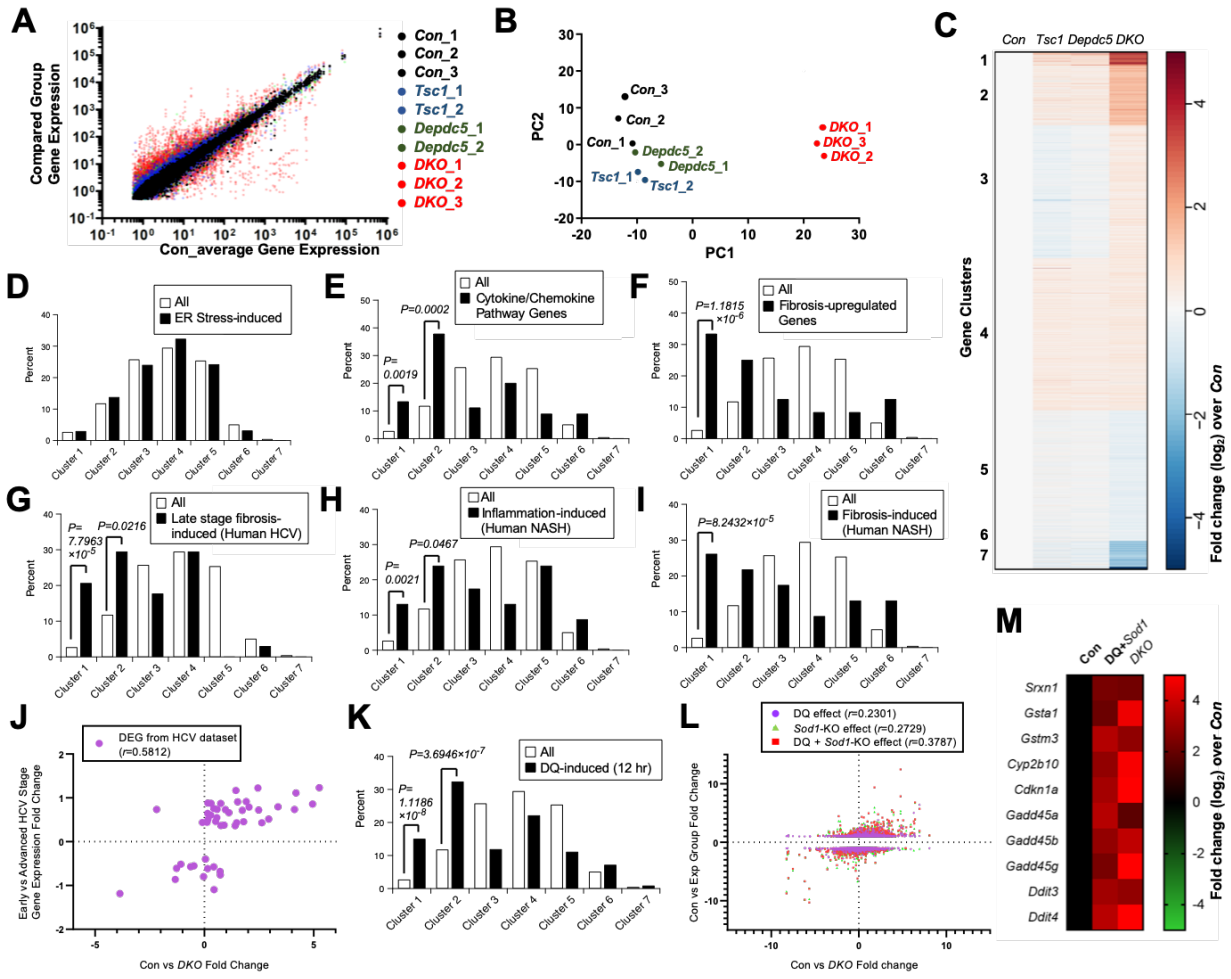

Figure 3.6: *Depdc5*/*Tsc1* double knockout (DKO) livers have distinct transcriptome profiles from single knockouts and specifically upregulate oxidative stress genes. Mouse cohort described in Fig. 3.2 was subjected to RNA-seq analyses. **(A)** Comparison of gene expression between averaged control profile and individual RNA-seq profiles from liver tissues of control (n=3), *Tsc1*$^{\Delta hep}$ (n=2), *Depdc5*$^{\Delta hep}$ (n=2) and DKO (n=3) mice. Each dot represents a single mRNA species in a dataset that is color-coded. For correlations between the datasets, see Supplementary Fig. S3.3a. **(B)** Principal component analysis (PCA) depicting the relationship between individual RNA-seq profiles. Each dot represents an entire RNA-seq profile from a single liver sample. Distinction is depicted spatially; similar profiles are clustered close together, while different profiles are located far from each other. **(C)** Transcript clusters were generated using a *k*-means algorithm (n = 7), using mRNA expression fold change values of *Tsc1*, *Depdc5,* and *DKO* samples over *Con* samples. **(D-I, K)** Bar graphs representing the distribution of all genes (white bars) and ER stress-inducible genes **(D)**, cytokine/chemokine pathway genes **(E)**, fibrosis-associated genes **(F)**, genes upregulated in late-stage fibrosis during human HCV infection **(G)**, genes upregulated in human NASH with lobular inflammation **(H)**, genes upregulated in human NASH with fibrosis **(I)** or genes induced in mouse liver at 12 hours after diquat (DQ) treatment **(K)**. Gene enrichments in clusters 1 and 2 were examined by Fisher's exact test, and *P* values were indicated on the graphs. **(J, L)** Comparison of gene expression fold changes induced in DKO livers (X axis in both panels)

and HCV pathology progression **(J)** or DQ injection, *Sod1* mutation and both **(L)**. Correlations were assessed by computing a nonparametric Spearman correlation (*r*); *P*<0.0001 for all correlation observations. **m,** List of representative genes that are consistently upregulated by DQ + *Sod1* mutation and DKO mutation. Heat map diagrams represent mRNA expression fold change from averaged control values (expressed as $\log_2$ values).

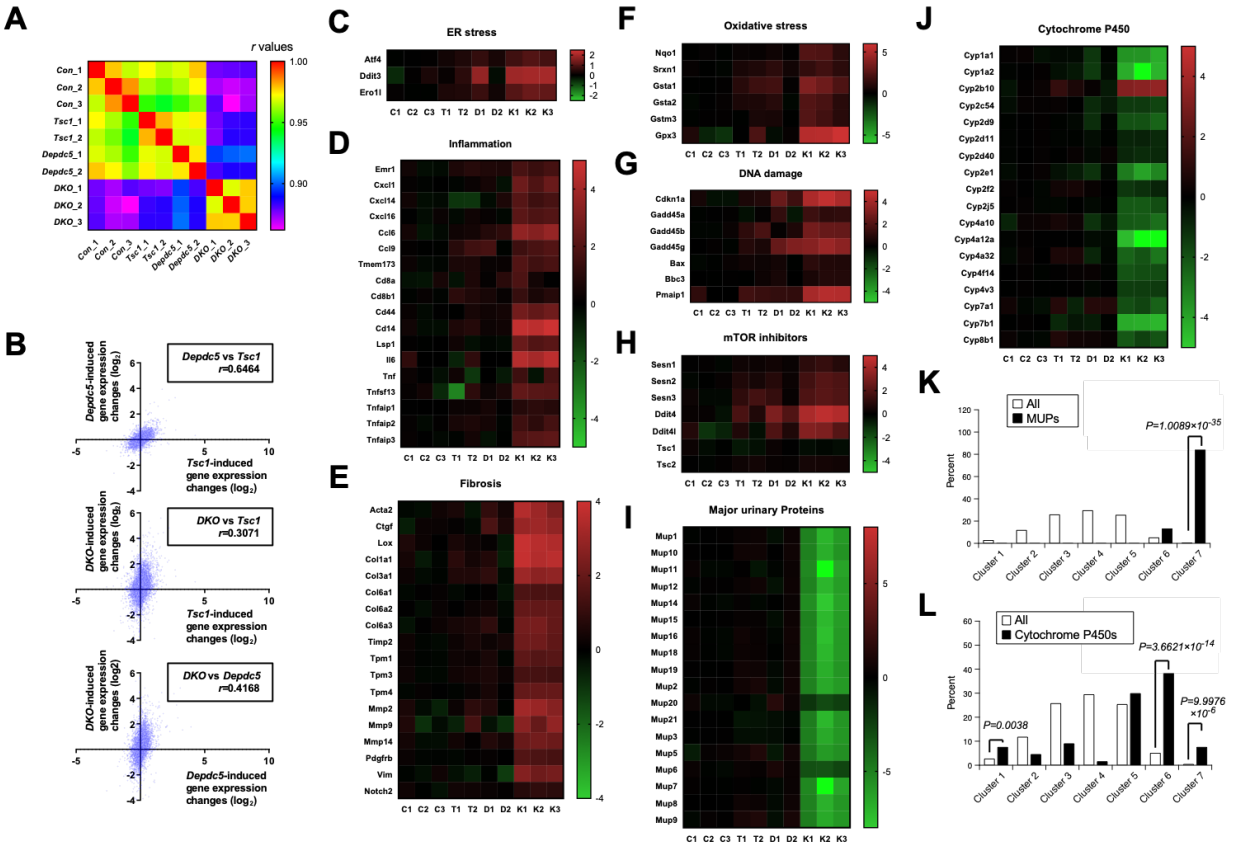

Figure S3.3: The DKO transcriptome profile is distinct from controls and single knockout mutants and is characterized by stress response. (A) Heat map diagram depicting the correlation between individual RNA-seq profiles. **(B)** Comparison of mRNA expression fold change over control liver samples between indicated liver samples. Individual dots represent single mRNA species. **(C-J)** Heat map diagrams representing mRNA expression fold change from averaged control values (expressed as log2 values). Each column represents a liver sample from a different *Con* (C1-3), *Tsc1*$^{\Delta hep}$(T1-2), *Depdc5*$^{\Delta hep}$(D1-2), or *DKO* (K1-3) mouse. **(K)** Gene cluster enrichment analysis of major urinary proteins (MUPs). **(L)** Gene cluster enrichment analysis of Cytochrome P450s. Correlations between RNA-seq datasets were assessed by computing a nonparametric Spearman correlation (*r*); *P*<0.0001 for all correlation observations. Statistical significance of gene enrichments in a specific cluster was examined by Fisher's exact test.

Figure S3.3B). All of these results congruently indicate that DKO livers have transcriptomic profiles distinct from control or single knockout liver tissues.

The DKO liver resembles diseased human livers with inflammation and fibrosis

To understand the nature of DKO-specific transcriptome differences, we classified the genes into 7 different categories through *k*-means clustering, according to their expression changes in *Tsc1*$^{\Delta hep}$, *Depdc5*$^{\Delta hep}$, and DKO livers (Figure 3.6C and Supplementary Table S2, available at: https://doi.org/10.1038/s41421-019-0131-9). Among the 7 clusters, only a small number of genes were strongly and consistently upregulated, clusters 1 and 2, or downregulated, clusters 6 and 7, in DKO mice (Figure 3.6C). Consistent with our immunoblotting findings (Figure 3.5A), ER stress-responsive genes, such as *Atf4* and *Chop/Ddit3*, were most upregulated in DKO mice (Supplementary Figure S3.3C). However, when we analyzed the whole known set of ER stress-inducible genes (26), they were not overrepresented in clusters 1 and 2 (Figure 3.6D), indicating that ER stress activation is not the major transcriptomic feature characterizing the DKO phenotype. This supports our pharmacological experiment showing that ER stress was not the conduit of liver pathology in DKO mice (Figure 3.5).

In contrast to this, genes belonging to cytokine and chemokine signaling pathways were highly enriched in clusters 1 and 2 (Figure 3.6E) and prominently upregulated in DKO livers (Supplementary Figure S3.3D), indicating that inflammatory pathways characterize the DKO transcriptome. In addition, genes upregulated during tissue fibrosis, such as collagens, matrix metalloproteinases (MMPs), tissue inhibitors of metalloproteinase (TIMPs) and TGF-beta pathway genes, were also highly enriched in clusters 1 and 2 (Figure 3.6F) and induced in DKO

livers (Supplementary Figure S3.3E). These are consistent with the extensive liver damage and fibrosis phenotypes we observed in the DKO mice.

Based on these observations, we were curious if the gene expression changes in DKO mouse livers had any resemblance to those induced by inflammation and fibrosis in human liver diseases. For this, we utilized recently published transcriptome profile datasets that were constructed using fibrotic human liver tissues associated with HCV infection (27) or nonalcoholic steatohepatitis (NASH) (28). Genes upregulated in late-stage fibrosis during HCV infection (Figure 3.6G), lobular inflammation (Figure 3.6H) and fibrosis (Figure 3.6I) in NASH were highly enriched in clusters 1 and 2 (Figure 3.6G-I). Since cluster 1 and 2 genes are strongly upregulated in the DKO mouse liver (Figure 3.6C), these results indicate that DKO mouse liver models human inflammatory and fibrotic liver diseases associated with HCV and NASH. Furthermore, the gene expression changes associated with HCV fibrosis progression showed positive correlation with the changes induced by DKO (Figure 3.6J). These results collectively indicate that DKO mice experience severe liver inflammation and fibrosis, transcriptomically similar to those associated with human HCV and NASH pathologies.

Oxidative damage response pathways were upregulated in the DKO transcriptome

Inspection of clusters 1 and 2 identified that, in addition to the upregulated inflammation and fibrosis genes (Supplementary Figure S3.3D, E), oxidative stress (Supplementary Figure S3.3F) and DNA damage (Supplementary Figure S3.3G) response genes were strongly upregulated in DKO mice. Sestrins (*Sesn1-3*) and Redds (*Ddit4* and *Ddit4l*), which are stress-inducible negative feedback regulators of the mTORC1 pathway (10,29), were also upregulated in DKO livers (Supplementary Figure S3.3H). Induction of Sestrin2 was detected at the protein level

(Supplementary Figure S3.2H), and activation of AMPK, a downstream target of Sestrin2, was also observed in DKO livers (Supplementary Figure S3.2H). In contrast, major urinary proteins (Supplementary Figure S3.3I) and cytochrome P450s (Supplementary Figure S3.3J), whose expression is reduced during decreased growth hormone signaling (30) or upon inflammation and oxidative stress (31-33), respectively, were strongly downregulated in DKO mouse liver (Supplementary Figure S3.3K, S3.3L). Although many of the cytochrome P450 genes were downregulated, some genes, such as *Cyp2b10* that is upregulated during hepatic damage and fibrosis (34,35), were upregulated (Supplementary Figure S3.3J) and found in cluster 1 (Supplementary Figure S3.3L). These transcriptomic features indicate that DKO mouse livers specifically upregulate pathways responding to oxidative stress and subsequent DNA damage.

DKO mouse liver exhibits excessive accumulation of superoxide radicals

Upregulation of oxidative stress response genes implicates the presence of oxidative stress. Oxidative damage can precipitate a plethora of liver pathologies through DNA damage, inflammation, fibrosis, liver injury and hepatocyte death (36), which were all observed from the DKO mouse liver. Therefore, we measured the level of hepatic oxidative stress by dihydroethidium (DHE) staining which visualizes superoxide radicals (37). DKO livers had pronounced elevation of DHE staining intensity (Figure 3.7A), which was blunted by rapamycin treatment (Figure 3.7B). Interestingly, DHE intensity became more upregulated when DKO was treated with TUDCA (Figure 3.7C), consistent with upregulation of mTORC1 and aggravation of liver pathologies (Figure 3.5). These results indicate that DKO livers suffer severe oxidative stress with excessive accumulation of superoxide radicals.

Superoxide insults produce transcriptomic changes similar to those of DKO

Superoxides can be formed by toxic chemicals such as diquat (DQ). Endogenous superoxide dismutase (*Sod1*) is important for reducing superoxides and suppressing their toxic effects (38). Genes whose hepatic expression is induced by DQ treatment (38) were highly enriched in clusters 1 and 2 (Figure 3.6K), suggesting that DKO livers upregulated DQ-induced genes. In addition, the gene expression changes induced by DQ treatment, *Sod1* mutation, or both showed a positive correlation at the whole transcriptome level with DKO-induced changes (Figure 3.6L). Accordingly, most of the DQ- and *Sod1* mutation-induced genes were also upregulated in DKO livers, and these genes included those involved in oxidative stress response, DNA damage response and ER stress (Figure 3.6M and Supplementary Figure S3.3). Taken together, we hypothesized that oxidative stress, especially the accumulation of superoxides, was one of the most characteristic features of DKO mouse livers.

Superoxide radicals mediate liver pathologies induced by hyperactive mTORC1

To test whether the superoxide accumulation is the pathological conduit of DKO-induced mTORC1 hyperactivation, we treated the mice with Tempol, a membrane-permeable superoxide dismutase mimetic (39,40). As expected, Tempol was highly effective in reducing DHE staining in DKO liver (Figure 3.7D). Interestingly, Tempol-treated DKO mice exhibited significant weight gain after 5 days of treatment (Figure 3.7E), indicating that like rapamycin, Tempol was able to release the DKO mice from systemic growth suppression. Furthermore, 10 days of Tempol administration was sufficient to reduce liver/body weight ratio (Figure 3.7F), as well as serum markers for liver damage (Figure 3.7G). Tempol also substantially reduced necrotic (Figure 3.7H)

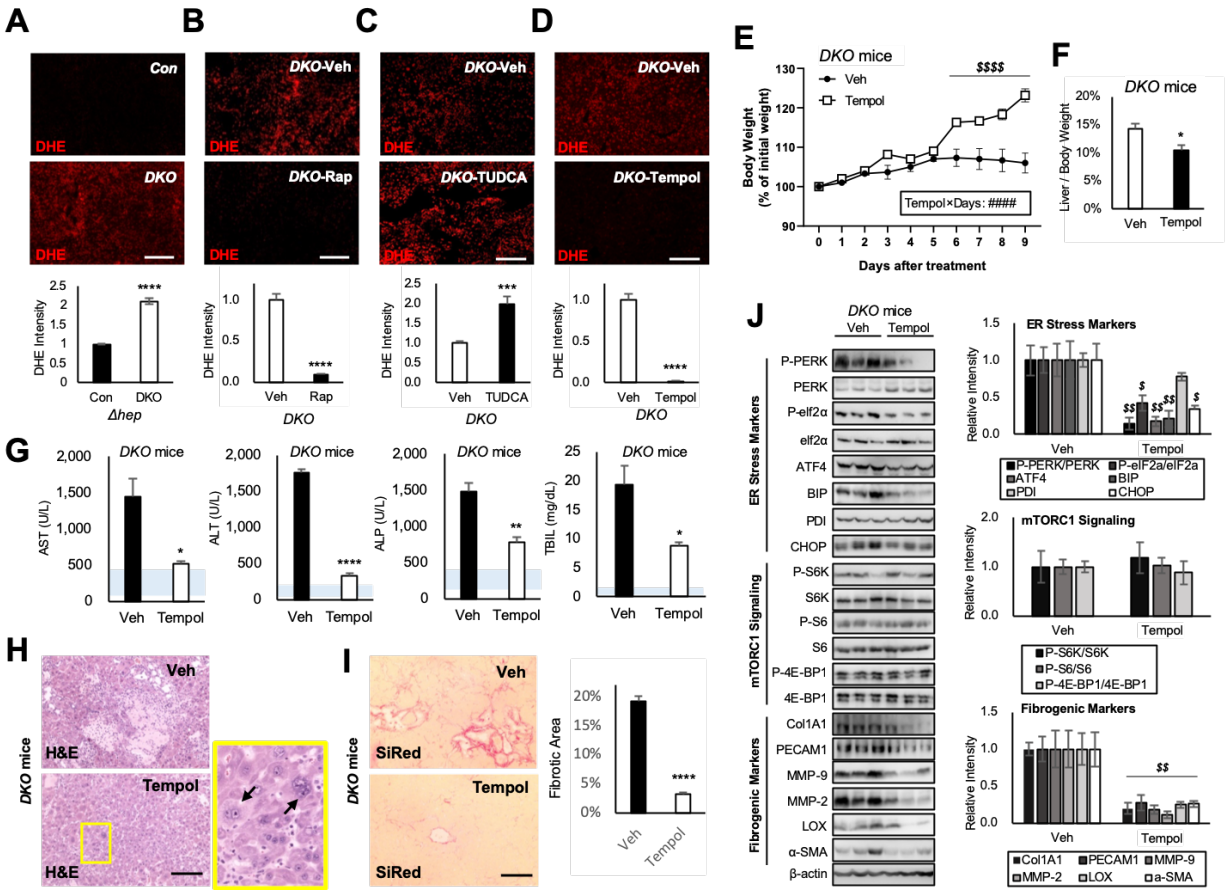

Figure 3.7: Superoxide dismutase mimetic Tempol corrects DKO liver pathologies. Mouse cohorts described in Figure 3.2, 3.4 and 3.5 were analyzed. Littermate cohorts of six-week-old DKO mice were kept on vehicle drinking water (Veh) or 0.064% Tempol-containing water for 10 days (n≥6). For drug treatment experiments, mice were gender-matched with both males and females. **(A-D)** Dihydroethidium (DHE) staining of liver sections and quantification. **(E)** Body weight was monitored throughout the course of the experiment. **(F)** Liver/body weight ratio was measured at the experimental endpoint. **(G)** Serum markers for liver damage were analyzed. Blue shaded regions indicate clinically normal ranges. **(H)** Liver sections were analyzed by H&E staining. Boxed area is magnified in right panel. **(I)** Liver sections were analyzed by SiRed staining. Fibrotic areas were quantified. **(J)** Liver lysates were subjected to immunoblotting (left panels) and quantification (right panels) to examine ER stress markers (top), mTORC1 signaling (middle), and fibrogenic markers (bottom). Data are presented as mean ± SEM (n=3). **P* < 0.05; ***P* < 0.01; ****P* < 0.001; *****P* < 0.0001 (Student's t-test). Interaction between Tempol and treatment days (Tempol×Days) were assessed through RM two-way ANOVA (####, P<0.0001), and differences in individual data points were assessed through Sidak's multiple comparison test (*$$$$*, *P*<0.0001). For western blot quantification, the Holm-Šídák method was used to compare groups (*$*, *P*<0.05; *$$*, *P*<0.01;). Scale bars, 200 μm.

and fibrotic (Figure 3.7I) lesions exhibited by the DKO mouse liver (Figure 3.7H, 3.7I). These observations were supported through western blot analyses, where Tempol treatment strongly reduced fibrotic marker expression in DKO mice (Figure 3.7J). Interestingly, ER stress marker expression was also decreased by Tempol, indicating that superoxide accumulation also contributed to the mTORC1-induced ER stress (Figure 3.7J). However, phosphorylation of mTORC1 downstream targets was not suppressed by Tempol, confirming that Tempol specifically reduced superoxide accumulation without affecting mTORC1 signaling (Figure 3.7J). Consistent with the observation that mTORC1 is still hyperactivated, Tempol administration did not suppress hepatocyte hypertrophy (Figure 3.7H, arrows), while other pathological features were substantially suppressed (Figure 3.7E-J).

Suppression of liver pathologies was again observed when DKO mice were treated with N-acetylcysteine (NAC), another antioxidant that scavenges superoxide radicals (Supplementary Figure S3.4). Collectively, these results indicate that production of reactive oxygen species, such as superoxide radicals, is the major pathological conduit of how hyperactive mTORC1 in DKO mice induces liver injury and precipitates pathologies.

DKO mice have defective glucose metabolism and hepatic insulin resistance.

DKO mice experienced hypoglycemia (Figure 3.8A and Supplementary Figure S3.5A), likely due to hepatic dysfunction and subsequent reduction in hepatic glucose output. Blood glucose levels of DKO mice were not reduced in response to insulin (Figure 3.8B and Supplementary Figure S3.5B, S3.5C), and DKO hepatocytes in intact livers did not activate AKT in response to insulin stimulation (Figure 3.8C). One potential explanation for this is due to

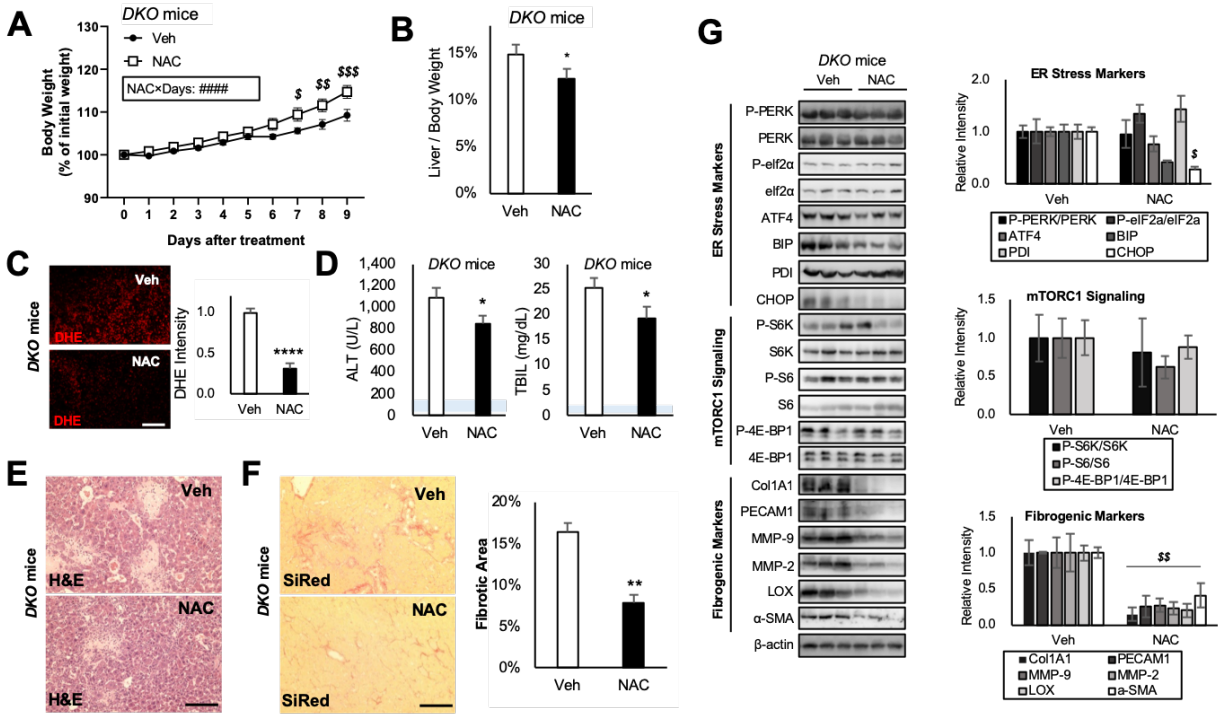

Figure S3.4: N-acetylcysteine (NAC) relieves DKO liver pathologies. Littermate cohorts of six-week-old DKO mice were injected daily with vehicle (Veh) or NAC (250 mg/kg) for 10 days (n≥10). For drug treatment experiments, mice were gender-matched with both males and females. **(A)** Body weight was monitored throughout the course of the experiment. **(B)** Liver/body weight ratio was measured at the experimental endpoint. **(C)** Dihydroethidium (DHE) staining of liver sections and quantification. **(D)** Serum markers for liver damage were analyzed. Blue shaded regions indicate clinically normal ranges. **(E)** Liver sections were analyzed by H&E staining. **(F)** Liver sections were analyzed by SiRed staining. Fibrotic areas were quantified. **(G)** Liver lysates were subjected to immunoblotting (left panels) and quantification (right panels) to examine ER stress markers (top), mTORC1 signaling (middle), and fibrogenic markers (bottom). Data are presented as mean ± SEM. **P* < 0.05; ***P* < 0.01; *****P* < 0.0001(Student's t-test). Interaction between NAC and treatment days (NAC×Days) were assessed through RM two-way ANOVA (####, P<0.0001), and differences in individual data points were assessed through Sidak's multiple comparison test (*$*, *P*<0.05; *$$*, *P*<0.01; *$$$*, *P*<0.001). For western blot quantification, the Holm-Šídák method was used to compare groups (*$*, *P*<0.05; *$$*, *P*<0.01). Scale bars, 200 μm.

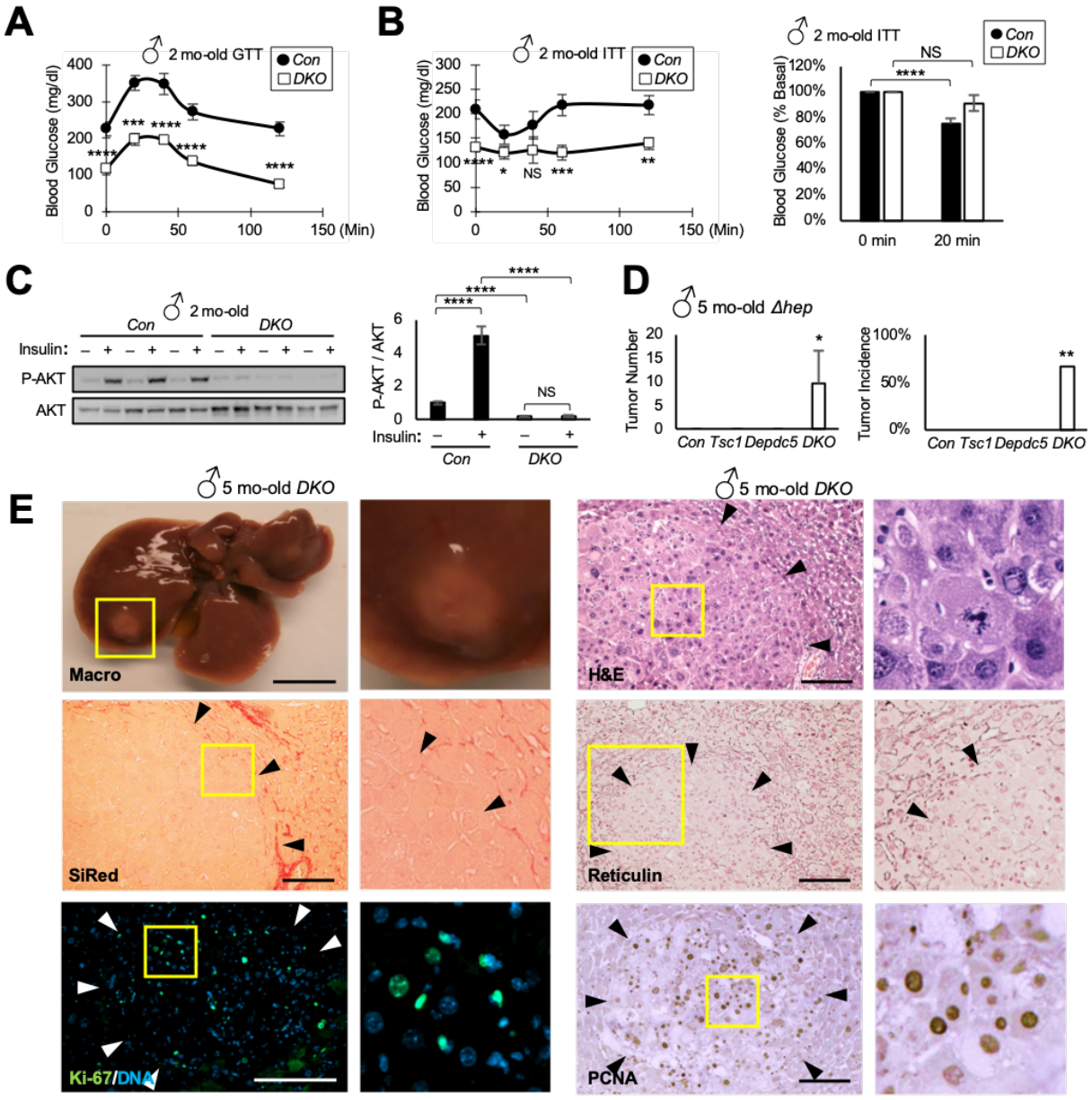

Figure 3.8: *Depdc5*/*Tsc1* double knockout mice exhibit insulin resistance and hepatocellular carcinoma. (A-C) After 4-6 hours of fasting, Two-month-old Con and DKO littermates (n≥9) were subjected to **(A)** glucose and **(B)** insulin tolerance tests (GTT and ITT, respectively). Data are normalized according to baseline glucose levels (**B**, right). **(C)** Livers were collected from Con and DKO littermates, after 4 hrs of fasting, before (–) or 5 min after (+) an insulin injection, homogenized and analyzed through immunoblotting (left) and quantification (right; n=6). **(D)** Tumor number and incidence of the indicated five-month-old mice (n≥3). All mouse strains except DKO were free of liver tumor. **(E)** Macroscopic images (Macro) and histology images of H&E, SiRed, Reticulin, Ki-67 and PCNA staining were shown for five-month-old DKO mouse livers. Arrowheads indicate approximate boundaries of tumor nodules. Boxed areas are magnified in right panels. Data are presented as mean ± SEM. **P*<0.05, ***P*<0.01, ****P*<0.001, *****P*<0.0001, NS

(*P*=0.0712, 0.1799 and 0.6796 in **B**-left, **B**-right and **C**, respectively) from a Student's t-test. Scale bars, 200 µm (histology) and 1 cm (whole liver).

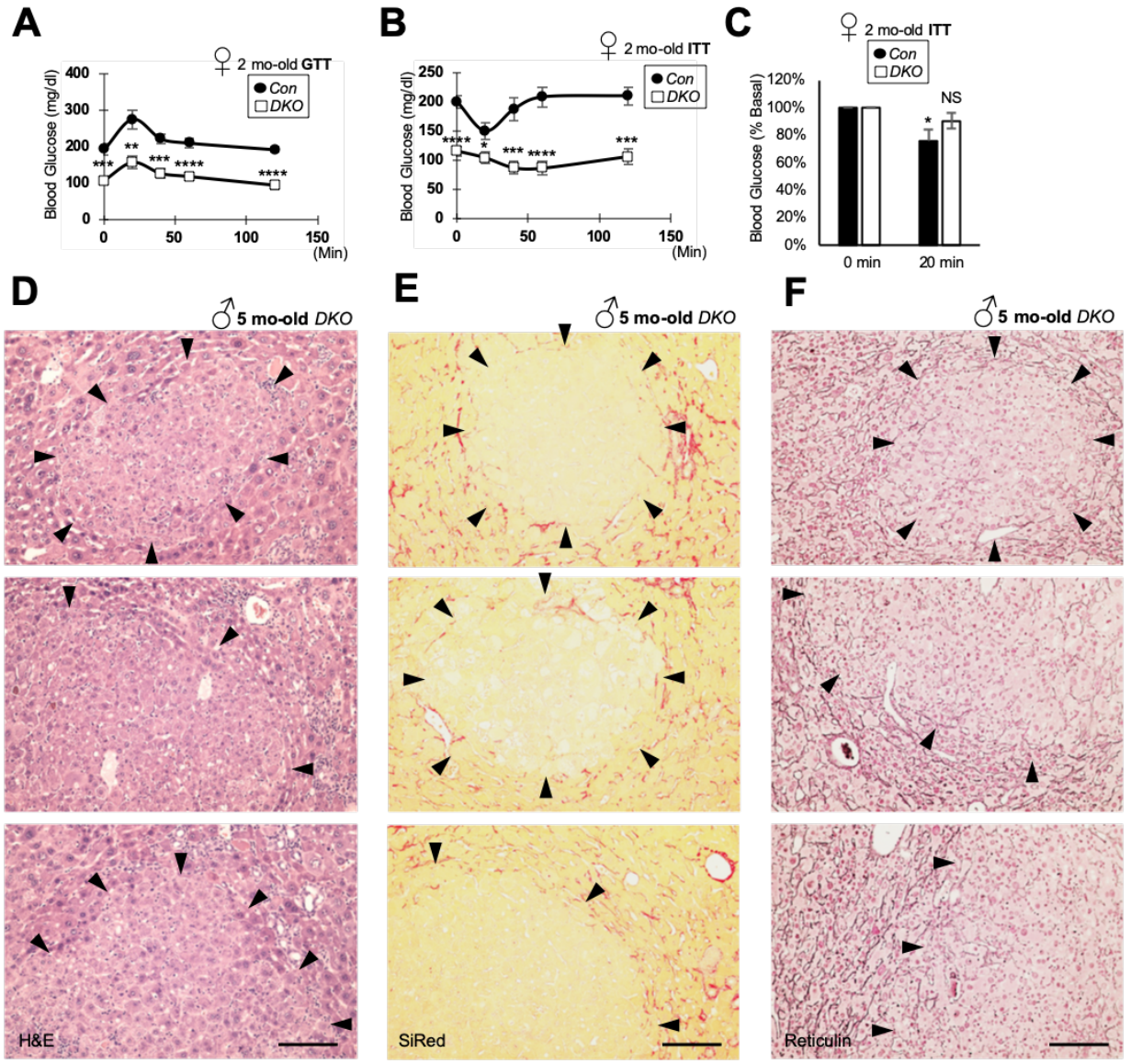

Figure S3.5: *DKO* mice have glucose metabolism defects and HCC development. (A-C) After 4-6 hours of fasting, two-month-old *Con* and *DKO* female littermates (n≥7) were subjected to (**a**) glucose and **(B)** insulin tolerance tests (GTT and ITT, respectively). Data are normalized according to baseline glucose levels **(C)**. **(D-F)** Additional histology images for Figure 3.8E upper right **(D)**, 8E middle left **(E)** and 8E middle right **(F)** are presented. Arrowheads indicate approximate boundaries of tumor nodules. Data are presented as mean ± SEM. **P*<0.05, ***P*<0.01, ****P*<0.001, *****P*<0.0001, NS (*P*=0.1050) from a Student's t-test. Scale bars, 200 µm.

mTORC1 and ER stress hyperactivation, both of which are known to provoke insulin resistance by blocking the insulin receptor-AKT pathway (24,41).

DKO mice develop hepatocellular carcinoma.

Although *Depdc5*$^{\Delta hep}$ or *Tsc1*$^{\Delta hep}$ mice developed mild inflammation at 5-6 months (Figure 3.1) (18), they did not exhibit liver cancer until they reached 9-15 months (17,18). Since DKO mice experienced more pronounced liver damage at a much earlier age, we hypothesized that DKO livers would more quickly progress to liver cancer. Indeed, five-month-old mice revealed macroscopically visible liver tumors (Figure 3.8D, 3.8E, Macro). More tumor nodules were discovered in histological sections (Figure 3.8E, H&E, and Supplementary Figure S3.5D), which frequently displayed atypical mitotic features (Figure 3.8E, H&E right panel). The nodules were surrounded by fibrotic tissue, but the nodules themselves were devoid of fibrosis (Figure 3.8E, SiRed, and Supplementary Figure S3.5E). Most of these nodules also displayed markedly decreased reticulin staining (Figure 3.8E, Reticulin, and Supplementary Figure S3.5F) and elevated frequency of Ki-67 and PCNA staining (Figure 3.8E, Ki-67 and PCNA), indicating that they are indeed hepatocellular carcinoma.

Discussion

mTORC1 is a protein kinase important for liver metabolism and is regulated by two small GTPases, Rheb and Rag (1-4). Rheb mediates growth factor regulation, while Rag mediates stress and nutrient control. Although the Rheb and Rag pathways were extensively studied, there have been no genetic studies of whether these two pathways interact for physiological mTORC1 regulation in an intact multicellular organism.

Rheb and Rag are regulated by their respective GAPs, TSC and GATOR1 (4,5). TSC1 and DEPDC5 are essential components of TSC and GATOR1, respectively. *Tsc1* deletion in mouse liver produced pleiotropic metabolic phenotypes such as suppression of fat oxidation (42) and ketogenesis (43), increased FGF21 production (44), and decreased insulin sensitivity and lipogenesis (22). However, *Tsc1* deletion in the liver ($Tsc1^{\Delta hep}$) did not cause gross pathologies in young mice, although it promoted age-associated liver inflammation and carcinogenesis in one-year-old mice (17,18). A physiological role for Depdc5 in the liver was not formerly investigated until the current study. Here, we showed that *Depdc5* deletion in mouse liver upregulated hepatic mTORC1 most prominently in zone 3, where oxygen and nutrients are relatively scarce. Since GATOR1 is important for suppressing mTORC1 in nutrient-depleted conditions (8), it is plausible that GATOR1 is critical for regulating mTORC1 in zone 3 hepatocytes. After maturation and aging of $Depdc5^{\Delta hep}$ mice, mTORC1 upregulation became more pronounced and resulted in phenotypes similar to $Tsc1^{\Delta hep}$ mice, such as mild inflammation and decreased fat levels. Consistent with their similar mild phenotypes, $Depdc5^{\Delta hep}$ and $Tsc1^{\Delta hep}$ mice had similar transcriptomic profiles that were only moderately different from the wild-type profile.

By crossing $Depdc5^{\Delta hep}$ mice with $Tsc1^{\Delta hep}$ mice, we showed that mutations in both *Depdc5* and *Tsc1* generate a synergistic genetic interaction and produce a very strong hyperactivation of mTORC1. This is the first genetic evidence in animal models confirming that the Rheb and Rag pathways indeed interact for mTORC1 regulation in a physiological context. mTORC1 hyperactivation in DKO mice resulted in liver dysfunction associated with prominent hepatocyte injury and fibrosis by two-months of age. This led to dramatic elevation of liver damage markers in the serum. Excessive bilirubin accumulation in serum led to an externally observable jaundice phenotype. In addition, since the liver is the primary source of insulin-like growth factors that are

essential for systemic growth, liver failure in DKO mice also suppressed growth. At the liver transcriptome level, specific stress response pathways, such as oxidative stress, inflammation, DNA damage and cell death pathways were strongly upregulated. All of these striking phenotypes were not manifested in either *Tsc1*$^{\Delta hep}$ or *Depdc5*$^{\Delta hep}$ single knockout strains or in any formerly described models of mTORC1 activation, such as *Deptor* knockout mice (45). Therefore, our current work provides a unique model of unregulated mTORC1 activation and shows that mTORC1 hyperactivation by itself can disrupt hepatocellular homeostasis, provoking liver injury and failure.

mTORC1 is regulated through multiple negative feedback loops. mTORC1 hyperactivation is known to inhibit Akt through S6K- or Grb10-mediated feedback inhibition of insulin signaling (41,46,47). Since Akt is an mTORC1 upregulator, Akt inhibition can limit mTORC1 activation. However, at the same time, inhibition of insulin-AKT signaling can also precipitate metabolic insulin resistance. Correspondingly, DKO mouse livers exhibited strong insulin resistance, and hepatocytes from DKO mice did not activate AKT in response to insulin. Although the DKO liver suffers strong insulin resistance, the blood glucose level was rather strongly decreased due to the deterioration of hepatocyte homeostasis and subsequent reduction in hepatic glucose output.

In addition to the feedback loop involving insulin signaling, Sestrins can also provide a negative feedback mechanism for the mTORC1 pathway. In Drosophila, Sestrin is an important feedback inhibitor of the mTORC1 pathway through Tsc1/2 (48) and Depdc5 (49) pathways. In the current work, we found that Sestrins expression levels were substantially elevated after deletion of Tsc1, Depdc5 or both. AMPK, one of the downstream effectors of Sestrins inhibiting mTORC1 (10), was subsequently activated in these tissues. Redd1 (*Ddit4*) and Redd2 (*Ddit4l*), which inhibit

mTORC1 through Tsc1/Tsc2 upregulation (29), were also upregulated in mTORC1-activated liver tissues. Therefore, it is possible that, in our mTORC1 activation models, Sestrins and Redds may have resulted in negative feedback inhibition to limit mTORC1 activities.

It was quite striking that all of the liver pathologies in DKO mice were almost completely rescued by only 10 days of rapamycin treatment. Liver/body weight ratios were restored to normal levels, and liver damage markers in the serum also recovered close to clinically normal ranges. Although rapamycin was historically considered a growth attenuator, rapamycin-mediated normalization of liver homeostasis actually promoted systemic growth in this specific DKO model. Upon rapamycin treatment, necrotic and fibrotic lesions in DKO mice disappeared, and hepatocellular ER stress, oxidative stress and apoptosis were all relieved. Therefore, mTORC1 is indeed the major conduit of how the Rheb and Rag pathways pathogenetically interact to produce liver injury and failure.

mTORC1 upregulation increases protein synthesis, which can put a burden on protein folding machinery and therefore induce accumulation of unfolded proteins in the ER, also known as ER stress (23). DKO mouse livers exhibited upregulation of ER stress signaling at the protein level, confirming that mTORC1 hyperactivation in DKO mice indeed precipitated unfolded protein accumulation and ER stress. However, the ER stress response pathway was not overrepresented in the DKO transcriptome, raising questions of whether the ER stress pathway is important for DKO pathologies. Indeed, TUDCA, a chemical chaperone that effectively suppressed hepatocellular ER stress in DKO mouse liver, was completely ineffective in rescuing DKO liver pathologies. Instead, TUDCA-treated DKO mice increased mTORC1 activation, further potentiating liver pathologies in DKO mice to the point of fatality. Even in the surviving mice, TUDCA administration increased expression of fibrogenic markers and more extensively

damaged hepatocytes. It is possible that ER stress signaling somehow limits mTORC1 activation, reducing its negative consequences on liver health. These data also indicate that ER stress signaling is not the major mechanism of how hyperactive mTORC1 disrupts hepatocellular homeostasis.

In addition to inducing ER stress, mTORC1 hyperactivation can elevate oxidative stress by altering mitochondrial metabolism (50,51), inhibiting autophagic elimination of dysfunctional mitochondria (48,52), and suppressing the superoxide-scavenging action of Sod1 (53). Indeed, DKO livers experienced severe oxidative stress associated with excessive accumulation of superoxide radicals and exhibited a transcriptomic profile that is similar to DQ-induced oxidative stress and *Sod1* loss. This high level of oxidative stress can damage cellular macromolecules including DNA. Consistent with this, the DKO transcriptome also exhibited upregulation of some DNA damage response genes. Administration of chemical antioxidants that scavenge superoxide radicals, such as Tempol and NAC, effectively reduced hepatic oxidative stress. Surprisingly, 10 days of antioxidant administration was sufficient to normalize almost every liver pathology parameter observed in DKO mouse liver and even restored normal growth. Since mTORC1 signaling itself was not suppressed by chemical antioxidants, these results indicate that hyperactive mTORC1 signaling provokes liver failure primarily through the induction of superoxide radicals that injure hepatocytes.

At the tissue level, mTORC1 hyperactivation produced crosstalk with a number of additional pathways. For instance, NF-kB target genes such as *Il6* (54) and *Cd44* (55), TGF-beta signaling targets genes *Acta2*, *Mmp2* and *Timp2* (56) and Hippo-Yap target genes *Ctgf* (57) and *Notch2* (58), were all upregulated in DKO mice. These signaling pathways were implicated in inflammation-dependent acceleration of carcinogenesis in previous studies (59). Consistent with

the finding and former studies, we found that the DKO mice spontaneously developed HCC at 5 months, a relatively early age.

Our observations also provide an explanation of how human genetic variations in the *DEPDC5* gene can accelerate HBV/HCV-associated liver pathologies such as hepatic fibrosis (14) and carcinogenesis (13,15). HBV and HCV infections upregulate mTORC1 by activating PI3K-AKT signaling and/or inhibiting TSC, both of which subsequently activate Rheb (60,61). Genetic variations suppressing DEPDC5 function would upregulate Rag signaling, and this would synergistically interact with the HBV/HCV infection that elevates Rheb signaling. Concomitant upregulation of both Rag and Rheb axes would lead to mTORC1 hyperactivation that can precipitate oxidative liver pathologies, as observed in the DKO mice described here. Furthermore, we found that our DKO liver transcriptome is closely related with human HCV and NASH transcriptomes. Therefore, our DKO mice provide a novel mouse model for investigating the role of human *DEPDC5* variations in accelerating liver pathologies associated with HCV and NASH. However, the DKO model currently described here does not involve an actual viral infection or virus-associated activation of adaptive immunity. Therefore, additional studies should be conducted in the context of actual HBV and HCV infection to gain a more direct translation of our findings into the corresponding human liver pathologies.

In conclusion, we show that the Rag and Rheb pathways are both required for maximum mTORC1 activation in tissues. Correspondingly, double knockout of the *Tsc1* and *Depdc5* genes provokes prominent upregulation of mTORC1, disrupts hepatocellular homeostasis, and subsequently precipitates oxidative injury and subsequent liver failure. Our work provides a valuable model for examining the consequences of mTORC1 hyperactivation, understanding human liver pathologies associated with HCV, NASH and *DEPDC5* variation, and developing

therapeutic strategies for treating such pathologies with mTORC1 inhibitors or antioxidant compounds.

Materials and Methods

Mice and Diet

Depdc5$^{F/F}$ (EM: 10459) mice, originated from the HEPD0734_3_G10 embryonic stem cell clone, were obtained from the European Mouse Mutant Archive. *Depdc5*$^{F/F}$ mice were bred to *Albumin* (*Alb*)-*Cre* to produce hepatocyte-specific knockout mice. DKO mice were generated by interbreeding *Depdc5*$^{F/F}$ and *Tsc1*$^{F/F}$ mice (17,62), then breeding progeny with *Alb-Cre* mice. *Depdc5* single knockout experiments were done in C57BL/6 background. *Tsc1* mice were originally produced in a 129S4/SvJae background (17,62) but were backcrossed to C57BL/6 for more than three generations for DKO experiments. To minimize genetic and environmental variations, littermate controls were used throughout the study, and mice were cohoused. For instance, *Depdc5*$^{\Delta hep}$ (*Alb-Cre*/*Depdc5*$^{F/F}$) and *Depdc5*$^{F/F}$ littermates were used for *Depdc5* single knockout experiments. *Alb-Cre*/*Tsc1*$^{F/+}$/*Depdc5*$^{F/+}$ and *Tsc1*$^{F/F}$/*Depdc5*$^{F/F}$ breeders produced control (*Alb-Cre* negative mice and *Alb-Cre*/*Tsc1*$^{F/+}$/*Depdc5*$^{F/+}$ mice), *Tsc1*$^{\Delta hep}$ (*Alb-Cre*/*Tsc1*$^{F/F}$/*Depdc5*$^{F/+}$), *Depdc5*$^{\Delta hep}$ (*Alb-Cre*/*Tsc1*$^{F/+}$/*Depdc5*$^{F/F}$), and *Tsc1*$^{\Delta hep}$/*Depdc5*$^{\Delta hep}$ (DKO, *Alb-Cre*/*Tsc1*$^{F/F}$/*Depdc5*$^{F/F}$) littermates that were analyzed for genetic interaction assays. *Alb-Cre*/*Tsc1*$^{F/F}$/*Depdc5*$^{F/F}$ males and *Tsc1*$^{F/F}$/*Depdc5*$^{F/F}$ females produced DKO littermate cohorts for drug intervention experiments. Mice were maintained in filter-topped cages with cob bedding and given free access to autoclaved regular chow/low fat diet (LFD, Lab Diet 5L0D), high fat diet (HFD, Bio-Serv S3282), and water, as previously described (63). When indicated, freshly made rapamycin (10 mg/Kg body weight), tauroursodeoxycholic acid (TUDCA, 500 mg/Kg body

weight), N-acetylcysteine (NAC, 250 mg/Kg body weight) or vehicle (5% Tween 80, 5% PEG400; or PBS) solutions were administered once daily through intraperitoneal (i.p.) injections for the last 10 days. A superoxide dismutase mimetic 4-hydroxy-2,2,6,6-tetramethylpiperidin-1-oxyl (Tempol, 0.064%) was administered to mice through drinking water. Acetaminophen (APAP, 400 mg/Kg body weight) was administered through a single i.p. injection after 12 hours of fasting. Glucose (1g/Kg glucose) and insulin (0.65 U/Kg insulin) tolerance tests (GTT/ITT) were done according to previously described procedures (25). For acute insulin response studies, mice were put under a surgical plane of isoflurane anesthesia. First, one part of the liver was collected as an untreated control. Then 0.8 U/Kg insulin, diluted in PBS, was injected intravenously through the vena cava. After 5 min, the other parts of the liver were collected as an insulin-treated sample. Information regarding mouse number, age, gender, diet duration, drug dose, route and frequency are indicated in the corresponding Figure and Figure legends. All animal procedures were ethically approved by the Institutional Animal Care & Use Committee and overseen by the Unit for Laboratory Animal Medicine at the University of Michigan.

Antibodies and Reagents

Antibodies for DEPDC5 were generated from Pocono Rabbit Farm & Laboratory using bacterially expressed recombinant proteins. We obtained COL1A1 (sc-293182), Pro-COL3A1 (sc-166316), PECAM-1 (sc-376764), MMP-2 (sc-53630), MMP-3 (sc-21732), MMP-9 (sc-393859), LOX (sc-373995), MMP-13 (sc-515284), CTGF (sc-365970), S6K (sc-230), eIF2α (sc-11386), ATF4 (sc-200 and sc-22800), and TIMP-3 (sc-373839) antibodies from Santa Cruz Biotechnology, Actin (9E10) antibody from Developmental Studies Hybridoma Bank, phospho-Thr389-S6K (9234), pThr172-AMPK (2535), pThr37/46-4E-BP (2855), 4E-BP (9452), pSer51-eIF2α (3398),

pThr980-PERK (3179), PERK (5683), PDI (3501), BIP (3177), CHOP (2895), pSer473-AKT (4060), AKT (4691), pSer236/239-S6 (2211) and S6 (2317) from Cell Signaling Technology, α-smooth muscle actin (α-SMA, ab5694) antibody from Abcam, and F4/80 (MF48000) antibody from Invitrogen. Acetaminophen, NAC and Tempol are from Sigma, TUDCA is from Cayman Chemical, and rapamycin is from LC labs.

Histology

Liver tissues were fixed in 10% buffered formalin, embedded in paraffin and subjected to hematoxylin and eosin (H&E) staining and immunohistochemical staining as previously described (63). In brief, paraffin-embedded liver sections were incubated with primary antibody (1:100), followed by incubation with biotin-conjugated secondary antibodies (Vector Lab, BA-9200 or BA-9401; 1:200) and horseradish peroxidase (HRP)-conjugated streptavidin (BD Biosciences, 554066; 1:300). The HRP activity was visualized with diaminobenzidine staining. Hematoxylin counterstaining was applied to visualize nuclei. For α-SMA and Ki-67 staining, Alexa Flour 488 or 594-conjugated secondary antibodies (Invitrogen) were used to visualize primary antibody staining. Terminal deoxynucleotidyl transferase dUTP Nick-End Labeling (TUNEL) assays were performed using In Situ Cell Death Detection Kit-TMR-Red (Roche). Dihydroethidium (DHE) staining was performed using freshly frozen liver sections and DHE (Thermo Fisher Scientific, D11347) as formerly described (25). To visualize collagen fibers, liver sections were stained with saturated picric acid containing 0.1% Sirius Red (SiRed, Sigma). For Oil Red O staining, OCT-embedded frozen liver sections were dried and stained with fresh 0.5% Oil Red O solution for 15 min then rinsed with 60% isopropanol. Reticulin staining was performed using a kit from

Polyscience (25094), following the manufacturer's recommendation. Histology samples were analyzed under an epifluorescence-equipped light microscope from Meiji.

Immunoblotting

Cells and tissues were lysed in radioimmunoprecipitation assay (RIPA) buffer (50mM Tris–HCl, pH 7.4; 150mM NaCl; 1% sodium deoxycholate; 1% NP-40; 1% Triton X-100; and complete protease inhibitor cocktail (Roche)). Lysates were clarified by centrifugation, and protein concentration was normalized using Bio-rad protein assay dye reagent. Protein lysates were boiled in SDS sample buffer for 5 min, separated by SDS-PAGE, transferred to PVDF membranes and subjected to immunoblotting procedures. 5% blocking grade non-fat milk (170-6404 from Bio-Rad) in TBST was used for membrane blocking and antibody incubation. 1X western blocking reagent (11 921 673 001 from Roche) in TBST was used for phospho-specific primary antibody incubation. Primary antibodies from Santa Cruz Biotechnology and Developmental Studies Hybridoma Bank were used at 1:100, and all the other primary antibodies were used at 1:1000. HRP-conjugated secondary antibodies were purchased from Bio-Rad and used at 1:2000. Chemiluminescence was detected using LAS4000 (GE) systems.

Serum Chemistry

Blood was obtained by cardiac puncture and separated by centrifugation to obtain serum. Serum chemistry markers associated with liver cytotoxicity (ALT, alanine aminotransaminase; AST, aspartate aminotransferase) or liver function (ALP, alkaline phosphatase; TBIL, total bilirubin) were obtained through standard operating procedures using the Liasys clinical chemistry

system (AMS Alliance) within the In Vivo Animal Core of the Unit for Laboratory Animal Medicine.

RNA-Seq Data Analysis

10 µg of DNAase I-treated total RNA, purified from liver tissues of control (*Tsc1*$^{F/F}$/*Depdc5*$^{F/F}$; n=3), *Tsc1*$^{\Delta hep}$ (*Alb-Cre*/*Tsc1*$^{F/F}$; n=2), *Depdc5*$^{\Delta hep}$ (*Alb-Cre*/*Depdc5*$^{F/F}$; n=2) and *DKO* (*Alb-Cre*/*Tsc1*$^{F/F}$/*Depdc5*$^{F/F}$; n=3) mice, were submitted to BGI for mRNA enrichment, library construction and sequencing (BGISeq 50SE), and processed through standard experimental and analytical pipelines. Each sample produced more than 20M clean reads, that were mapped to the mm9 reference genome using STAR (64). Then, Cufflinks was used to generate Fragments Per Kilobase of transcript per Million mapped reads (FPKM) table (65), supplied as Supplementary Table S1. Genes with more than 0.5 FPKM values in every dataset were used to perform correlation and *k*-means clustering analyses. The accession number for the RNA-seq data reported in this paper is GSE136684.

As formerly described (66), gene enrichment analyses were performed to identify whether a subset of genes were significantly overrepresented in specific gene clusters. Inflammation and fibrosis upregulated gene lists were obtained from recent transcriptome data on human liver samples with HCV-associated fibrosis (27) and nonalcoholic steatohepatitis (NASH) (28). From the HCV dataset, disease progression-associated fold changes of differentially expressed genes (the most stringent set with study-wide significance; both up- and down-regulated genes) were compared with the *DKO*-induced gene expression fold changes. The oxidative stress-upregulated gene list was obtained from livers of mice acutely treated with Diquat (DQ) for 12 hrs (38). From the same dataset, DQ-treated and *Sod1*-knockout induced fold changes of differentially expressed

genes (both up- and down-regulated genes; 1 hr DQ treatment) were compared with the *DKO*-induced gene expression fold changes. The ER stress-upregulated gene list was obtained from tunicamycin-treated mouse embryonic fibroblasts (26). Cytokine and chemokine pathway gene lists were generated by selecting relevant genes from the list of genes whose names begin with *Ccl/Ccr*, *Cxcl*/*Cxcr*, *Il/Ilr*, *Ifn/Ifnr* and *Tnf/Tnfr*. The fibrosis-associated gene list was generated by selecting relevant genes from the list of genes whose names begin with *Col*, *Mmp*, *Timp* and *Tgfb*. Cytochrome P450 and major urinary protein gene lists were generated by selecting relevant genes from the list of genes whose names begin with *Cyp* and *Mup*, respectively.

Quantification and Statistics

Immunoblot images were quantified by densitometry, and protein expressions were expressed as relative band intensities. Histological images were analyzed by densitometric or fluorometric methods as appropriate. When indicated, data are shown as mean ± SEM. Statistical significance between two groups was calculated using a Student's t-test (*, $P<0.05$; **, $P<0.01$; ***, $P<0.001$; ****, $P<0.0001$). When multiple parameters were assessed, the Holm-Šídák method was used to compare groups (*$*, $P<0.05$; *$$*, $P<0.01$; *$$$*, $P<0.001$; *$$$$*, $P<0.0001$). A two-way ANOVA was used to evaluate the effect of *Tsc1* and *Depdc5* mutations and assess interactions and synergy between them (#, $P<0.05$; ##, $P<0.01$; ###, $P<0.001$; ####, $P<0.0001$), and statistical significance between two individual groups were assessed through Tukey's multiple comparison test (*$$*, $P<0.01$; *$$$*, $P<0.001$; *$$$$*, $P<0.0001$). The effect of drugs on body weights was assessed through repeated measures (RM) 2-way ANOVA to evaluate the interaction between treatment and time (####, $P<0.0001$). Differences in individual data points were assessed through Sidak's multiple comparison test (*$*, $P<0.05$; *$$*, $P<0.01$; *$$$*, $P<0.001$; *$$$$*, $P<0.0001$). Survival

curves were compared with a log-rank test. Statistical significance of gene enrichment in a specific cluster was calculated using Fisher's Exact test. Correlations between RNA-seq datasets were assessed by computing nonparametric Spearman correlation (r); $P<0.0001$ for all correlation observations. GraphPad Prism 8 was used for all statistical analyses except k-means clustering analyses and gene enrichment analyses, which were performed using R.

References

1. Hay, N., and Sonenberg, N. (2004) Upstream and downstream of mTOR. *Genes Dev* **18**, 1926-1945

2. Wullschleger, S., Loewith, R., and Hall, M. N. (2006) TOR signaling in growth and metabolism. *Cell* **124**, 471-484

3. Zoncu, R., Efeyan, A., and Sabatini, D. M. (2011) mTOR: from growth signal integration to cancer, diabetes and ageing. *Nat Rev Mol Cell Biol* **12**, 21-35

4. Gonzalez, A., and Hall, M. N. (2017) Nutrient sensing and TOR signaling in yeast and mammals. *EMBO J* **36**, 397-408

5. Bar-Peled, L., and Sabatini, D. M. (2014) Regulation of mTORC1 by amino acids. *Trends Cell Biol* **24**, 400-406

6. Inoki, K., Li, Y., Zhu, T., Wu, J., and Guan, K. L. (2002) TSC2 is phosphorylated and inhibited by Akt and suppresses mTOR signalling. *Nat Cell Biol* **4**, 648-657

7. Inoki, K., Zhu, T., and Guan, K. L. (2003) TSC2 mediates cellular energy response to control cell growth and survival. *Cell* **115**, 577-590

8. Bar-Peled, L., Chantranupong, L., Cherniack, A. D., Chen, W. W., Ottina, K. A., Grabiner, B. C., Spear, E. D., Carter, S. L., Meyerson, M., and Sabatini, D. M. (2013) A Tumor suppressor complex with GAP activity for the Rag GTPases that signal amino acid sufficiency to mTORC1. *Science* **340**, 1100-1106

9. Panchaud, N., Peli-Gulli, M. P., and De Virgilio, C. (2013) Amino acid deprivation inhibits TORC1 through a GTPase-activating protein complex for the Rag family GTPase Gtr1. *Sci Signal* **6**, ra42

10. Ho, A., Cho, C. S., Namkoong, S., Cho, U. S., and Lee, J. H. (2016) Biochemical Basis of Sestrin Physiological Activities. *Trends Biochem Sci* **41**, 621-632

11. Dibbens, L. M., de Vries, B., Donatello, S., Heron, S. E., Hodgson, B. L., Chintawar, S., Crompton, D. E., Hughes, J. N., Bellows, S. T., Klein, K. M., Callenbach, P. M., Corbett, M. A., Gardner, A. E., Kivity, S., Iona, X., Regan, B. M., Weller, C. M., Crimmins, D., O'Brien, T. J., Guerrero-Lopez, R., Mulley, J. C., Dubeau, F., Licchetta, L., Bisulli, F., Cossette, P., Thomas, P. Q., Gecz, J., Serratosa, J., Brouwer, O. F., Andermann, F., Andermann, E., van den Maagdenberg, A. M., Pandolfo, M., Berkovic, S. F., and Scheffer, I. E. (2013) Mutations in DEPDC5 cause familial focal epilepsy with variable foci. *Nat Genet* **45**, 546-551

12. Ishida, S., Picard, F., Rudolf, G., Noe, E., Achaz, G., Thomas, P., Genton, P., Mundwiller, E., Wolff, M., Marescaux, C., Miles, R., Baulac, M., Hirsch, E., Leguern, E., and Baulac,

S. (2013) Mutations of DEPDC5 cause autosomal dominant focal epilepsies. *Nat Genet* **45**, 552-555

13. Miki, D., Ochi, H., Hayes, C. N., Abe, H., Yoshima, T., Aikata, H., Ikeda, K., Kumada, H., Toyota, J., Morizono, T., Tsunoda, T., Kubo, M., Nakamura, Y., Kamatani, N., and Chayama, K. (2011) Variation in the DEPDC5 locus is associated with progression to hepatocellular carcinoma in chronic hepatitis C virus carriers. *Nat Genet* **43**, 797-800

14. Burza, M. A., Motta, B. M., Mancina, R. M., Pingitore, P., Pirazzi, C., Lepore, S. M., Spagnuolo, R., Doldo, P., Russo, C., Lazzaro, V., Fischer, J., Berg, T., Aghemo, A., Cheroni, C., De Francesco, R., Fargion, S., Colombo, M., Datz, C., Stickel, F., Valenti, L., and Romeo, S. (2016) DEPDC5 variants increase fibrosis progression in Europeans with chronic hepatitis C virus infection. *Hepatology* **63**, 418-427

15. Liu, W., Ma, N., Zhao, D., Gao, X., Zhang, X., Yang, L., and Dianwu, L. (2019) Correlation between the DEPDC5 rs1012068 polymorphism and the risk of HBV-related hepatocellular carcinoma. *Clin Res Hepatol Gastroenterol*

16. Umemura, A., Park, E. J., Taniguchi, K., Lee, J. H., Shalapour, S., Valasek, M. A., Aghajan, M., Nakagawa, H., Seki, E., Hall, M. N., and Karin, M. (2014) Liver Damage, Inflammation, and Enhanced Tumorigenesis after Persistent mTORC1 Inhibition. *Cell Metab* **20**, 133-144

17. Kenerson, H. L., Yeh, M. M., Kazami, M., Jiang, X., Riehle, K. J., McIntyre, R. L., Park, J. O., Kwon, S., Campbell, J. S., and Yeung, R. S. (2013) Akt and mTORC1 have different roles during liver tumorigenesis in mice. *Gastroenterology* **144**, 1055-1065

18. Menon, S., Yecies, J. L., Zhang, H. H., Howell, J. J., Nicholatos, J., Harputlugil, E., Bronson, R. T., Kwiatkowski, D. J., and Manning, B. D. (2012) Chronic activation of mTOR complex 1 is sufficient to cause hepatocellular carcinoma in mice. *Sci Signal* **5**, ra24

19. Chen, W., Zhang, X., Fan, J., Zai, W., Luan, J., Li, Y., Wang, S., Chen, Q., Wang, Y., Liang, Y., and Ju, D. (2017) Tethering Interleukin-22 to Apolipoprotein A-I Ameliorates Mice from Acetaminophen-induced Liver Injury. *Theranostics* **7**, 4135-4148

20. Borude, P., Bhushan, B., Gunewardena, S., Akakpo, J., Jaeschke, H., and Apte, U. (2018) Pleiotropic Role of p53 in Injury and Liver Regeneration after Acetaminophen Overdose. *Am J Pathol* **188**, 1406-1418

21. Lee, D. H., Lee, B., Park, J. S., Lee, Y. S., Kim, J. H., Cho, Y., Jo, Y., Kim, H. S., Lee, Y. H., Nam, K. T., and Bae, S. H. (2018) Inactivation of Sirtuin2 protects mice from acetaminophen-induced liver injury: possible involvement of ER stress and S6K1 activation. *BMB Rep*

22. Yecies, J. L., Zhang, H. H., Menon, S., Liu, S., Yecies, D., Lipovsky, A. I., Gorgun, C., Kwiatkowski, D. J., Hotamisligil, G. S., Lee, C. H., and Manning, B. D. (2011) Akt stimulates hepatic SREBP1c and lipogenesis through parallel mTORC1-dependent and independent pathways. *Cell Metab* **14**, 21-32

23. Ozcan, U., Ozcan, L., Yilmaz, E., Duvel, K., Sahin, M., Manning, B. D., and Hotamisligil, G. S. (2008) Loss of the tuberous sclerosis complex tumor suppressors triggers the unfolded protein response to regulate insulin signaling and apoptosis. *Mol Cell* **29**, 541-551

24. Ozcan, U., Yilmaz, E., Ozcan, L., Furuhashi, M., Vaillancourt, E., Smith, R. O., Gorgun, C. Z., and Hotamisligil, G. S. (2006) Chemical chaperones reduce ER stress and restore glucose homeostasis in a mouse model of type 2 diabetes. *Science* **313**, 1137-1140

25. Park, H. W., Park, H., Ro, S. H., Jang, I., Semple, I. A., Kim, D. N., Kim, M., Nam, M., Zhang, D., Yin, L., and Lee, J. H. (2014) Hepatoprotective role of Sestrin2 against chronic ER stress. *Nat Commun* **5**, 4233

26. Han, J., Back, S. H., Hur, J., Lin, Y. H., Gildersleeve, R., Shan, J., Yuan, C. L., Krokowski, D., Wang, S., Hatzoglou, M., Kilberg, M. S., Sartor, M. A., and Kaufman, R. J. (2013) ER-stress-induced transcriptional regulation increases protein synthesis leading to cell death. *Nat Cell Biol* **15**, 481-490

27. Ramnath, D., Irvine, K. M., Lukowski, S. W., Horsfall, L. U., Loh, Z., Clouston, A. D., Patel, P. J., Fagan, K. J., Iyer, A., Lampe, G., Stow, J. L., Schroder, K., Fairlie, D. P., Powell, J. E., Powell, E. E., and Sweet, M. J. (2018) Hepatic expression profiling identifies steatosis-independent and steatosis-driven advanced fibrosis genes. *JCI Insight* **3**

28. Gerhard, G. S., Legendre, C., Still, C. D., Chu, X., Petrick, A., and DiStefano, J. K. (2018) Transcriptomic Profiling of Obesity-Related Nonalcoholic Steatohepatitis Reveals a Core Set of Fibrosis-Specific Genes. *J Endocr Soc* **2**, 710-726

29. Ellisen, L. W. (2005) Growth control under stress: mTOR regulation through the REDD1-TSC pathway. *Cell Cycle* **4**, 1500-1502

30. Knopf, J. L., Gallagher, J. F., and Held, W. A. (1983) Differential, multihormonal regulation of the mouse major urinary protein gene family in the liver. *Mol Cell Biol* **3**, 2232-2240

31. Morgan, E. T. (2001) Regulation of cytochrome p450 by inflammatory mediators: why and how? *Drug Metab Dispos* **29**, 207-212

32. El-Kadi, A. O., Bleau, A. M., Dumont, I., Maurice, H., and du Souich, P. (2000) Role of reactive oxygen intermediates in the decrease of hepatic cytochrome P450 activity by serum of humans and rabbits with an acute inflammatory reaction. *Drug Metab Dispos* **28**, 1112-1120

33. Aitken, A. E., Richardson, T. A., and Morgan, E. T. (2006) Regulation of drug-metabolizing enzymes and transporters in inflammation. *Annu Rev Pharmacol Toxicol* **46**, 123-149

34. Shan, W., Nicol, C. J., Ito, S., Bility, M. T., Kennett, M. J., Ward, J. M., Gonzalez, F. J., and Peters, J. M. (2008) Peroxisome proliferator-activated receptor-beta/delta protects against chemically induced liver toxicity in mice. *Hepatology* **47**, 225-235

35. Koga, T., Yao, P. L., Goudarzi, M., Murray, I. A., Balandaram, G., Gonzalez, F. J., Perdew, G. H., Fornace, A. J., Jr., and Peters, J. M. (2016) Regulation of Cytochrome P450 2B10 (CYP2B10) Expression in Liver by Peroxisome Proliferator-activated Receptor-beta/delta Modulation of SP1 Promoter Occupancy. *J Biol Chem* **291**, 25255-25263

36. Parola, M., and Robino, G. (2001) Oxidative stress-related molecules and liver fibrosis. *J Hepatol* **35**, 297-306

37. Zhao, H., Kalivendi, S., Zhang, H., Joseph, J., Nithipatikom, K., Vasquez-Vivar, J., and Kalyanaraman, B. (2003) Superoxide reacts with hydroethidine but forms a fluorescent product that is distinctly different from ethidium: potential implications in intracellular fluorescence detection of superoxide. *Free Radic Biol Med* **34**, 1359-1368

38. Han, E. S., Muller, F. L., Perez, V. I., Qi, W., Liang, H., Xi, L., Fu, C., Doyle, E., Hickey, M., Cornell, J., Epstein, C. J., Roberts, L. J., Van Remmen, H., and Richardson, A. (2008) The in vivo gene expression signature of oxidative stress. *Physiol Genomics* **34**, 112-126

39. Muscoli, C., Cuzzocrea, S., Riley, D. P., Zweier, J. L., Thiemermann, C., Wang, Z. Q., and Salvemini, D. (2003) On the selectivity of superoxide dismutase mimetics and its importance in pharmacological studies. *Br J Pharmacol* **140**, 445-460

40. Thiemermann, C. (2003) Membrane-permeable radical scavengers (tempol) for shock, ischemia-reperfusion injury, and inflammation. *Crit Care Med* **31**, S76-84

41. Um, S. H., D'Alessio, D., and Thomas, G. (2006) Nutrient overload, insulin resistance, and ribosomal protein S6 kinase 1, S6K1. *Cell Metab* **3**, 393-402

42. Kucejova, B., Duarte, J., Satapati, S., Fu, X., Ilkayeva, O., Newgard, C. B., Brugarolas, J., and Burgess, S. C. (2016) Hepatic mTORC1 Opposes Impaired Insulin Action to Control Mitochondrial Metabolism in Obesity. *Cell Rep* **16**, 508-519

43. Sengupta, S., Peterson, T. R., Laplante, M., Oh, S., and Sabatini, D. M. (2010) mTORC1 controls fasting-induced ketogenesis and its modulation by ageing. *Nature* **468**, 1100-1104

44. Cornu, M., Oppliger, W., Albert, V., Robitaille, A. M., Trapani, F., Quagliata, L., Fuhrer, T., Sauer, U., Terracciano, L., and Hall, M. N. (2014) Hepatic mTORC1 controls

locomotor activity, body temperature, and lipid metabolism through FGF21. *Proc Natl Acad Sci U S A* **111**, 11592-11599

45. Caron, A., Mouchiroud, M., Gautier, N., Labbe, S. M., Villot, R., Turcotte, L., Secco, B., Lamoureux, G., Shum, M., Gelinas, Y., Marette, A., Richard, D., Sabatini, D. M., and Laplante, M. (2017) Loss of hepatic DEPTOR alters the metabolic transition to fasting. *Mol Metab* **6**, 447-458

46. Hsu, P. P., Kang, S. A., Rameseder, J., Zhang, Y., Ottina, K. A., Lim, D., Peterson, T. R., Choi, Y., Gray, N. S., Yaffe, M. B., Marto, J. A., and Sabatini, D. M. (2011) The mTOR-regulated phosphoproteome reveals a mechanism of mTORC1-mediated inhibition of growth factor signaling. *Science* **332**, 1317-1322

47. Yu, Y., Yoon, S. O., Poulogiannis, G., Yang, Q., Ma, X. M., Villen, J., Kubica, N., Hoffman, G. R., Cantley, L. C., Gygi, S. P., and Blenis, J. (2011) Phosphoproteomic analysis identifies Grb10 as an mTORC1 substrate that negatively regulates insulin signaling. *Science* **332**, 1322-1326

48. Lee, J. H., Budanov, A. V., Park, E. J., Birse, R., Kim, T. E., Perkins, G. A., Ocorr, K., Ellisman, M. H., Bodmer, R., Bier, E., and Karin, M. (2010) Sestrin as a feedback inhibitor of TOR that prevents age-related pathologies. *Science* **327**, 1223-1228

49. Kim, J. S., Ro, S. H., Kim, M., Park, H. W., Semple, I. A., Park, H., Cho, U. S., Wang, W., Guan, K. L., Karin, M., and Lee, J. H. (2015) Sestrin2 inhibits mTORC1 through modulation of GATOR complexes. *Sci Rep* **5**, 9502

50. Zid, B. M., Rogers, A. N., Katewa, S. D., Vargas, M. A., Kolipinski, M. C., Lu, T. A., Benzer, S., and Kapahi, P. (2009) 4E-BP extends lifespan upon dietary restriction by enhancing mitochondrial activity in Drosophila. *Cell* **139**, 149-160

51. Khan, N. A., Nikkanen, J., Yatsuga, S., Jackson, C., Wang, L., Pradhan, S., Kivela, R., Pessia, A., Velagapudi, V., and Suomalainen, A. (2017) mTORC1 Regulates Mitochondrial Integrated Stress Response and Mitochondrial Myopathy Progression. *Cell Metab* **26**, 419-428 e415

52. Bartolome, A., Garcia-Aguilar, A., Asahara, S. I., Kido, Y., Guillen, C., Pajvani, U. B., and Benito, M. (2017) MTORC1 Regulates both General Autophagy and Mitophagy Induction after Oxidative Phosphorylation Uncoupling. *Mol Cell Biol* **37**

53. Tsang, C. K., Chen, M., Cheng, X., Qi, Y., Chen, Y., Das, I., Li, X., Vallat, B., Fu, L. W., Qian, C. N., Wang, H. Y., White, E., Burley, S. K., and Zheng, X. F. S. (2018) SOD1 Phosphorylation by mTORC1 Couples Nutrient Sensing and Redox Regulation. *Mol Cell* **70**, 502-515 e508

54. Kannabiran, C., Zeng, X., and Vales, L. D. (1997) The mammalian transcriptional repressor RBP (CBF1) regulates interleukin-6 gene expression. *Mol Cell Biol* **17**, 1-9

55. Hinz, M., Lemke, P., Anagnostopoulos, I., Hacker, C., Krappmann, D., Mathas, S., Dorken, B., Zenke, M., Stein, H., and Scheidereit, C. (2002) Nuclear factor kappaB-dependent gene expression profiling of Hodgkin's disease tumor cells, pathogenetic significance, and link to constitutive signal transducer and activator of transcription 5a activity. *J Exp Med* **196**, 605-617

56. March, J. T., Golshirazi, G., Cernisova, V., Carr, H., Leong, Y., Lu-Nguyen, N., and Popplewell, L. J. (2018) Targeting TGFbeta Signaling to Address Fibrosis Using Antisense Oligonucleotides. *Biomedicines* **6**

57. Zhao, B., Ye, X., Yu, J., Li, L., Li, W., Li, S., Yu, J., Lin, J. D., Wang, C. Y., Chinnaiyan, A. M., Lai, Z. C., and Guan, K. L. (2008) TEAD mediates YAP-dependent gene induction and growth control. *Genes Dev* **22**, 1962-1971

58. Yimlamai, D., Christodoulou, C., Galli, G. G., Yanger, K., Pepe-Mooney, B., Gurung, B., Shrestha, K., Cahan, P., Stanger, B. Z., and Camargo, F. D. (2014) Hippo pathway activity influences liver cell fate. *Cell* **157**, 1324-1338

59. Shalapour, S., and Karin, M. (2015) Immunity, inflammation, and cancer: an eternal fight between good and evil. *J Clin Invest* **125**, 3347-3355

60. Bose, S. K., Shrivastava, S., Meyer, K., Ray, R. B., and Ray, R. (2012) Hepatitis C virus activates the mTOR/S6K1 signaling pathway in inhibiting IRS-1 function for insulin resistance. *J Virol* **86**, 6315-6322

61. Wang, Z., Jin, W., Jin, H., and Wang, X. (2014) mTOR in viral hepatitis and hepatocellular carcinoma: function and treatment. *Biomed Res Int* **2014**, 735672

62. Kwiatkowski, D. J., Zhang, H., Bandura, J. L., Heiberger, K. M., Glogauer, M., el-Hashemite, N., and Onda, H. (2002) A mouse model of TSC1 reveals sex-dependent lethality from liver hemangiomas, and up-regulation of p70S6 kinase activity in Tsc1 null cells. *Hum Mol Genet* **11**, 525-534

63. Cho, C. S., Park, H. W., Ho, A., Semple, I. A., Kim, B., Jang, I., Park, H., Reilly, S., Saltiel, A. R., and Lee, J. H. (2018) Lipotoxicity induces hepatic protein inclusions through TANK binding kinase 1-mediated p62/sequestosome 1 phosphorylation. *Hepatology* **68**, 1331-1346

64. Dobin, A., Davis, C. A., Schlesinger, F., Drenkow, J., Zaleski, C., Jha, S., Batut, P., Chaisson, M., and Gingeras, T. R. (2013) STAR: ultrafast universal RNA-seq aligner. *Bioinformatics* **29**, 15-21

65. Trapnell, C., Roberts, A., Goff, L., Pertea, G., Kim, D., Kelley, D. R., Pimentel, H., Salzberg, S. L., Rinn, J. L., and Pachter, L. (2012) Differential gene and transcript

expression analysis of RNA-seq experiments with TopHat and Cufflinks. *Nat Protoc* **7**, 562-578

66. Namkoong, S., Ho, A., Woo, Y. M., Kwak, H., and Lee, J. H. (2018) Systematic Characterization of Stress-Induced RNA Granulation. *Mol Cell* **70**, 175-187 e178

Chapter IV

Conclusions and Future Directions

Summary

Sestrins are stress-induced proteins that protect against the pathological progression of many age and metabolic phenotypes. With two established anti-aging functions, reducing ROS and inhibiting mTORC1, Sestrins are well-positioned to protect cells from damage and disease progression. In this thesis, I have expanded our knowledge of Sestrin biology by defining a new mechanism of Sestrin2 regulation, where Sestrin2 activates AKT through GATOR2 and mTORC2. In addition to characterize other components in the Sestrin signaling network, I have generated a new mouse model with a hyperactive mTORC1 liver for use as a new model of both NASH and HCC liver diseases. However, further questions still remain regarding each of these topics.

Sestrin2 and GATOR2 activate mTORC2 and AKT

In Chapter 2, I first showed that Sestrin2 overexpression was sufficient to improve glucose and lipid regulation in HFD mice. We found improved responses to ITT, decreased lipid accumulation in the liver, and decreased gluconeogenic and lipogenic gene transcription (Figure 2.1). Next, I wanted to understand mechanistically how this was occurring and saw huge AKT activation in the livers of the HFD mice with Sestrin2 overexpression, even without insulin stimulation (Figure 2.2A). This relationship between Sestrin2 expression and AKT activation also corresponded to an improvement in insulin sensitivity in cultured HepG2 cells (Figure 2.2B,

2.2C). Furthermore, I used a chemical inhibitor of mTORC1 and an *AMPK*-null cell line to establish that the mechanism of Sestrin2-induced AKT activation occurred independently of previously established Sestrin2 mechanisms (Figure 2.2E, 2.2F). To dissect this mechanism further, we performed kinase assays of established kinases upstream of AKT, PI3K and mTORC2. We found that Sestrin2 overexpression did not increase PI3K activity but did increase mTORC2 activity (Figure 2.3D, 2.3E).

Next, we wanted to know whether GATOR2 was involved in the mechanism of Sestrin2-induced AKT activation. Sestrin2 is known to bind GATOR2 through its D406 and D407 residue sites (1). Therefore, we tested if overexpressing Sestrin2 mutants that have lost their GATOR2 binding function could still activate AKT and found that when Sestrin2 lost GATOR2, it also lost its ability to activate AKT (Figure 2.4A). I also confirmed this functional requirement for GATOR2 through knockdown and knockouts of WDR24, the GATOR2 subcomponent that binds to Sestrin2 (2). Furthermore, mice with liver-specific knockout of WDR24 were not able to benefit from Sestrin2 overexpression (Figure 2.4D-G). Determining that GATOR2 was involved in the mechanism of Sestrin2-induced AKT activation identified a novel function for GATOR2.

Through a series of immunoprecipitation assays, we found that GATOR2 bridged Sestrin2 and mTORC2. Sestrin2 was already known to bind WDR24, and I found that the GATOR2 protein WDR59 was both critical and sufficient to bind Rictor, a key mTORC2 component (Figure 2.5B). The functional requirement of WDR59 for Sestrin2-induced AKT activation was also confirmed in a WDR59 KO cell line (Figure 2.5D).

Finally, I found that Sestrin2 regulates the subcellular localization of AKT by inducing its translocation to the plasma membrane. Not only did I find a physical association between Sestrin2 and AKT (Figure 2.6A-C), but I also found a strong association between Sestrin2 and the PH

domain of AKT (Figure 2.6C). The PH domain is important for AKT translocation to the plasma membrane (3), so I wanted to determine if Sestrin2 was in fact regulating AKT subcellular localization. It is possible that Sestrin2 binding to the PH domain is releasing AKT from its inhibitory conformation. Using both immunocytochemistry (Figure 2.6D) and fractionation experiments (Figure 2.6E-H), I was able to confirm that Sestrin2 overexpression enriches AKT on the membrane and requires GATOR2 to do so.

Overall, this work defined a novel signaling mechanism for Sestrin2 in regulating mTORC2 through GATOR2. Some questions still remain, however, about the details of this mechanism. First, I only identified the requirements of WDR24 and WDR59 for this mechanism, so future work could determine the requirement for the other three subcomponents of GATOR2: Seh1L, SEC13, and Mios. It is possible that only part of the GATOR2 complex is involved in the mechanism of Sestrin2-induced AKT activation, since other investigators have also found independent functions of GATOR2 subcomponents (4,5). Secondly, the exact mechanism of how Sestrin2 and GATOR2 induces membrane translocation and activation of AKT should be clarified. For example, one possibility is that Sestrin2, GATOR2, and mTORC2 are all shuttling AKT to the plasma membrane. However, it is also possible that Sestrin2, GATOR2, and mTORC2 are promoting Ser473 phosphorylation on AKT, and this subsequently promotes translocation to the plasma membrane. Finally, the next steps would be to evaluate Sestrin2 as a therapeutic candidate to improve glucose and lipid regulation in diabetic patients. Some challenges may be to determine mechanisms for effective delivery to the liver, developing Sestrin mimetics that can activate AKT in vivo, and determining appropriate, safe dosages to achieve clinical benefits.

Hyperactive mTORC1 liver mouse model

In Chapter 3, I generated and characterized two new mouse models. First, I generated *Depdc5*$^{\Delta hep}$ mice, which showed zone 3 hepatocyte enlargement, inflammation, and liver injury as they aged (Figure 3.1, S3.1). Then I generated a *Tsc1*$^{\Delta hep}$*/Depdc5*$^{\Delta hep}$ DKO mouse, which showed systemic growth suppression and severe liver injury, even at a young age (Figure 3.2, S3.2, 3.3). Comparing DKO mice to littermate controls, I noticed three categories of significantly increased phenotypes: mTORC1 activity, ER stress, and liver injury. To which, I then tested three different interventions for each phenotype.

First, we treated the DKO mice with rapamycin, an mTORC1 inhibitor. Strikingly, all pathological phenotypes were reversed with only 10 days of IP injections. This included resuming normal growth, reduced liver injury, inflammation, cell death, and fibrosis (Figure 3.4). Because our genetic modifications result in a hyperactive mTORC1 liver, this experiment confirmed that the pathological progression was, in fact, occurring through hyperactive mTORC1 signaling.

The next intervention we tested was TUDCA, an ER stress reducer, that has been shown to be beneficial for WT mice (6,7). Surprisingly, TUDCA injections resulted in less than a 50% survival rate of the DKO cohort by 10 days (Figure 3.5B). Despite a reduction in most ER stress markers, all other liver injury phenotypes such as inflammation and fibrosis were significantly increased (Figure 3.5D, 3.5E). This data suggests that a potential negative feedback mechanism occurs through ER stress signaling that actually tempers the pathological progression of the hyperactive mTORC1 liver.

To look at the DKO phenotype on a larger scale, we also performed transcriptomic analysis of WT, *Depdc5*$^{\Delta hep}$, *Tsc1*$^{\Delta hep}$, and DKO livers. We found that DKO transcriptomes had distinct profiles from WT and single knockout livers (Figure 3.6B). In addition, DKO livers had selective

upregulation of oxidative stress genes (Figure S3.3F) and transcriptomic profiles that resembled transcriptomes of patients with NASH (Figure 3.6H, 3.6I). Based on these findings, we then performed the third intervention, treating the DKO mice with Tempol, a reactive oxygen species reducer, to counter the oxidative stress. Tempol was also able to reverse the DKO pathologies: resuming normal growth, reducing liver injury, inflammation, and fibrosis (Figure 3.7). Taken together with the transcriptomic analysis, this suggests that the hyperactive mTORC1 liver injury was occurring through oxidative stress signaling.

Finally, we also characterized the DKO mice under conditions of no interventions. We found that by 2 months of age, not only were the DKO mice exhibiting liver fibrosis (Figure 3.2E), but they were also insulin resistant (Figure 3.8A-C). These phenotypes may potentially make the DKO mouse a good model for NASH because of the quick fibrosis progression. Current models such as diet-induced NASH models, using methionine choline deficiency (MCD) or MCD-HFD, require 2 months of aging with an additional minimum 2 months of feeding (8), so our DKO model not only does not require a special diet but also no intervention and half of the time for NASH development. Furthermore, we found that 5-month-old DKO mice spontaneously generated hepatocellular carcinoma (HCC) with an incidence greater than 50% (Figure 3.8D). Current HCC mouse models require much longer time periods until tumorigenesis. For example, diethylnitrosimine (DEN) requires administration of the carcinogen in 15-day-old mice, then a 9-month incubation period (8). Other chemical inducers such as carbon tetrachloride (CCl_4) and thioacetamide (TAA) require repeat administration or combinatorial treatments with shortest times of HCC development of 5 months but this ranges to a year or longer (8). Diet-induced HCC models also exist, but HCC incidence is only 60-89% and may require 12 months of feeding (8). Finally, genetic models also exist but still require a latency period of a minimum of 8 months (8).

Therefore, our 5-month spontaneous HCC DKO mouse model may be a quick, low-maintenance HCC model for future studies.

Overall, this work examined the genetic effect of deleting specific regulators upstream of mTORC1 in the liver. First, the *Depdc5*$^{\Delta hep}$ mice showed some mild inflammation and liver injury in 5-month-old mice. Then, *Tsc1*$^{\Delta hep}$*/Depdc5*$^{\Delta hep}$ DKO mice showed huge pathological phenotypes by 2-months with transcriptomic profiles similar to NASH patients and exhibiting insulin resistance. By 5 months, the majority of the mice developed HCC without chemical administration. Mechanistically, we found that the liver injury seen in these DKO mice resulted from increased oxidative stress and could be recovered with daily injections of both rapamycin and Tempol for 10 days. One major caveat to this mouse model is that the mice are quite sick, as witnessed by their significantly lower body weight. However, they are still reproductively viable, making them amenable to simple, littermate controlled breeding schemes for experimental setups.

Perspectives

From these two major experimental studies, this dissertation furthers our understanding of the Sestrin2 signaling network. First, I identified and defined a novel cell signaling pathway for Sestrin2 as a regulator of mTORC2. Sestrin2 is a concurrent mTORC1 inhibitor and mTORC2 activator. These parallel mechanisms of regulation position Sestrin2 well for therapeutic evaluation because Sestrin2 is able to improve glucose and lipid regulation without the deleterious effects of mTORC1 activation. Sestrin2 mimetics or other chemicals that can strategically target this pathway may potentially improve glucose and lipid homeostasis in diabetic patients without promoting tumorigenesis.

Secondly, I generated a novel genetic mouse model with a hyperactive mTORC1 liver that replicates NASH and eventually HCC without subsequent intervention. This mouse model may be utilized for future investigation in liver disease because it is quick, thus cost-efficient, and low-maintenance because it does not require chemical administration or a long latency period for NASH or HCC development.

References

1. Kim, H., An, S., Ro, S. H., Teixeira, F., Park, G. J., Kim, C., Cho, C. S., Kim, J. S., Jakob, U., Lee, J. H., and Cho, U. S. (2015) Janus-faced Sestrin2 controls ROS and mTOR signalling through two separate functional domains. *Nat Commun* **6**, 10025

2. Parmigiani, A., Nourbakhsh, A., Ding, B., Wang, W., Kim, Y. C., Akopiants, K., Guan, K. L., Karin, M., and Budanov, A. V. (2014) Sestrins inhibit mTORC1 kinase activation through the GATOR complex. *Cell Rep* **9**, 1281-1291

3. Manning, B. D., and Toker, A. (2017) AKT/PKB Signaling: Navigating the Network. *Cell* **169**, 381-405

4. Platani, M., Samejima, I., Samejima, K., Kanemaki, M. T., and Earnshaw, W. C. (2018) Seh1 targets GATOR2 and Nup153 to mitotic chromosomes. *J Cell Sci* **131**

5. Cai, W., Wei, Y., Jarnik, M., Reich, J., and Lilly, M. A. (2016) The GATOR2 Component Wdr24 Regulates TORC1 Activity and Lysosome Function. *PLoS Genet* **12**, e1006036

6. Park, H. W., Park, H., Ro, S. H., Jang, I., Semple, I. A., Kim, D. N., Kim, M., Nam, M., Zhang, D., Yin, L., and Lee, J. H. (2014) Hepatoprotective role of Sestrin2 against chronic ER stress. *Nat Commun* **5**, 4233

7. Ozcan, U., Yilmaz, E., Ozcan, L., Furuhashi, M., Vaillancourt, E., Smith, R. O., Gorgun, C. Z., and Hotamisligil, G. S. (2006) Chemical chaperones reduce ER stress and restore glucose homeostasis in a mouse model of type 2 diabetes. *Science* **313**, 1137-1140

8. Carlessi, R., Kohn-Gaone, J., Olynyk, J. K., and Tirnitz-Parker, J. E. E. (2019) Mouse Models of Hepatocellular Carcinoma. in *Hepatocellular Carcinoma* (Tirnitz-Parker, J. E. E. ed.), Brisbane (AU). pp